University of Southampton Research Repository

UNIVERSITY OF SOUTHAMPTON

Faculty of Engineering and Physical Sciences
School of Physics and Astronomy

Data-driven analyses of supersymmetric models and their cosmological and phenomenological consequences

by

Adam Forster
Msc, Bsc

A thesis for the degree of
Doctor of Philosophy

June 2022

University of Southampton

Abstract

Faculty of Engineering and Physical Sciences
School of Physics and Astronomy

Doctor of Philosophy

Data-driven analyses of supersymmetric models and their cosmological and phenomenological consequences

by Adam Forster

With such a rich plethora of models to explain the mysteries of modern theoretical physics, the role of phenomenology is critical in ascertaining the viability of said models against experimental result. Furthermore, as the ambition and scope of these models grows, sophisticated data science techniques are more relevant than ever in handling such models.

In this thesis, I present the work I have done in applying data techniques to extensions of supersymmetric models which remains one of the most attractive candidates for physics beyond the Standard Model. In particular, I present the results of my work developing and applying algorithmic frameworks for analysing high scale parameters of these models and linking phenomenological tools in order to analyse various experimental results of these models. In essence, the models presented display two different approaches to the fine-tuning problems in supersymmetry where in one we fix parameters to be natural, and in the second we allow for non-minimal-flavour-violation.

In this manuscript, I first briefly introduce the Standard Model and its shortcomings as well as supersymmetric extensions to the Standard Model and some alternative approaches to beyond the Standard Model physics.

I then show the results of a no-scale supergravity model where the universal scalar mass is zero. We have a particular focus on the recent muon g-2 experimental results as well as dark matter and the Higgs boson mass. These models naturally arise from string theory and are also inspired by Starobinsky inflation which places further phenomenological constraints on the model. We find that certain regions of parameter space can satisfy these constraints with requisite light sleptons close to the LHC excluded region.

I also display the work I did in implementing a Markhov chain MonteCarlo scan of a supersymmetric grand unified theory of flavour. In this analysis, a huge number of phenomenological constraints were applied to examine the allowed flavour structure. The model naturally predicted large sleptonic mixing explaining their LHC evation and light winos and gluinos suggesting the good prospect for discovering these particles in up-coming collider runs.

This thesis contains work based on two preprint publications with arXiv numbers arXiv:2111.10199, and arXiv:2111.10199.

Contents

List of Figures

List of Tables

Declaration of Authorship

I declare that this thesis and the work presented in it is my own and has been generated by me as the result of my own original research.

I confirm that:

1. This work was done wholly or mainly while in candidature for a research degree at this University;
2. Where any part of this thesis has previously been submitted for a degree or any other qualification at this University or any other institution, this has been clearly stated;
3. Where I have consulted the published work of others, this is always clearly attributed;
4. Where I have quoted from the work of others, the source is always given. With the exception of such quotations, this thesis is entirely my own work;
5. I have acknowledged all main sources of help;
6. Where the thesis is based on work done by myself jointly with others, I have made clear exactly what was done by others and what I have contributed myself;
7. Parts of this work have been published as:

Signed:... Date:..................

Acknowledgements

At many points in the past four years I have had real doubts that I would make it this far and it is testimony to the great network of colleagues, friends, and family that I have achieved what I have.

Firstly I would like to thank Steve King, my PhD supervisor. Your wise council has been absolutely pivotal in guiding me to this point. Thank you for your great ideas and for the fascinating physical phenomena we explored.

Thank you to my various collaborators along the way. Without your contributions and expertise I certainly would not have developed my projects to where they are. Special thanks to Jordan Bernigaud; you were always willing to discuss the queries and conundrums I conjured up (and to play a cheeky chess game or two).

Thanks to the wonderful friends I made in the High Energy Physics group. Particular thanks to Matthew Russell and Michele Santagata; you guys brightened up my life with heated discussions, long days in the department, and long nights in the pub.

I certainly would not be here without the support of my great friends Andy Cornforth and Joe Woodall. You two are the best friends a guy could have.

Particular thanks to Eddie Fitzgerald-Barron. Your sage leadership of C Free enabled me to thrive in this endeavour. Without your great sacrifices we would never be where we are. I hope many more great things are in our future.

Most of all I would like to thank my family, Mough, Dough, Ough, Wough, and Emji the Dwarf. Thank you for your unwavering support.

Finally I would like to thank Marcella. Thanks for sharing in the highs and lows with me.

Chapter 1

The Standard Model

1.1 Overview

The rather stalely entitled Standard Model of Particle Physics (SM) was developed predominantly in the mid-20th century and is still a remarkably powerful theory in modern physics. Modern science has rarely, if ever, seen such a successful model in terms of the accuracy and scope of its predictions. It is by far the most powerful application of quantum field theory (QFT), utilising a number of imposed symmetry groups in order to describe three of the four fundamental forces of nature and the constituents of matter that make up the world around us. Indeed, the model makes a number of astonishingly successful prediction including decay rates, bound states, etc [1–9]. With the discovery of the Higgs boson in 2012 at the LHC, the final building blocks of the model fell into place, experimentally confirming and completing the theory [10, 11].

As alluded to previously, the SM is a QFT. As such, it is a natural framework for imposing symmetry groups on top of well established quantum physical descriptions. In particular, special relativity (or the Poincaré group) is combined with the local symmetry group $G_{SM} = SU(3)_C \times SU(2)_L \times U(1)_Y$. These so-called gauge groups provides a mechanism for generating the force particles of the Standard Model. Here, the subscripts C, L, and Y denote the different interactions described by each group. These shall be delved into further later in this chapter. However, I shall make note of the critical role of the Higgs boson here as, after spontaneous symmetry breaking, $SU(2)_L \times U(1)_Y \rightarrow U(1)_{em}$ forms the basis for electromagnetic interactions via the Higgs mechanism. Therefore, the electric charge, Q, is given in terms of the generators of the broken symmetry groups; Y, the hypercharge associated to $U(1)_Y$ and T^3, the third generator of the $SU(2)_L$ group, as follows.

$$Q = T^3 + \frac{Y}{2} \tag{1.1}$$

This peculiar relation is the direct result of the specific breaking pattern of the symmetry group and of the Higgs mechanism as we shall see later.

Having spoken in such glowing terms about this theory, cracks have emerged in its previously iron-clad arsenal of experimental successes. There are now a number of observations that cannot be easily accommodated for in the theory. Furthermore, there are some aesthetic principals that hint at physics beyond the Standard Model.

As an example of these issues, galaxy rotation curves suggest the presence of some invisible, weakly interacting source of gravity sitting in the galaxies. The cosmic microwave background (CMB) contains key features that are only possible with reference to a similar weakly interacting source of gravity [12]. We call this source dark matter. Although alternative theories have been suggested, the common consensus is that this source is a particle. However, no Standard Model particle represents a good candidate. The CMB also demonstrates the horizon problem, in which causally disconnected parts fo the universe appear homogenous and isotropic [13]. Furthermore, the SM has no explanation for the large matter antimatter asymmetry we observe.

Looking a little closer to home, we find further limitations of the Standard Model. Recent experiments have shown that the treatments of the different flavours is not universal as the Standard Model would predict. Indeed, the recent measurement at brookhaven and fermilab's have shown a 4.2σ discrepancy between the Standard Model and experimental results for the muon magnetic moment, muon $g-2$ [14–34]. Furthermore, neutrinos have been observed to oscillate between different generations [35]; such a trick is only possible if neutrinos, previously thought to be massless, have mass.

On the more theoretical side, one can argue that the Standard Model does not address the hierarchy problem concerning the vast discrepancy between the electroweak scale of physics and the scale at which gravitational affects become important on the quantum level [36]. Indeed, the Standard Model suffers from a further naturalness problem; the flavour problem. Why do the free parameters of the Standard Model take the particular values that they do? In the immortal words of Isidor Isaac Rabi, "who ordered that?".

With these limitations manifest, the Standard Model cannot be the final story, but is an effective field theory (EFT) of some theory beyond the Standard Model. That is to say, the extraordinary successes of the Standard Model must re-emerge from our BSM theory at low energies, once the new physics is "integrated out".

With this said, I will now endeavour to give a very brief introduction to the Standard Model in order to give context to the Beyond the Standard Model (BSM) physics I wish to explore. Furthermore, certain notation and stylistic choices will be made to give clarity to the following chapters. Having said this, I will not go into detail. Many excellent works are available to readers of all abilities to get a richer context for the Standard Model.

1.2 The Fermions

Fermions are particles theorised by a number of phsyicists in the early 20th century. They have spin half and obey the Pauli exclusion principle. As we impose the above symmetries on the theory, they are representations of the Poincare group and thus obey special relativity. Under this condition, the wave function must be anti-symmetric in order to prevent negative energy eigenstates thus realising the Pauli exclusion principle. These fermions obey the Dirac equation given by,

$$(\not{p} - m)\psi = 0 \tag{1.2}$$

where ψ is the wave function of the fermion, $\not{p}$ is the Dirac operator $\gamma^\mu p_\mu$ and γ^μ are Dirac matrices. Therefore, the Dirac Lagrangian is given by

$$\mathcal{L}_f = \overline{\psi}(i\not{\partial} - m)\psi \tag{1.3}$$

where $\overline{\psi} = \psi^\dagger\gamma^0$. These wave-function include 4-dimensional Dirac spinors. These can in turn by constructed from two dimensional Weyl spinors. Although this formalism is not necessary, we will find later (when we consider supersymmetry) that these objects can be useful. One can define chirality projectors that apply to the Dirac spinors and pull out the left or right handed parts as follows

$$P_L = \frac{1-\gamma^5}{2}, P_R = \frac{1+\gamma^5}{2}, \tag{1.4}$$

where $\gamma^5 = i\gamma^0\gamma^1\gamma^2\gamma^3$. Therefore $P_L\psi = \eta_L$ and $P_R\psi = \eta_R$ where η_L is the left handed Weyl spinor and η_R is its right handed equivalent.

With these in hand, let us return to the aforementioned Poincaré group and, more specifically, its subgroup, the Lorentz group, $SO(1,3)$. This group is comprised of both spatial rotations, and so-called Lorentz boosts. We can therefore split the generators of the group into the corresponding operators; the boosts, K_i, and the spatial rotations, J_i. From these, we can define the further operators

$$\begin{aligned} N_i^+ &= \frac{1}{2}(J_i + iK_i), \\ N_i^- &= \frac{1}{2}(J_i - iK_i) \end{aligned} \tag{1.5}$$

This may seem like a curious definition, but one can use these, and the commutations relations of K_i and J_i to show that

$$\begin{aligned} [N_i^+, N_j^+] &= \epsilon_{ijk} N_k^+, \\ [N_i^-, N_j^-] &= \epsilon_{ijk} N_k^-, \\ [N_i^+, N_j^-] &= 0 \end{aligned} \tag{1.6}$$

This is precisely the commutation relations of the product of two special unitary groups, $SU(2)$, with generators N_k^+ and N_k^-. Therefore, $SO(1,3) \approx SU(2) \times SU(2)$.

But what is the point of all of this? We can express representations of the Lorentz group, and therefore construct a theory that inherently obeys special relativity, as objects transforming under the two $SU(2)$ groups. These are as follows:

$$\begin{aligned} \text{Scalar} &: (0,0) \\ \text{Left handed spinor} &: (\frac{1}{2}, 0) \\ \text{Right handed spinor} &: (0, \frac{1}{2}) \\ \text{Vector} &: (\frac{1}{2}, \frac{1}{2}) \end{aligned} \tag{1.7}$$

With these four components, we can make the entire Standard Model as our friends, the Weyl spinors, satisfy this algebra and thus give us a natural framework for the theory. Therefore, I give the Dirac lagrangian in terms of its constituent Weyl fermions.

$$\mathcal{L}_f = i\overline{\eta}_L \sigma^\mu \partial_\mu \eta_L + i\overline{\eta}_R \overline{\sigma}^\mu \partial_\mu \eta_R + (\overline{\eta}_L m \eta_R + h.c) \tag{1.8}$$

where is $\sigma = (I, \sigma^i)$ and $\overline{\sigma} = (I, -\sigma^i)$, and σ_i are the Pauli matrices that generate the $SU(2)$ group, and I is the unitary matrix. Notice that the Dirac mass term inherently mixes the lift and right spinors while the kinetic term leaves them independent. Here we can manifestly see that a theory constructed from such creatures cannot maintain the $SU(2)_L \times U(1)_Y$ symmetry. This will be addressed explicitly later.

Now with these building blocks defined, we will turn to the content of the Standard Model itself. There are two instantiations of fermions in the Standard Model; the leptons and the quarks distinguished by there $SU(3)_c$ representations; the leptons are colourless and therefore are not affected by the strong force, where as quarks are charged under this group.

1.2.1 The Leptons

The charged leptons are separated into three different generations; the electron (e), the muon (μ), and the tauon (τ). Each generation has exactly the same quantum numbers as the others excepting their masses, which differ vastly (see Figure 1.2). They are charged under $SU(2)_L \times U(1)_Y$ and thus interact electromagnetically, and via the weak gauge bosons.

To compliment this set of three particles, an additional set of brother particles exists called neutrinos. These neutrinos reflect the same generational structure, electron neutrino (ν_e), muon neutrino (ν_μ), tauon neutrino (ν_τ). We refer to this structure as the flavour of the particles.

We combine a given flavour of charged lepton and it's respective neutrino into an $SU(2)_L$ doublet, denoted by L_i, where $i \in 1, 2, 3$ represents the different generations. This is convenient notation to guarantee that our theory obeys they imposed symmetries. We can then derive the charge of these particles by using equation 1.1. The eigenvalue of T^3 is $-1/2$ for the charged leptons and $1/2$ for the neutrinos. The doublets hypercharge is -1 and therefore the electric charge of the neutrino is 0 and -1 for the charged leptons. As is the case in many families, one brother interacts magnetically, while the other is shy, only weakly interacting.

The right handed leptons are not charged under $SU(2)_L$ and therefore their eigenvalue fo T^3 is 0. The hypercharge of the right handed charged leptons is 2 but that of the right handed neutrinos is 0. Therefore, the right handed neutrinos are completely uncharged. For this reason, they have been precluded from the Standard Model. Furthermore, with reference to equation 1.8 we know that without both right and left handed states, a particle cannot have a Dirac mass term. Therefore, the Standard Model predicts massless neutrinos.

All leptons are completely uncharged under $SU(3)_c$ making them interesting candidates to study flavour physics as they are not affected by the powerful physics of the strong force.

1.2.2 The Quarks

Like the leptons, there are three generations of quarks. They are divided into up-type and down-type; the three up type quarks are name up (u), charm (c), and top (t) whilst the down type quarks are named down (d), strange (s), and bottom (b). Again, these are perfect copies of each other excepting their vastly varying masses. Again they are organised into $SU(2)_L$ doublets, Q_{L_i} comprised of up-type and down-type quarks. However, unlike the leptons, the quarks are charged under $SU(3)_c$ forming colour triplets with three colours; red, green, and blue. As they respond to the strong force, they cannot be observed on their own but rather form bound states. This is how, so few particles lead to the great tapestry of mesons and hadrons we observe in modern experiments.

The charge assignments and representations of the quarks is summarised in Tables 1.2 and 1.2.

1.2.3 Matter Content Summary

For convenience, I give a number of tables here to clarify the matter content of the Standard Model. Firstly, in Tables 1.2 I give a table summarising the field representations under each of the Standard Model symmetry groups. We see that the left handed fields are collected into doublets of $SU(2)_L$ and that the quarks are triplets under $SU(3)_c$. I then give a break down of the charges under key generators and the resulting electric charge of the Standard Model fermions in Table 1.2.

Field	$U(1)_Y$	$SU(2)_L$	$SU(3)_c$
L_i	-1	2	1
e_{R_i}	-2	1	1
Q_{L_i}	$1/3$	1	3
u_{R_i}	$4/3$	2	3
d_{R_i}	$-2/3$	1	3

TABLE 1.1: The representations under the SM gauge group for the matter content is presented. Q_L and L_L are the left handed SU(2) doublet represntations.

Particle	Y	T^3	$SU(3)_c$	Q
e_{L_i}	-1	$-1/2$	1	-1
e_{R_i}	-2	0	1	-1
ν_i	-1	$1/2$	1	0
u_{L_i}	$1/3$	$1/2$	3	$2/3$
u_{R_i}	$4/3$	0	3	$2/3$
d_{L_i}	$1/3$	$-1/2$	3	$-1/3$
d_{R_i}	$-2/3$	0	3	$-1/3$

TABLE 1.2: The charge under the hypercharge, third isospin component, and $SU(3)$. The resultant electric charge of each state is also presented.

With this summary in hand, we have described the full matter content of the SM. This is all well and good, but a theory with all these particles in it but no interactions between them cannot be the theory I have previously described in such glowing terms. We will therefore move on to the interactions of the Standard Model by taking a closer look at the symmetry groups I have been referring to thus far.

1.3 Symmetries of the Standard Model

The symmetry groups of the Standard Model serve to constrain the overall form of the theory. They are the key to understanding the fascinating dynamics that play out on the quantum level. In particular, by promoting symmetry groups to local symmetries, and thereby enforcing a gauge structure, the fundamental interactions between the particles can be described.

1.3.1 Local Symmetries

The Standard Model obeys three local symmetry groups, G_{SM}. Local symmetry groups are a classification of symmetries where by the transformations under this group can depend on the position in space and time. We will see that, by imposing these symmetries, we will introduce a new type of particle, the gauge bosons.

Let us continue to consider the Dirac Lagrangian.

$$\mathcal{L}_f = \overline{\psi}(i\partial\!\!\!/ - m)\psi \tag{1.9}$$

Consider a global $U(1)$ symmetry transformation, $\psi \to e^{i\alpha Q}\psi$, where Q is the generator of the $U(1)$ symmetry and alpha parameterises the transformation. Clearly, the given Lagrangian is symmetric under this transformation. Now let's promote this symmetry to a local (gauge) symmetry. Therefore,

$$\psi \to e^{i\alpha(x)Q}\psi \tag{1.10}$$

Now, there is a problem. Although the mass term will remain unchanged, the derivative will draw out an extra term leaving the Lagrangian changed. To solve this problem, we introduce the covariant derivative whose behaviour will change depending on its position in space time.

$$D_\mu\psi = (\partial_\mu - igA_\mu)\psi \tag{1.11}$$

Here, we have introduced the gauge boson, A_μ. This will transform as,

$$A_\mu \to A_\mu + \frac{1}{g}\partial_\mu\alpha(x) \tag{1.12}$$

where g is the gauge coupling. With this redefinition, the above Lagrangian becomes invariant under the local symmetry for both the mass and kinetic terms. We can also write down kinetic terms for this new field of the form

$$\mathcal{L}_{gauge} = -\frac{1}{4}F^{\mu\nu}F_{\mu\nu} \tag{1.13}$$

where $F_{\mu\nu} = \partial_\mu A_\nu - \partial_\nu A_\mu$ is the field strength tensor. We have now naturally included gauge bosons that couple to the fermion fields we have already introduced.

However, what if we want our theory to describe massive gauge bosons? Naively, including a mass term for the gauge bosons, such as $M_A A_\mu A^\mu$, leads to the same problem we had before; our symmetry is again broken under the given transformations. For the time being our theory must only contain massless gauge bosons.

Now that we have some understanding of the technical side of these symmetries we can inspect the practical applications.

1.4 QCD

Although my research, in general does not pertain to the nuances of QCD, for completeness I include a brief discussion of the theory.

Quantum chromodynamics (QCD) is the theory associated with the non-abelian $SU(3)_c$ gauge group [37] and is responsible for the mechanisms that bind the quarks into the menagerie of hadrons observed by experimentalists. The force mediators are called gluons, G^a, come in eight varieties, corresponding to the eight generators of $SU(3)$. Recalling that leptons are uncharged under $SU(3)_c$ and therefore do not feel its affects, the QCD Lagrangian is given by,

$$\mathcal{L}_{QCD} = \overline{\psi_q}(i\not{D} - m)\psi_q - \frac{1}{4}G^a_{\mu\nu}G^{\mu\nu}_a \tag{1.14}$$

where $G^{\mu\nu}_a$ is the field strength tensor associated with this gauge transformation and ψ_q represents the quark fields. The field strength tensor, and the covariant derivative are given by

$$\begin{aligned} D_\mu &= \partial_\mu - ig_s G^a_\mu T^a \\ G^{\mu\nu}_a &= \partial_\mu G^a_\nu - \partial_\nu G^a_\mu + ig_s f^{abc} G^b_\mu G^c_\nu \end{aligned} \tag{1.15}$$

where f^{abc} are the fine structure constants, G^a_μ are the gluon fields, and g_s is the coupling strength. Indeed, the particular behaviour of the coupling strength in QCD gives rise to the phenomena of colour confinement, in which $SU(3)$ charged states cannot be observed alone, instead always appearing bound together into a hadronic state. However, due to RGE running (a phenomena I will discuss later) this theory is asymptotically free. That is to say, at high energy scales, the coupling runs such that the confinement effects wane away leaving a free quarks to stand alone.

1.5 Electroweak Field Theory

Having dealt with the $SU(3)_c$ part of G_{SM}, we are left with $U(1)_Y \times SU(2)_L$. This combination comprise electroweak (EW) field theory. There are three primary components to the electroweak Lagrangian

$$\mathcal{L}_{EW} = \mathcal{L}_{Kinetic} + \mathcal{L}_{Yukawa} + \mathcal{L}_{Higgs} \tag{1.16}$$

We will start with the kinetic part. The gauge fields for the Electroweak theory are W^i_μ for $SU(2)_L$ and B_μ for $U(1)_Y$, where i runs from 1 to 3. Therefore, we can construct our covariant derivative as follows

$$D_\mu = \partial_\mu + ig_2 W^i_\mu T^i + \frac{1}{2} ig_1 B_\mu \tag{1.17}$$

where g and g' are the gauge couplings and T^i are the generators of $SU(2)_L$. Therefore, the kinetic Lagrangian is given by

$$\mathcal{L}_{Kinetic} = \sum_{\alpha,\beta} \overline{\psi}_\alpha \not{D} \psi_\beta - \frac{1}{4} W^b_{\mu\nu} W^{\mu\nu\, b} - \frac{1}{4} B_{\mu\nu} B^{\mu\nu} \tag{1.18}$$

where $W^{\mu\nu}$ and $B^{\mu\nu}$ are the field strength tensors for the gauge bosons, $\not{D} = \gamma_\mu D^\mu$, and α and β represent the different fermion flavours. As there are three $SU(2)_L$ generators, there are three corresponding gauge bosons. Although I have precluded the index that runs over the three generators to avoid clutter, I will include it in the following definition so as to explicitly demonstrate the structure of the field strength tensors.

$$W^b_{\mu\nu} = \partial_\mu W^b_\nu - \partial_\nu W^b_\mu + g_2 \epsilon^{bcd} W^c_\mu W^d_\nu \tag{1.19}$$

where ϵ^{bcd} is the antisymmetric tensor for $SU(2)_L$.

With the dynamics of this sector defined, we can take a look a the Yukawa sector. The $\mathcal{L}_{Yukawa}$ terms link the Higgs field, ϕ, with the fermion of the model via dimensionless Yukawa couplings which control the strength of these interactions.

Before continuing it is import to quickly introduce the Higgs field. The Higgs is a complex scalar field It is in the fundamental representation of $SU(2)_L$ with hypercharge $1/2$. As we will see later, this field is critical for mass generation in the Standard Model.

The Yukawa sector Lagrangian is then given by

$$\mathcal{L}_{Yukawa} = -\sqrt{2}(\lambda_u^{ij}\overline{Q}_{L_i}\phi^c u_{R_j} + \lambda_d^{ij}\overline{Q}_{L_i}\phi d_{R_j} + \lambda_e^{ij}\overline{L_i}\phi e_{R_j}) + h.c. \tag{1.20}$$

where i, j represent the usual family indices, λ_{ij} are the Yukawa couplings and $h.c.$ stands for hermitian conjugate.

Finally we have the Higgs Lagrangian itself

$$\mathcal{L}_{Higgs} = (D_\mu\phi)^\dagger(D^\mu\phi) - \mu^2|\phi|^2 - \lambda|\phi|^4 \tag{1.21}$$

introduced by Peter Higgs, François Englert and Robert Brout [38, 39]. We shall see in the next section how the parameters μ and λ ultimately cause the phenomena of spontaneous symmetry breaking giving masses to the fermions in the model.

1.5.1 The Higgs Mechanism

In the early universe, the SM symmetry group, G_{SM} was intact and thus, as we have seen, the fermions were all massless. However, as the universe cooled, the electroweak symmetry group underwent spontaneous symmetry breaking to the QED symmetry group. That is to say $SU(2)_L \times U(1)_Y \to U(1)_Q$. This phenomena is driven by the particular properties of the Higgs field.

The Higgs field is an $SU(2)_L$ doublet and can be expressed as follows

$$\phi = \begin{pmatrix} \phi^+ \\ \phi^0 \end{pmatrix} = \begin{pmatrix} \phi_1 + i\phi_2 \\ \phi_3 + i\phi_4 \end{pmatrix} \tag{1.22}$$

where $\phi_{1,2,3,4}$ are the real degrees of freedom. The spontaneous symmetry breaking is driven by the evolution of the parameters, μ and λ in Equation 1.21. λ must always be positive in order to bound potential from below. However, as the universe evolves, μ^2 transitions from positive to negative. This has the effect of modifying the shape of the

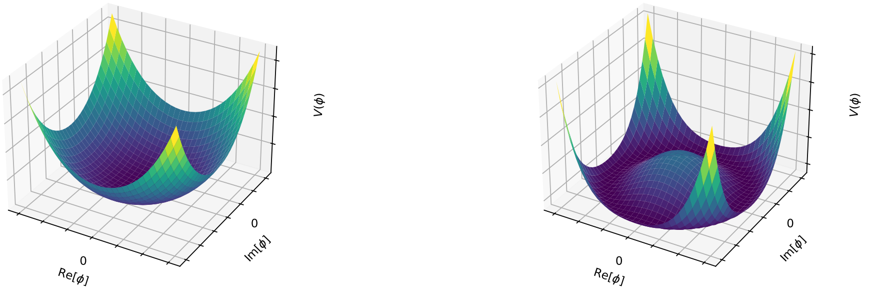

FIGURE 1.1: On the left is the symmetric Higgs potential where on the right is the broken Higgs potential where the Higgs potential is given by $V(\phi) = \mu^2|\phi|^2 + \lambda|\phi|^4$. The minimum of the potential moves from zero in field space to a non zero value V.

Higgs potential and thereby breaking the electroweak symmetry. Initially the vacuum expectation value $< 0|\phi|0 >= 0$. Transformations generated by the Standard Model symmetry group leave this state unchanged. But after symmetry breaking, the effect of applying such transformation generated by the original symmetry no longer leaves the vacuum state invariant; thus the symmetry is broken.

From Figure 1.1 above, we can see how the minimum of the potential has shifted to a non zero value, $< 0|\phi|0 >= v \neq 0$. We can now express the Higgs field as follows

$$\phi = \begin{pmatrix} \phi^+ \\ \phi^0 \end{pmatrix} = \begin{pmatrix} \phi_1 + i\phi_2 \\ v + h(x) + i\phi_4 \end{pmatrix} \tag{1.23}$$

where we have chosen the ϕ_3 degree of freedom to take on the vev. Here, v represents the vacuum expectation value and $h(x)$ is the physical degree of freedom represented by radial fluctations away from the vev. Due to the rotational symmetry, we are always free to do this. Now we are left with three non physical degrees of freedom. We can eliminate these by re-expressing the Higgs field as follows

$$\phi = e^{i\tau^i\phi_i} \begin{pmatrix} 0 \\ v + h(x) \end{pmatrix} \tag{1.24}$$

where τ^i are again the $SU(2)$ generators. This expression is perfectly equivalent to what we had before, with some redefinition of ϕ_i. Now we can use our $SU(2)$ gauge symmetry to gauge away the extra degrees of freedom and move to the unitary gauge

$$\phi \to e^{-i\tau^i\phi_i}\phi = \begin{pmatrix} 0 \\ v + h(x) \end{pmatrix} \tag{1.25}$$

so we now see we are left only with the massive mode, i.e. the physical degree of freedom $h(x)$, the Higgs field. In the following section we will see what has happened to these extra degrees of freedom.

The Higgs Boson was ultimately discovered at the large hadron collider by both the ATLAS and CMS collaborations in 2012 with a mass of $125GeV$ [10, 11]. This was a great achievement of particle physics, experimentally confirming a crucial mechanism of the Standard Model; a mechanism we shall se momentarily.

This whole phenomena is referred to as spontaneous symmetry breaking where we have broken the Electroweak symmetry group $SU(2)_L \times U(1)_Y \rightarrow U(1)_Q$ where we have broken three of the generators of the original symmetry group leaving one in tact to form the basis of the $U(1)_Q$ symmetry group. This symmetry can be seen manifestly by inspection of the right panel of Figure 1.1 where you can imagine rotating the diagram about the z-axis where our unbroken generator corresponds to such a rotation.

1.5.2 Massive Gauge Bosons

Although our trick to gauge away the degrees of freedom in the Higgs doublet was useful, degrees of freedom cannot simply vanish. So where are they? Goldstone theorem tells us that for each broken generator after symmetry breaking, there is a so called "Goldstone Boson". These become extra longitudinal degrees of freedom for the three gauge bosons corresponding to the broken generators. With these extra degrees of freedom, they become massive. Lets look at the kinetic term for the Higgs

$$\mathcal{L}_{Kinetic,\phi} = (D^\mu \phi)^\dagger (D_\mu \phi) \tag{1.26}$$

Sticking with the unitary gauge and precluding kinetic terms for the Higgs and gauge bosons we are left with mass terms for the gauge bosons.

$$\mathcal{L}_m = [(-ig_2 W_a^\mu \tau^a - i\frac{g_1}{2} B^\mu Y) \begin{pmatrix} 0 \\ v \end{pmatrix}]^\dagger [(-ig_2 W_a^\mu \tau^a - i\frac{g_1}{2} B^\mu Y) \begin{pmatrix} 0 \\ v \end{pmatrix}] \tag{1.27}$$

Since the theory will ultimately be $U(1)_Q$ invariant, we want to express the theory such that its invariance is manifest, i.e. in eigenstates of the operator Q. This can be done using the following redefinitions,

$$\begin{aligned} W_\mu^\pm &\equiv \frac{1}{\sqrt{2}}(W_\mu^1 \mp iW_\mu^2), \\ Z_\mu &\equiv \frac{1}{\sqrt{g_1^2+g_2^2}}(g_2 W_\mu^3 - g_1 B_\mu), \quad A_\mu \equiv \frac{1}{\sqrt{g_1^2+g_2^2}}(g_2 W_\mu^3 + g_1 B_\mu), \end{aligned} \tag{1.28}$$

$W_\mu^\pm$ and Z_μ are the massive gauge bosons of the broken weak symmetry group while A_μ is the photon associated to the remaining $U(1)_Q$ symmetry group. As the Higgs vev is invariant under the symmetry group Q acting on the vacuum will vanish and thus A_μ remains massless. We can parameterise the mismatch between the different bases with the Weinberg angle

$$\begin{pmatrix} Z_\mu \\ A_\mu \end{pmatrix} = \begin{pmatrix} cos(\theta_W) & -sin(\theta_W) \\ sin(\theta_W) & cos(\theta_W) \end{pmatrix} \begin{pmatrix} W_\mu^3 \\ B_\mu \end{pmatrix} \tag{1.29}$$

Applying the new definitions we are left with mass terms for the gauge bosons

$$\mathcal{L}_m = v^2[\frac{g_2^2}{4} W_\mu^+ W^{\mu,-} + \frac{g_1+g_2}{4}(Z_\mu)^2] \tag{1.30}$$

and so the masses are given by

$$\begin{aligned} M_W &= v g_2/2, \\ M_Z &= \frac{v}{2}\sqrt{g_1^2+g_2^2} \end{aligned} \tag{1.31}$$

1.5.3 Fermion Masses

Finally, let's return to Equation 1.20 and the Yukawa sector. By introducing the Higgs scalar doublet, the symmetry groups allow us numerous new terms that couple the doublet to the fermions. The strength of these couplings are determined by three by three matrices called Yukawa couplings and take the form, $\lambda_u Q_u \phi u_R$. After spontaneous symmetry breaking, the higgs field take on a vev. This then acts like a mass term for all the massive Standard Model fermions. Therefore we have a Lagrangian of the form

$$\mathcal{L}_{Yukawa} = m_u^{ij} \overline{u}_L^i u_R^j + m_d^{ij} \overline{d}_L^i d_R^j + m_e^{ij} \overline{e}_L^i e_R^j \tag{1.32}$$

where $m_f^{ij} = vY_f^{ij}$. Notice the lack of a neutrino mass term. This is due to the underlying symmetry groups of the Standard Model precluding such a Yukawa term without right handed neutrinos.

These mass matrices are under no impetus to be diagonal. Indeed, they are not. This is due to a misalignment between the flavour basis of pure interaction, and the physical mass basis. This ultimately manifests itself in flavour changing charged currents as we will see in the following.

1.5.4 The Cabibbo–Kobayashi–Maskawa Matrix

Having constructed these fermion mass matrices, we would like to extract the mass eigenstates for the fermions. However, there is no reason to expect that these matrices are diagonal. Therefore, we must move from the purely interacting flavour basis, to the physical mass basis. This is done by applying a unitary transformation V_f such that $f' = V_f f$ where f' is the flavour basis Weyl states, and f denotes the new mass basis. Therefore

$$V_f^\dagger m_f V_f = \begin{pmatrix} m_{f1} & 0 & 0 \\ 0 & m_{f2} & 0 \\ 0 & 0 & m_{f3} \end{pmatrix} \tag{1.33}$$

For the vast majority of the terms in the lagrangian, these unitary matrices cancel, as usually each term conjoins one such matrix to its inverse i.e. $m\overline{f}V_f^\dagger V_f f = m\overline{f}f$. However, this is not the case for the charged currents. $W^\pm$ couples up type quarks with down type quarks and the respective unitary matrices, V_u and V_d do not necessarily cancel. Indeed, they do not. It should be noted that as there are no right handed neutrinos in the SM, the misalignment between the mass basis and flavour basis does not occur for the Standard Model leptons.

To parameterise this misalignment issue, we introduce the so called Cabibbo–Kobayashi–Maskawa matrix (V_{CKM}) [40, 41]. This is a generalisation of the Cabibbo mixing angles to 6 quark fields. The Lagrangian contains terms of the following form

$$\mathcal{L} \supset \overline{u}_i V_{CKM}^{ij} \gamma^\mu W_\mu^+ V_{CKM} d_j \tag{1.34}$$

where $V_{CKM}^{ij} = V_u^{i\dagger} V_d^j$ and u_i, d_i are the left handed fields. The CKM matrix then parameterises the degree of flavour violation in the SM. In particular, the off-diagonal elements.

A priori, this matrix will have nine independent parameters. A common parameterisation is to assign it three angles and six phases. However, by redefining the quark fields, one can absorb the five of the six phases into the quark fields. This leaves us with four parameters; three angles and one phase. We can therefore construct the CKM matrix by considering three independent rotation matrices

$$\begin{aligned} V_{CKM} &= \begin{pmatrix} 1 & 0 & 0 \\ 0 & c_{23} & s_{23} \\ 0 & -s_{23} & c_{23} \end{pmatrix} \begin{pmatrix} c_{13} & 0 & s_{13}e^{-i\delta} \\ 0 & 1 & 0 \\ -s_{13}e^{i\delta} & 0 & c_{13} \end{pmatrix} \begin{pmatrix} c_{12} & s_{12} & 0 \\ -s_{12} & c_{12} & 0 \\ 0 & 0 & 1 \end{pmatrix} \\ &= \begin{pmatrix} c_{12}c_{13} & s_{12}s_{13} & s_{13}e^{i\delta} \\ -s_{12}c_{23} - c_{12}s_{23}s_{13}e^{i\delta} & c_{12}c_{23} - s_{12}s_{13}s_{23}e^{i\delta} & s_{23}c_{13} \\ -s_{12}s_{23} - c_{12}c_{23}s_{13}e^{i\delta} & c_{12}s_{23} - s_{12}s_{13}c_{23}e^{i\delta} & c_{23}c_{13} \end{pmatrix} \end{aligned} \tag{1.35}$$

where s_{ij} and c_{ij} are the sin and cos of θ_{ij}, the given angle, and δ is the a-for mentioned phase. This phase controls the degree of CP violation in these interactions as complex valued CKM element will imply the biased treatment of a particle vs its antiparticle. The values of these parameters are very well measured by a number of experiments generally involving the rare decays of mesons. Now we see that the presence of off-diagonal elements in this matrix gives couplings between different generations proportional to that element. For instance, $W^{+}\bar{c}d \propto s_{12}s_{13}$.

Further to this parameterisation, there is also a the Wolfenstein parameterisation. Although it is an approximation, this formulation is helpful for model building.

$$V_{CKM} = \begin{pmatrix} 1-\lambda^2/2 & \lambda & A\lambda^3 \\ -\lambda & 1-\lambda^2/2 & A\lambda^2 \\ A\lambda^3(1-\rho-i\eta) & -A\lambda^2 & 1 \end{pmatrix} + \mathcal{O}(\lambda^4) \tag{1.36}$$

where $\lambda \approx s_{12} \approx 0.22$.

As a final note I have already expressed that, in the Standard Model, there is no equivalent to this matrix for the leptons due to the lack of massive neutrinos. But experimentally we know that neutrino's do indeed have masses. Without jumping ahead of ourselves we should briefly pay lip service to the Pontecorvo–Maki–Nakagawa–Sakata matrix (PMNS) [42]. By introducing right handed neutrinos we can form a matrix very similar to the CKM matrix. This is introduced in more detail in Chapter 3.1.

1.6 Global Symmetries

In addition to the gauge symmetries of the SM, there are a number of global symmetries that can be useful. These correspond to conserved quantities of the SM, some of which are only conserved under certain interactions; others are conserved absolutely. These include the familiar energy and momentum which correspond to the Poincaré group. I will now give a brief outline of some of these symmetries.

1.6.1 Time Reversal (T)

As the name suggested, time reversal reverses the order of time. In a theory that respects this symmetry (unlike the SM) switching the final states with the initial states will leave physical quantities such as the scattering amplitude unchanged. By reversing the order of time particle states will have the same position but opposite spin and momentum. Using the co-ordinates $x = (x_0, \overrightarrow{x})$ time reversal has the effect

$$x \to x_T = (-x_0, \overrightarrow{x}) \tag{1.37}$$

The precise form of this operator can be complicated; particularly for the fermions. However, their properties under the transformation are given as follows.

$$\begin{aligned} T\psi(x_0, \overrightarrow{x})T^{-1} &= \gamma^1\gamma^3\psi(-x_0, \overrightarrow{x}) \\ T\phi(x_0, \overrightarrow{x})T^{-1} &= \phi(-x_0, \overrightarrow{x}) \end{aligned} \tag{1.38}$$

where γ^1 and γ^3 are Dirac matrices.

1.6.2 Charge Conjugation (C)

Charge conjugation turns a particle into its antiparticle. As such, all its charges under the SM are reversed. This is not a symmetry of the universe as, if it were, there would be no matter anti-matter asymmetry. Indeed, this symmetry is explicitly broken by the Weak interaction who does not act upon left handed anti-particles.

We define the charge conjugation transformation as follows.

$$\begin{aligned} &\psi(x) \to \eta^C_\psi \psi^C(x) = \eta^C_\psi \widehat{C}\gamma^0\psi^*(x) \\ &\phi \to \eta^C\phi = \eta^c\phi^* \end{aligned} \tag{1.39}$$

where ψ is a Dirac fermion and ϕ is a scalar and $\eta^C = \pm 1$. The form of $\widehat{C}$ is fixed by the requirement that the Dirac equation be satisfied under charge conjugation. Therefore,

$$\widehat{C} = \begin{pmatrix} i\sigma_2 & 0 \\ 0 & i\sigma_2 \end{pmatrix} \tag{1.40}$$

where σ_2 is the second Pauli matrix.

The Lagrangian will include QED interaction terms of the form, $\overline{\phi}\gamma^\mu\phi A_\mu$. It can be shown that the combination $\overline{\phi}\gamma^\mu\phi \to -\overline{\phi}\gamma^\mu\phi$ under charge conjugation. In order for the QED Lagrangian to respect this symmetry

$$\widehat{C}A_\mu\widehat{C}^{-1} = -A_\mu \tag{1.41}$$

such that the combination is invariant. Therefore, particles with $\eta^C = 1$ such as pions cannot decay into a final state with an odd number of photons.

1.6.3 Parity Transformation (P)

Parity is in some sense the partner to time reversal where instead of reversing the time coordinates, we reverse the spacial coordinates. Similarly, parity is not a symmetry of nature. As with charge conjugation, the weak interactions are the source of this violation. The weak bosons couple only to the left handed fields. A parity transformation will reverse the momentum and therefore the chirality. As before, we define the transformation such that

$$x \to x_P = (x_0, -\overrightarrow{x}) \tag{1.42}$$

This has the following properties for the fields.

$$\begin{aligned} P\psi(x_0, \overrightarrow{x})P^{-1} &= \eta_P\gamma^0\psi(t, -\overrightarrow{x}) \\ P\phi(x_0, \overrightarrow{x})P^{-1} &= \eta_P\phi(t, -\overrightarrow{x}) \end{aligned} \tag{1.43}$$

where η_P is the intrinsic parity of the field.

1.6.4 CP

Having seen that charge conjugation and parity transformations are violated by by weak interactions, it was thought that their composite transformation was a symmetry, known as CP-symmetry. After all, charge conjugating and then parity transforming a left handed fermion does, at least, get you a state that is again charged under $SU(2)_L$ (a right handed antifermion). However, CP violation was discovered in 1964 through some Kaon decays and since then, much more evidence has been gathered in a range of meson decays.

The Standard Model parameterises the amount of CP violation in the CKM matrix with δ phase. CP-violation therefore requires the existence of three generations of quarks as, with fewer quarks, complex phases can be reabsorbed into field definitions. CP-violation is crucial in generating baryogenesis, the imbalance in number densities between matter and antimatter, in the early universe by satisfying the Sakharov conditions.

1.6.5 CPT

Although CP is violated, the combination of charge conjugation, parity transformation, and time reversal is a symmetry of the SM. Indeed, CPT theorem states that CPT must be a symmetry of any theory that is Lorentz invariant [43]. Therefore, such a theory cannot distinguish between a left handed particle travelling forwards in time, and a right handed antiparticle travelling backwards in time. Ofcourse, if CPT is a symmetry of the SM but CP isn't, there must be some time reversal violation.

1.7 RGEs

Although the technical details of renormalisation group running are beyond the scope of this document, it is important to discuss them as they have great importance for any phenomenologically successful model. The quantum field theories of the SM produce problematic infinite quantities. These must be eradicated in order to make the theory physical. Renormalisation Group Equations, pioneered by Richard Feynman, Julian Schwinger and Shinichiro Tomonaga, who ultimately received a Nobel prize for their contributions in 1965, offer a systematic tool kit for removing these infinities and therefore, connecting the theory with experiment.

The process of renormalisation has the effect of causing parameters to vary with the renormalisation scale, μ. The RGEs inform us about the nature of this variation. The information is contained in the β-function who is calculated by considering a finite set of loop contributions to the given parameter. They must be valid only up to a scale called the cut-off scale Λ who parameterises our ignorance. That is to say, we understand that our theory is not the final answer, and therefore set a scale above which our theory can no longer be taken seriously as a description of physics. Indeed, in the case of SM, the plank scale $\Lambda_P \approx 10^{19} GeV$ is the scale at which gravitational effects come into play.

These RGE effects are critical to understanding a number of features of the Standard Model but in particular, the RGE flow causes the strong force to confine all quarks into bound states at low scales. But the dependance on μ varies the coupling strength, g_c, such that at high scales the quarks become asymptotically free.

Furthermore RGE effects are critical to understanding models beyond the Standard Model and connecting their phenomenology to experiment. One must pay careful attention to the scale at which a given parameter is calculated such that it matches experimental results.

1.8 Clues of Physics Beyond the Standard Model

Having given a brief introduction to the wonders of the SM, I will now draw your attention to its short comings. In particular, a number of experimental breakthroughs have been made demonstrating the weakness of the Standard Model. Here-in I give a set of such limitations that my work has pertained to. Therefore, this list is by no means exhaustive. Some critical problems that I do not specifically address here include matter-antimatter asymmetry [44, 45] and unification with gravity [46].

1.8.1 The Flavour Puzzle

In the SM, there is no natural requirement for 3 generations; I simply postulated the fermionic states, and wrote down the theory. Furthermore, there is mechanism to explain the structure of the Yukawa matrices and therefore, the origin of the particular mass hierarchy between the fermions.

Although experimentally it is clear there are (at least) three generations of fermions, from a theoretical point of view there is a mystery; why three in particular?

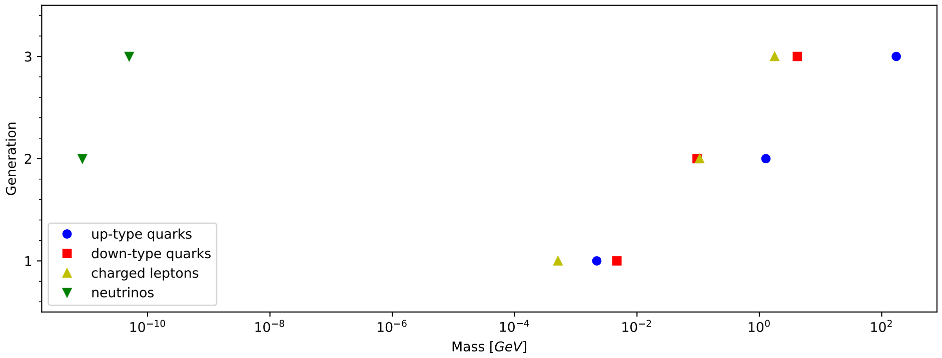

FIGURE 1.2: The masses of the Standard Model fermions are given in GeV against their generation. We have assumed normal ordering for the neutrinos masses and do not give a mass for the lightest neutrino.

Figure 1.2 is a vivid demonstration of the flavour puzzle. Not only are we confronted with the vast divergence in masses but also strange ordering within each generation.

The flavour problem can then be summarised with these four questions [47].:

- Why are there three fermionic generations?
- What causes the mass hierachy?
- What is the origin of quark and lepton mixing?
- What causes neutrino masses?

Although this last point pertains to a separate issue with the Standard Model, I include it here as neutrino masses are fundamentally linked to the mysteries of flavour hierarchy and perhaps the flavour problem more generally.

1.8.2 The Hierarchy Problem

Upon inspecting the scales of the Standard Model we find a surprise. That is that the plank scale M_P is so so much greater than the electroweak scale M_W. Although these two parameters appear to pertain to completely different physics there is a link. We know that new physics must exist at the plank scale, if not far before given the orders of magnitude between the current experimentally observable range and the gravity scales. If this is the case, the small value of the Higgs mass is a mystery.

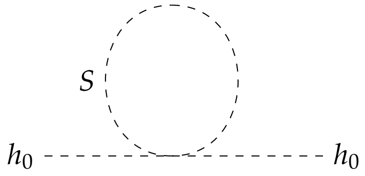

FIGURE 1.3: New scalar particle loop interactions with the Higgs boson lead to Higgs mass sensitivity to the mass of the new scalar.

The Higgs boson mass uniquely receives quantum corrections from new physics that couples to the Higgs. To see this consider a heavy complex scalar particle S that couples to the Higgs with a term in the Lagrangian like $-\lambda_S|h|^2|S|^2$. Then the diagram shown in Figure 1.3 will lead to Higgs mass corrections like

$$\Delta m_h^2 = \frac{\lambda_S}{16\pi^2}[\Lambda_{UV}^2 - 2m_S^2 \ln(\Lambda_{UV}/m_S) + ...] \tag{1.44}$$

where m_S is the scalar's mass [36]. As we can see, this particles will give quadratic contributions to the Higgs mass corresponding to the ultraviolet cut-off scale of new physics. Therefore the Higgs mass should be at the same scale as that of the new physics and of course, all the masses of the Standard Model are connected to the Higgs and would thus be perturbed to the new scales too.

Although this problem is unsolved in the standard model, there are many extensions to the standard model proposed to solve this problem. The one I have focussed on and will introduce in the coming chapters is supersymmetry.

1.8.3 Neutrino Masses

The experimental discovery of neutrino masses is perhaps the most viscerally striking evidence that the SM is incomplete. Originally believed to be massless, they were found to oscillate between mass eigenstates over time. This implies that the physical mass eigenstates are not the same as the flavour basis and therefore, there must exist a mass eigenbasis [48, 49].

As we have already seen, the SM has no right handed neutrinos. This means that the SM cannot accommodate Yukawa terms for the neutrinos and thus does not generate Dirac type mass terms for the neutrino. One could argue that there is a simple solution; in the same way that we wrote down fields for all the other fermions, let's include right handed fermions. However, the right handed neutrinos cannot be naturally accommodated into any representation of the SM symmetry group other than a singlet representation. Although this is a valid possibility, it seems somewhat ad-hoc and perhaps less aesthetically pleasing.

Unlike the CKM, where the mixing is small, the mixing between the neutrinos is quite large. Furthermore, the masses are exceptionally small, thus evading experimental observation for so long. Indeed, the experimentally measuring neutrino masses is a real challenge. Modern experiments can only measure the probabilities of a given state transitioning to another. Therefore, they are only sensitive to the mass differences squared between the states, $\Delta m_{ij}^2 = m_i^2 - m_j^2$. Current data is consistent with two possible orderings; normal ordering, in which the mostly electron mass state is lightest and the state with the most tauon is heaviest, and inverse ordering [48], where the highest tauon state is lightest, as can be seen in Figure 1.4.

With the advent of the seesaw mechanism, we have a theoretical framework to generate neutrino masses, with the inclusion of majorana mass terms, and explain the vast hierarchy between the other fermionic states and the neutrinos themselves. We will introduce this mechanism later.

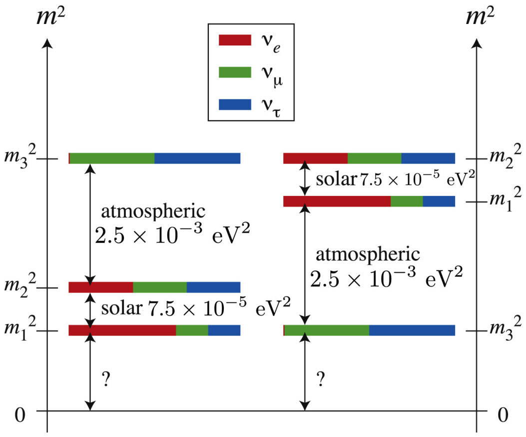

FIGURE 1.4: The mixing and masses of the neutrinos with thee experimentally determined mass gaps. On the left, normal ordering is shown, while on the right inverse ordering is shown. The colour in each bar represents the flavour composition of the given mass eigenstate. This figure was produced by [47].

1.8.4 Muon g-2

By taking the QED Dirac equation, one finds that, at tree level, the muon magnetic moment should be $g = 2$. However, loop corrections contribute to this parameter slightly perturbing it from this value. The anomalous magnetic moment of the muon (muon $g - 2$) refers to these quantum contributions to the magnetic moment of the muon.

As, classically we expect $g = 2$, it is useful to define the quantity $a_\mu = \frac{g-2}{2}$ to parameterise the anomalous part. Experimentally this quantity is very difficult to measure and indeed, theoretically very difficult to calculate. None-the-less, great efforts have been made to calculate the Standard Model contributions to a_μ using lattice techniques. Furthermore, in the year of writing, experimental break throughs have been made to measure this quantity. The Fermilab Muon collaboration announced measurements strengthening the significance of the two original Brookhaven National Laboratory results. The combined results now give a 4.2σ discrepancy between the Standard Model (SM) and the experimental value [14–34].

$$a_\mu^{EXP} - a_\mu^{SM} = (2.51 \pm 0.59) \times 10^{-9} \tag{1.45}$$

It seems that nature has picked out the muon for a special role and therefore this result could play a key role in unwinding the flavour problem. Although there is some controversy in the physics community about the validity of the Standard Model calculations that lead to this result, if they are truly robust, this is a clear sign of new physics as new loop diagrams are needed to explain this inconsistency.

1.8.5 Motivation for Dark Matter

The discovery of Dark Matter was perhaps some of the most humbling results in modern physics. Only 5% of the universe is comprised of baryonic matter. Roughly 25% is made up of a mysterious particle known as Dark Matter. It appears that there is a particle that does not interact with either itself or with light (hence "dark") that none-the-less has a huge influence on the universe through its gravitational effects. It should be noted that modified gravity models have also been proposed to explain the experimental observations. However, these are very difficult to get right and the scientific consensus at the time of writing is that these phenomena are mostly naturally explained by a new particle. Certainly, this is what I have focussed on.

After observing the rotation curves of many galaxies, it was found that the angular velocities of the outer bodies were higher than expected given the amount of visible matter in the galaxy [50, 51]. In order to explain the anomalously large angular velocities, there must be invisible sources of gravity distributed amongst the galactic bodies.

Observations of the famous Bullet Cluster gave further evidence of the existence of Dark Matter [52, 53]. In this famous example, two galaxy clusters have collided and passed through each other. However, the distribution of matter is not consistent with just baryonic matter interactions. Instead, a weakly interacting source of gravity must have played a role in the collision, silently passing though the cluster collision and warping the resultant matter distribution.

In order to satisfactorily explain these observations, a stable, neutral, weakly interacting and cold particle should exist. Although many models exist, a popular mechanism for Dark Matter production is that it is a relic particle, left over from some primordial processes, leaving the universe with an abundance of these particles. Indeed the relic abundance was measured by the Planck satellite [54] as

$$\Omega h^2 = 0.1200 \pm 0.0012 \tag{1.46}$$

where h^2 is the Planck constant. This measured is of course made with the assumption that a cold Dark Matter relic particle is the explanation of the experimental phenomena previously discussed.

1.8.6 Horizon Problem

Simply put, the Horizon Problem can be listed as follows; why is the universe, consistent with the cosmological principles, so homogenous and isotropic? On the face of it this may seem like a strange question. Why wouldn't it be?

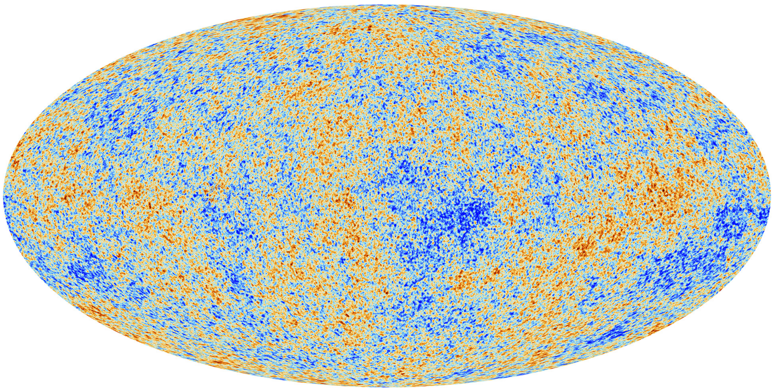

FIGURE 1.5: The anisotropies of the Cosmic microwave background (CMB) as observed by Planck. The CMB is a snapshot of the oldest light in our Universe, imprinted on the sky when the Universe was just ≈ 400000 years old. It shows tiny temperature fluctuations that correspond to regions of slightly different densities, representing the seeds of all future structure: the stars and galaxies of today. This figure was produced by ESA and the Planck Collaboration [49].

In some sense, the universe is bigger than it is old. That is to say that, patches of space are so far apart that they could not possibly have been in causal contact [55]. And yet the uniformity of the Cosmic Microwave Background (CMB) tells us that these regions must have been in contact with each other.

The CMB, shown in Figure 1.5, is an imprint of universe $400,000$ years after the Big Bang [55]. The colour variations correspond to tiny temperature fluctuations $\frac{\Delta T}{T} = \mathcal{O}(10^{-5})$. Therefore, the early universe is exceptionally homogenous and isotropic but showing some minor anisotropies and inhomogeneities that ultimately lead to all the amazing structure of the universe. One might postulate that there is only one allowed initial condition of the universe but this cannot explain the small temperature variations. Although it is possible to simply impose these in the initial conditions of the universe this is rather artificial. Instead, some mechanism must explain the common past of these seemingly disparate regions.

Chapter 2

Supersymmetry

In this Chapter I will give a very brief introduction into Supersymmetry (SUSY) only to the extent that is required for proper comprehension of the rest of this manuscript. Therefore, much of the technical detail is precluded. For more on this, many exceptional references are available.

I begin with a brief motivation for SUSY models followed by a brief introduction into the symmetry group itself. Having discussed how to build the symmetry, I will then discuss how to break it. Finally, I will give an introduction to the Minimal Supersymmetric Standard Model (MSSM); as the name suggests, the most minimal Supersymmetric extension of the Standard Model.

2.1 Solving the Hierarchy Problem

As we have already seen, m_h gets huge corrections from any new physics one tries to introduce. This is a severe impediment to the introduction of the new physics required to solve some of the problems previously elucidated. SUSY provides and elegant solution from this seemingly intractable problem.

We have already seen the contributions one would expect from a new scalar at high scales in Equation 1.44 diagrammatically represented in Figure 1.3.

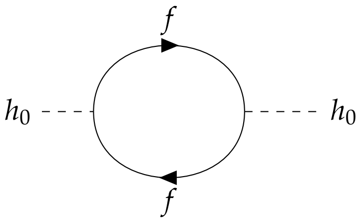

FIGURE 2.1: New fermion particle loop interactions with the Higgs boson lead to Higgs mass sensitivity to the mass of the new particle. Critically, these are of the opposite sign to similar scalar contributions.

Consider also the contributions from a high scale fermion in Figure 2.1. This contribution is given in [36] as

$$\Delta m_h^2 = -\frac{|\lambda_f|^2}{8\pi^2}\Lambda_{UV}^2 + ... \tag{2.1}$$

Critically, we notice the sign difference between the two terms. Now, without some miraculous cancellations, these terms will provide an intractable problem. However, by enforcing supersymmetry, a symmetry group (that I will more formally introduce later) that enforces that for every fermionic degree of freedom, there exists two scalar degrees of freedom, known as SUSY partners, with the same properties (except for intrinsic spin). Therefore, $\lambda_s = |\lambda_f|^2$ providing the miraculous cancellation we require. Indeed, these cancellations continue beyond one loop level.

With SUSY, any BSM model ones cares to introduce will not suffer form this sensitivity to new physics. This is the great motivation for supersymmetry as it liberates model builders to solve problems with out destroying the masses of the Standard Model.

2.2 Extending Spacetime Symmetries

Having discussed the practical motivation of the hierachy problem, there is a further motivation. Supersymmetry would complete the set of spacetime symmetries obeyed by physics i.e. it is a natural extension of the Poincaré group. In some sense, if supersymmnetry were to be realised, it would be very aesthetically pleasing.

SUSY is generated by the generator Q. We note that, in principle, one could add as many supersymmetries, Q_i for i up to N, as you please. However, I will focus on the case where $N = 1$. Q is an anticommuting spinor with spin $\frac{1}{2}$. It should transform a bosonic state to a fermionic one and vice versa. Then we have

$$\begin{aligned} Q|Boson> &= |Fermion> \\ Q|Fermion> &= |Boson> \end{aligned} \tag{2.2}$$

We also have $Q^\dagger$, the hermitian commutator of the generator. In order to recreate the Standard Model gauge group the algebra of such a commutator is limited. Therefore, we have the following algebra

$$\begin{aligned} \{Q, Q^\dagger\} &= P^\mu \\ \{Q, Q\} &= \{Q^\dagger, Q^\dagger\} = 0 \\ [P^\mu, Q] &= [P^\mu, Q^\dagger] = 0 \end{aligned} \tag{2.3}$$

where P^μ is the 4-momentum generator. As with the SM symmetries, it is useful to contain the fields inside representations (in this case the irreducible representation) in order to manifestly produce symmetric Lagrangians. We call these supermultiplets. They contain any given field, and its sypersymmetric partner. As P^μ commutes with Q, both members of these multiplets must have the same eigenvalues under this generator and therefore, must have the same mass. Furthermore, the Standard Model symmetry group generators also commute with Q and therefore each member of the multiplet must also have the same charges under the Standard Model.

As we have already seen, it is useful to work with Weyl fermions so as to see the difference between the left and right handed degrees of freedom. With this in mind we will construct two types of supermultiplet; the chiral multiplet and the gauge multiplet. The chiral will contain one Weyl fermionic degree of freedom and its superpartner, the sfermion, a complex scalar degree of freedom. Typically this will house the SM fermionic degrees of freedom. As left and right handed fermions are charged differently under the Standard Model, we have separate mutliplets for each chirality. The SM gauge bosons belong to the chiral multiplet along with one Weyl fermionic degree of freedom, known as a gaugino. As the gauge bosons transform in the adjoint representation, so must the gauginos, and as this represntation is self conjugate, left and right handed gauginos must have the same properties under the gauge group. In general, superpartners to Standard Model particles are expressed will a ˜ to distinguish them and multiplets are denoted with ˆ . Therefore, a chiral mutliplet would be expressed

$$\widehat{\Phi} = \begin{pmatrix} \phi \\ \widetilde{\phi} \end{pmatrix} \tag{2.4}$$

As the Higgs is a spin zero particle, it must reside in a chiral mutliplet with a fermionic superpartner. In fact, just one multiplet is not enough; two are required. There are multiple reasons for this which can be found in [36]. One such reason is that the partner to the Higgs boson, higgsino, will represent a new source of hypercharge. This is problematic as the sum of the fermionic hypercharges will no longer be zero (as it is in the SM). This in turn will cause a gauge anomaly, breaking the gauge symmetries of the theory at the loop level. To remedy this, we introduce a second Higgs doublet with opposite hypercharge. This are refferred to as H_u and H_d.

2.3 Soft SUSY breaking

Having read the previous, the eagle eyed among you may have asked yourself this; "if these particles have precisely the same properties including mass, where are they?". In order to explain this phenomenological conundrum, SUSY must be a broken symmetry. By breaking the symmetry, the SUSY particles will get extra mass terms such that they are hidden at the energy scales of modern particle accelerators.

Unlike the Standard Model, we cannot dynamically break the symmetry. To see why we should remind ourselves of the initial motivation for introducing the theory; the hierarchy problem. In order to cancel the problematic contributions to the higgs mass, we need $\lambda_s = |\lambda_f|^2$. If this relation is not preserved, the Higgs will again receive radiative corrections. Furthermore, some forms of breaking can lead to colour charge breaking.

Instead, we must softly break the theory. That is to say that the Lagrangian can be split into a part respecting the symmetry and some additional part that does not

$$\mathcal{L} = \mathcal{L}_{SUSY} + \mathcal{L}_{soft} \tag{2.5}$$

where $\mathcal{L}_{SUSY}$ respected SUSY and $\mathcal{L}_{soft}$ does not. Now, from the additional part of the $\mathcal{L}$ we do get some corrections to the Higgs mass of the form,

$$\Delta m_h^2 = m_{soft}^2 [\frac{\lambda}{16\pi^2} \ln(\Lambda_{UV})] \tag{2.6}$$

where m_{soft} is taken to be the largest mass scale associated with the SUSY breaking Lagrangian. We note that in the limit where $m_{soft} \to 0$ these corrections vanish. The existence of these contributions does place something of an upper limit on the masses of the superpartners as, if we still wish to solve the hierarchy problem, the contributions cannot be too large, and therefore, m_{soft} must also be small.

With this in mind, one might wonder, why the SUSY particles are so much larger than the their Standard Model conterparts. Or rather, is it natural that such a hierarchy exists. The answer is yes. But for electroweak symmetry breaking, none of the Standard Model particles would have masses. On the other hand, all the superpartners have the opposite feature; by the symmetries of the Standard Model they can have mass terms. The partners to the fermions as well as the Higgs are scalars and therefore can have simple mass terms of the form $m^2\phi$ (as per the Klein-Gordan Equation). As the gauge bosons must be in the adjoint representation, their partners must be in a real representation and therefore can accommodate mass terms without violating the Standard Model symmetries. Therefore, it is quite natural to expect that the superpartners have larger masses than their SM brothers.

There are many well established mechanisms to accommodate supersymmetry breaking but its precise nature is unknown. Indeed, the SUSY respecting part of the Lagrangian is very constrained by the symmetries. However the SUSY breaking part is still a mystery and in many ways, the subject of my research.

2.4 The MSSM

Having given a minimal introduction to supersymmetry itself, I will now give a minimal introduction to the minimal supersymmetric Standard Model (MSSM). That is, the minimal particle content to satisfy supersymmetry and phenomenological requirements.

2.4.1 The Lagrangian and Particle Content

As seen in equation 2.7, the Lagrangian is split into a SUSY respecting part, and a non-SUSY respecting part. I will treat each of them individually but first, we must consider our particle content. To generate the MSSM from the usual SM, one can simply promote the SM particles to super multiplets. However, as I have already argued here, there must be a further Higgs doublet. I will now give a brief list of the set of physical fields involved in the MSSM.

Table 2.1 summarises the particle content of the chiral multiplets as well as their properties under the SM group. To preserve readability, family and colour indices

	Content		Representation		
Multiplet	Spin-0	Spin-1/2	$SU(3)_c$	$SU(2)_L$	$U(1)_Y$
$\widehat{Q}$	$(\widetilde{u}_L, \widetilde{d}_L)$	(u_L, d_L)	3	2	1/3
$\widehat{U}$	$\widetilde{u}_R$	u_R	3	1	4/3
$\widehat{D}$	$\widetilde{d}_R$	d_L	3	1	-2/3
$\widehat{L}$	$(\widetilde{e}_L, \widetilde{\nu}_L)$	(e_L, ν_L)	1	2	-1
$\widehat{E}$	$\widetilde{e}_R$	e_R	1	1	-2
$\widehat{H}_u$	(H_u^+, H_u^0)	$(\widetilde{H}_u^+, \widetilde{H}_u^0)$	1	2	1
$\widehat{H}_d$	(H_d^0, H_d^-)	$(\widetilde{H}_d^0, \widetilde{H}_d^-)$	1	2	-1

TABLE 2.1: The particle content belonging to the chiral multiplets of the MSSM are displayed. Sparticles are spin-0 complex scalars and SM fermions are two component Weyl spinnors.

	Content		Representation		
Multiplet	Spin-1	Spin-1/2	$SU(3)_c$	$SU(2)_L$	$U(1)_Y$
$\widehat{G}$	g	$\widetilde{g}$	8	1	0
$\widehat{W}$	W^i	$\widetilde{W}^i$	1	3	0
$\widehat{B}$	B	$\widetilde{B}$	1	1	0

TABLE 2.2: The particle content belonging to the gauge multiplets of the MSSM are displayed. Gauginos are spin-1/2 Weyl fermions and the SM bosons are spin-1 vector bosons.

have been suppressed. The additional Higgs doublets are given with subscripts u and d denoting the opposite hypercharge. This difference ultimately has the affect of modifying the electric charges of the relevant states. Therefore, the electric charges have been given in the superscript. Table 2.2 gives the vector multiplets of the MSSM along with its symmetry group properties where lorentz and colour indices have again been suppressed.

These two tables summarise the entire MSSM. Now we turn our attention to the Lagrangian itself.

2.4.1.1 The Superpotential

The superpotential of the SUSY theory contains all the information about the non-kinetic terms of the SUSY Lagrangian. This includes the Higgs couplings to matter fields and the Higgs doublet interactions. By conducting the appropriate integrals over Grassman variables, one can generate the afore mentioned parts of the Lagrangian using a very succinct notation. The superpotential for the MSSM is given in [36] as

$$W_{MSSM} = \overline{u}Y_uQH_u - \overline{d}Y_dQH_d - \overline{e}Y_eLH_d + \mu H_uH_d \tag{2.7}$$

where the fields u, d, Q, e, L, H_u and H_d correspond to the superfields associated with the previously given supermultiplets. Y_u, Y_d, and Y_e are the 3 by 3 dimensionless yukawa couplings matrices. Again, I have suppressed the gauge and family indices. Finally there is the "μ-term". This acts as a mass term or the higgs doublet. This term is unique in that self coupling terms such as $H_uH_u^*$ that are used in the regular Standard Model to give mass to the Higgs are forbidden as the superpotential must be holomorphic. This is yet another justification for the two Higgs doublet requirement. This can also be seen in the other terms of the superpotential who also rely on the two multiplets in order to generate the relevant mass terms.

In addition to the parts of the Lagrangian that can be contained by the superpotential, there is also a the supersymmetry respecting interaction terms. The explicit content and make up of such terms is beyond the scope of this manuscript and has therefore been excluded.

2.4.1.2 Soft Breaking Part of the MSSM

As mentioned previously, the exact nature of SUSY breaking is unknown. Therefore, the MSSM has the most general form in order to accommodate the different potential mechanisms. Thus, we have

$$\begin{aligned}\mathcal{L}_{soft} = &-\frac{1}{2}(M_3\widetilde{g}\widetilde{g} + M_2\widetilde{W}\widetilde{W} + M_1\widetilde{B}\widetilde{B} + c.c)- \\ &-(\overline{\widetilde{u}}A^u\widetilde{Q}H_u + \overline{\widetilde{d}}A^d\widetilde{Q}H_d + \overline{\widetilde{e}}A^e\widetilde{L}H_d + c.c)- \\ &-\widetilde{Q}^\dagger m_Q^2\widetilde{Q} - \widetilde{L}^\dagger m_L^2\widetilde{L} - \widetilde{u}^\dagger m_u^2\widetilde{u} - \widetilde{d}^\dagger m_d^2\widetilde{d} - \widetilde{e}^\dagger m_e^2\widetilde{e}- \\ &-m_{H_u}^2 H_u^* H_u - m_{H_d}^2 H_d^* H_d - (B_0\mu H_u H_d + c.c.)\end{aligned} \tag{2.8}$$

where I have suppressed the gauge group indices on the gauginos. $M_{1,2,3}$ are the soft terms associated with the bino, wino, and gluinos respectively. On the following line, we have the trilinear terms that link the chiral superpartners with the Higgs doublets. They are parameterised by the trilinear matrices, A^i, which are 3 by 3 in flavour space. On the subsequent line, we have soft masses for the squarks and sleptons. Again these are 3 by 3 in flavour space. Finally, we have the soft mass contributions to the two Higgs doublet, H_u and H_d, and the bilinear coupling parameterised by B_0.

As previously argued, the scale of the new physics cannot be too high in order to avoid problematic contributions to the Higgs mass. Therefore, all these terms should be approximately proportional to the general scale m_{soft}.

Unlike in $\mathcal{L}_{SUSY}$, where all parameters have already been seen in the Standard Model, an array of new masses, phases, and mixing angles have been introduced; 105 to be precise. It seems that SUSY breaking introduces a huge set of new parameters. Indeed, leaving these parameters leads to large flavour and CP violating effects that are very suppressed by experiment.

In later chapters we will examine two different approaches to understanding this parameterisation: supergravity in which this huge array of variables are reduced to a small list of governing parameters that determine the entire breaking scenario; and the use of Flavour and GUT symmetries to suppress the terms by construction.

2.4.2 Electroweak Symmetry Breaking

Having added the extra Higgs doublet, electroweak symmetry breaking must be modified in order to accommodate this new state. Ofcourse, our theory must still generate mass terms through the usual Yukawa mechanism and give the 125GeV scalar mass state in accordance with LHC observations [10, 11].

As in traditional electroweak breaking, we minimise the scalar potential such that the vacuum expectation value of the Higgs fields is non-zero. However, In SUSY we have many scalars making the potential quite complicated. Fortunately, a number of tricks are available in order to avoid working with such a bloated animal. Firstly, the squarks and sleptons have large positive masses and therefore will not get vevs and therefore can be excluded from our considerations. Furthermore, as in SM EWSB we can use the SU(2) symmetry to rotate the fields such that one of the directions in field space, in this case H_u^+, is zero at the minimum. As electromagnetism is unbroken we also know that $H_d^+ = 0$. With these tricks in mind, we are left with a scalar potential

$$\begin{aligned} V =&(|\mu|^2 + m_{H_u}^2)|H_u^0|^2 + (|\mu|^2 + m_{H_d}^2)|H_d^0|^2 - (B\mu H_u^0 H_d^0 + c.c) \\ &+ \frac{1}{8}(g_1^2 + g_2^2)(|H_u^0|^2 - |H_d^0|^2)^2 \end{aligned} \tag{2.9}$$

The B term is the only one that depends on the phase of H_u^0 and H_d^0. We can therefore absorb the phase by redefining one or other of the neutral Higgses. Furthermore, we can use the $U(1)_Y$ symmetry to rephase H_u^0 and H_d^0 such that their vacua are real and positive. This implies that CP will be unbroken by the vev.

We now require V to be bounded from below. This amounts to the condition

$$2b < 2|\mu|^2 + m_{H_u}^2 + m_{H_d}^2 \tag{2.10}$$

Then for the vev to appear near $H_u^0 = H_d^0 = 0$ we require

$$b^2 > (|\mu|^2 + m_{H_u}^2)(|\mu|^2 + m_{H_d}^2) \tag{2.11}$$

Now that we have stated the conditions required for the scalar potential to take the requisite shape in phase space, we turn to phenomenology to inform the specific breaking pattern. Setting $< H_u^0 >, < H_d^0 >= v_u, v_d$ we know that the vevs will be related to the Z mass by

$$v_u^2 + v_d^2 = \frac{2m_Z^2}{g_1^2 + g_2^2} \tag{2.12}$$

The exact values of the vevs is not determined. Instead, we write the ratio of the vevs as $\tan(\beta) \equiv v_u/v_d$. Now in order for the scalar potential to satisfy these conditions, we can extract a set of equations required by electroweak symmetry breaking. Therefore, by requiring that $\partial V/\partial H_u = \partial V/\partial H_d = 0$ we have

$$\begin{aligned} \sin(2\beta) &= \frac{2\mu B}{m_{H_u}^2 + m_{H_d}^2 + 2|\mu|^2} \\ m_Z^2 &= \frac{|m_{H_u}^2 - m_{H_d}^2|}{\sqrt{1 - \sin^2(2\beta)}} - (m_{H_u}^2 + m_{H_d}^2 + 2|\mu|^2) \end{aligned} \tag{2.13}$$

Here we have established the parameter requirements for electroweak symmetry breaking. These equations will be useful for some of the analysis in later chapters.

As with SM EWSB, this process generates goldstone bosons. As we have two $SU(2)_L$ higgs doublets, we have eight degrees of freedom. Three of these are "eaten" by the massive electroweak bosons, leaving five massive Higgs states; two oppositely electrically charged mass eigenstates, two electrically neutral CP-even mass states, and one neutral CP-odd state. The lightest of the two CP-even, neutral states is the SM Higgs. At tree level, the mass is bounded from above such that it would have been discovered long ago. Fortunately, as we have already seen, loop order contributions come into play to remove this impossibility.

2.4.3 R-Parity

In principle, terms are allowed by supersymmetry that lead to baryon and lepton number violation. These are rather troubling as they lead to decays that are not realised in nature; such as a short life time proton decay. To prevent these terms appearing in our Lagrangian, we introduce a new symmetry to forbid them while maintaining the benefits of supersymmetry we have already established. This symmetry is known as R-parity defined as

$$P_R = (-1)^{3(B-L)+2s} \tag{2.14}$$

where s is the spin of the given state. Here we can see that, for any given mutliplet, the R-parity eigenstates will be different between the constituents due to the difference in spin. We say that the Standard Model particles, including the Higgs, have even R parity, $P_R = +1$, and that the sparticles have odd R-parity, $P_R = -1$.

Taking R-parity to be an exact symmetry we produce three consequences of note, beyond the motivation we opened this section with.

- The lightest supersymmetric partner particle (odd R-parity) will be stable. In the case where this particle is uncharged under the Standard Model gauge group (as with the neutral gauginos, or neutralinos) this particle will interact with the Standard Model only weakly, and therefore makes for an excellent dark matter candidate (to be discussed later) [56].

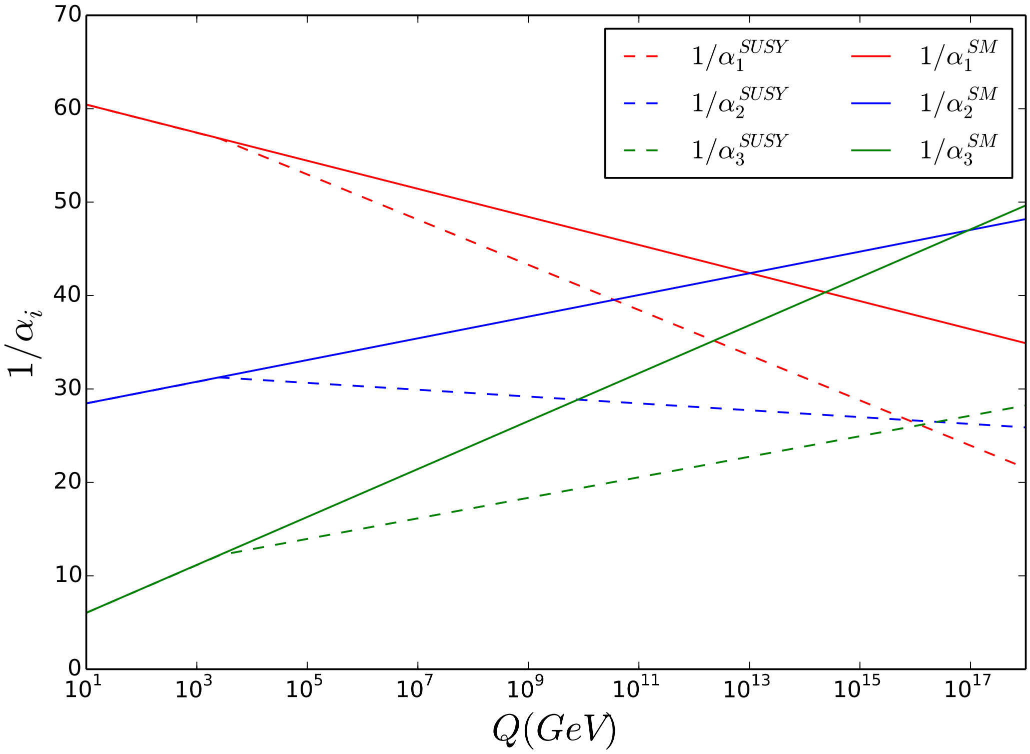

FIGURE 2.2: Gauge coupling running in the SM and MSSM. The SUSY scale is assumed to be around 3TeV. The Standard Model gauge couplings are marked with solid lines while the SUSY couplings are marked with dashed lines. The SUSY parameters almost perfectly converge at approximately $10^{16} GeV$.

- Sparticles must decay into a final state with an odd number of sparticles.
- Colliders will produce SUSY partners in even numbers.

In order for the theory to be viable, it is very useful (from a model building perspective) that the symmetry be imposed. From the theoretical standpoint, this seems rather artificial, but experimentally it is very well motivated given the long life of the proton, the lack of collider evidence, and the search for dark matter.

2.4.4 Gauge Coupling Unification

As we have already seen, the couplings run as we change the energy scale. Ofcourse, the introduction of all these new particles will mean new loop diagrams and therefore a different RG flow. Interestingly, if we assume the SUSY scale to be $\mathcal{O}(1TeV)$, we find remarkable convergence in the gauge coupling parameters, demonstrated in Figure 2.2, where α_i are functions of the $U(1)$, $SU(2)$, and $SU(3)$ gauge group couplings derived from the renormalisation process.

This could be a very exciting clue as to the origin of the SM gauge group, perhaps hinting at the exciting possibility that the symmetry groups are born of one parent symmetry, who is broken in much the same way we have broken electroweak symmetry, to give the familiar SM group. Indeed, this is yet another motivation for SUSY as it helps build models that unify the Standard Model forces. One example of such a model is studied in detail in subsequent chapters.

2.4.5 Flavour Mixing

By construction, the flavour structure of the SUSY respecting part of the Lagrangian reflects that of the SM. Therefore, it contains no new sources of flavour violation beyond that of the CKM. This is referred to as minimal flavour violation (MFV) [57]. However, MFV is broken by the soft masses whose parameters can lead to large flavour violating effects. This is known as non-minimal flavour violation (NMFV).

Before continuing, it is useful to define the super CKM basis (SCKM). In this basis, we simply apply the same rotations required to diagonalise the SM masses to the SUSY flavour basis. This is useful for phenomenological reasons as it allows us to work in the mass basis of the SM fermions and thereby study the flavour violating effects and other observables associated with the model. We have defined the rotations necessary to diagonalise the Yukawa matrices in Equation 1.33. Therefore we have

$$\widetilde{u}'_L = V_{u_L}\widetilde{u}_L,\ \widetilde{u}'_R = V_{u_R}\widetilde{u}_R,\ \widetilde{d}'_L = V_{d_L}\widetilde{d}_L,\ \widetilde{d}'_R = V_{d_R}\widetilde{d}_R \tag{2.15}$$

where the primed basis is the mass basis and the unprimed is the SCKM basis.

With the aside in mind, we now return to the issue of flavour violation. In order to eradicate the strong flavour violating effects, it is often simply assumed that soft matrices are diagonal in the SCKM basis. Therefore, as the SUSY respecting part of the Lagrangian has diagonal masses in this basis, the sfermion masses will be completely diagonal.

Although this strategy is effective in quickly and simply producing viable results, it is strangely ad hoc. That is, there is no systematic mechanism for setting the off-diagonal elements to zero and no theoretical motivation. It is motivated only by experiment.

Instead of this approach, one can choose to embrace the NMFV paradigm. This may seem suicidal from a phenomenological perspective. However, some recent work [58, 59] has studied this framework with some interesting results. The motivation for such study is as follows. Firstly, this is the most general framework and doesn't involve the artificial suppression of model parameters. Additionally, these off-diagonal elements lead to large squark and slepton mixing. This can hide the sparticles, who otherwise would be accessible at current energy scales, from collider experiments as new decay channels open up. Finally, these non-minimal flavour violating models are very well motivated by GUTs with additional flavour symmetry. In such scenarios, SUSY not only converges the gauge couplings, but the flavour symmetry can serve to constrain the off-diagonal elements.

Having discussed this NMFV paradigm, I will now give a very brief and very non-exhaustive introduction to some of the flavour violating constraints. In particular, I will focus on those that have influenced my research. However, many more are currently under research. Particularly constraining results come from meson mixing. In particular, NMFV SUSY gives new diagrams to B and K meson mixing. These diagrams are proportional to the off-diagonal elements of the soft matrices. Furthermore, there are new channels that contribute to meson decays. Although these channels are open in an MFV context, they will be suppressed by the CKM. In Figure 2.3 I give an example SUSY contribution to $b \to s\ \gamma$.

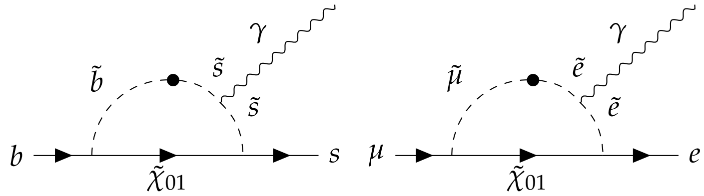

FIGURE 2.3: Example SUSY loop contribution to $b \to s\ \gamma$ on the left and $\mu \to e\ \gamma$ on the right. The dots mark NMFV transitions between different generations of sparticles controlled by off diagonal elements in soft breaking matrices.

Another source of flavour violating constraints come from leptonic decays. A particularly stringent experimental limit comes from $\mu \to e\ \gamma$ in the context of NMFV. From Figure 2.3, we see that this diagram is proportional to the flavour mixing transition between $\tilde{\mu}$ and $\tilde{e}$.

2.4.6 Muon g-2 in SUSY

In Chapter 1.8.4 I introduced the experimental breakthrough associated with the magnetic moment of the muon. Although there is some controversy about this result, such strong experimental significance is hard to ignore.

Supersymmetry provides an excellent framework for explaining such anomalous flavour behaviour due to loop corrections. An example Feynman diagram that contributes to Δa_μ is given in Figure 2.4.

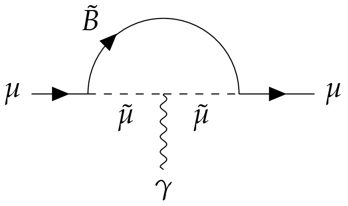

FIGURE 2.4: Example SUSY loop contribution to muon g-2. The left handed muon emits a bino and smuon and ultimately transitions into a right handed muon.

With the right blend of parameters [60] it has been shown that the MSSM can successfully accommodate the g-2 prediction. In particular, given sufficiently light electroweak gauginos, smuons, and smuon neutrinos, these contributions will be non vanishing.

Chapter 3

Beyond The Standard Model and Cosmology

Although we have spent quite some time focusing on SUSY, there is, of course, much more to beyond the Standard Model (BSM) physics than that. In particular, taking just the most minimal version of supersymmetry leaves a whole host of problems left unsolved (for a non comprehensive list see Chapter 1.8). Having said this, it is often true, and is the case in my research, that BSM models are often very well complimented by SUSY. Therefore, I have given it special consideration in this manuscript.

I will now explore a small set of further BSM considerations. I have structured the chapter in such a way that each subsection addresses one or more of the issues raised in Chapter 1.8.

3.1 Massive Neutrinos

Perhaps the most obvious short coming of the SM is the lack of neutrino masses. The charged leptons get mass through the usual Yukawa mechanism coupling left and right handed fields together. This ofcourse cannot apply to the neutrinos who, in the Standard Model, do not have a right handed field.

By simply including such right handed neutrinos we can introduce a mechanism for generating neutrino masses [47]. However, in order to predict experimentally viable masses, we would require Yukawa coupling $\mathcal{O}(10^{-11})$. This raises an issue of naturalness as there is a huge difference in magnitude between the next smallest Yukawa coupling; that of the electron, $\mathcal{O}(10^{-6})$.

As the right handed neutrinos are neutral under the Standard Model gauge group, charge conjugation has no effect on them. Therefore, they are there own antiparticle and thus called Majorana fermions. As they are singlets there are no symmetry constraints controlling their mass scale and they can have their own mass term, called a Majorana mass term, which is a free parameter of the theory and can therefore be arbitrarily large.

By utilising both the Yukawa structure for generating mass and the Majorana structure, we can construct the Seesaw Mechanism [61–65]. This provides a natural framework for setting the effective mass of the left handed neutrinos to be very light. There are number of Seesaw mechanisms, the first of which was introduced in [66]. I will focus on the Type-I seesaw for its relevance to later chapters. However, for a review of further means of generating neutrinos masses I refer you to [67].

3.1.1 The Seesaw Mechanism

With the introduction fo the right handed majorana neutrinos, we have the following possible neutrino mass terms

$$\mathcal{L} = -\frac{1}{2} M_R \overline{\nu_R^c} \nu_R - m_D \overline{\nu_L} \nu_R + H.c. \tag{3.1}$$

where M_R is the right handed Majorana mass matrix and m_D is the neutrino mass matrix arising from the Yulawa coupling $-H_u Y^\nu \overline{L} \nu_R$. Therefore, $m_D = v_u Y^\nu$ where is the (up-type) Higgs vev.

Combing our terms we can construct the seesaw mass matrix for the neutrino part of the Lagrangian

$$\begin{pmatrix} \overline{\nu_L} & \overline{\nu_R^c} \end{pmatrix} \begin{pmatrix} 0 & m_D \\ (m_D)^T & M_R \end{pmatrix} \begin{pmatrix} \nu_L^c \\ \nu_R \end{pmatrix} \tag{3.2}$$

As M_R is unrestricted we can make the assumption that $M_R >> m_D$. Under this assumption, this matrix can then be diagonalised to give the effective Majorana Masses as follows

$$m^\nu = -m_D M_R^{-1} (m_D)^T \tag{3.3}$$

Now we can see why this is called the Seesaw mechanism. The effective light neutrinos are suppressed by the large M_R scale where as the right handed neutrinos are at the M_R scale. This provides a natural explanation as to the smallness of the SM handed neutrinos.

This model is phenomenologically viable with only two right handed neutrinos [48]. In such a model, one of the light neutrinos will be massless. However, perhaps a more natural model includes three right handed neutrinos and gives mass to all three light neutrinos.

3.1.2 The PMNS

As with the quark sector, where the up and down Yukawa matrices don't perfectly align, the introduction of neutrino masses means a similar diagonalisation process must be applied and, yet again, there are two transformations required to diagonalise the basis. Y_e is diagonalised by U_{e_L} and m_ν is diagonalised by U_ν. Therefore, we can define the so-called PMNS matrix [68, 69] as follows.

$$U_{PMNS} = U_{e_L}^\dagger U_\nu \tag{3.4}$$

This matrix describes the mixing in the lepton sector. Indeed, in the mass basis of the charged leptons the lagrangian will have terms of the form

$$\mathcal{L} \supset \frac{-g}{2} \begin{pmatrix} \bar{e} & \bar{\mu} & \bar{\tau} \end{pmatrix} U_{PMNS} \gamma^\mu W_\mu \begin{pmatrix} \nu_1 \\ \nu_2 \\ \nu_3 \end{pmatrix} + H.c. \tag{3.5}$$

then the PMNS matrix describes the mixing between the flavour states that form the mass states. Therefore,

$$\begin{pmatrix} \nu_e \\ \nu_\mu \\ \nu_\tau \end{pmatrix} = \begin{pmatrix} U_{e1} & U_{e2} & U_{e3} \\ U_{\mu 1} & U_{\mu 2} & U_{\mu 3} \\ U_{\tau 1} & U_{\tau 2} & U_{\tau 3} \end{pmatrix} \begin{pmatrix} \nu_1 \\ \nu_2 \\ \nu_3 \end{pmatrix} \tag{3.6}$$

where $\nu_{1,2,3}$ are the mass basis states and $\nu_{\epsilon,\mu,\tau}$ are the flavour states.

There are only 3 angles and 3 phases on the PMNS as 3 phases associated with the charged leptons can be absorbed. However, in the case of the Majorana fermions two phases cannot be eliminated. The PMNS can be parameterised in many different ways. I give here the parameterisation consistent with the PDG. It has the same structure as the CKM matrix but with the additional Majorana phases.

$$U_{PMNS} = \begin{pmatrix} c_{12}c_{13} & s_{12}s_{13} & s_{13}e^{i\delta} \\ -s_{12}c_{23} - c_{12}s_{23}s_{13}e^{i\delta} & c_{12}c_{23} - s_{12}s_{13}s_{23}e^{i\delta} & s_{23}c_{13} \\ -s_{12}s_{23} - c_{12}c_{23}s_{13}e^{i\delta} & c_{12}s_{23} - s_{12}s_{13}c_{23}e^{i\delta} & c_{23}c_{13} \end{pmatrix} \begin{pmatrix} e^{i\eta_1} & 0 & 0 \\ e0 & ^{i\eta_2} & 0 \\ 0 & 0 & 1 \end{pmatrix} \quad (3.7)$$

where η_1 and η_2 are the Majorana phases.

3.1.3 Neutrinoless Double-beta Decay

With the introduction of right handed neutrinos and new terms in the lagrangian, new decay channels are exposed. In particular, if the right handed neutrinos are majorana in nature, the process of neutrinoless double beta decay would be allowed [70]. In such a process, two neutrons could decay into two protons and two electrons without emitting a neutrino.

The decay rate of this process is of the form

$$\Gamma^{0\nu}_{\beta\beta} \propto |m_{ee}| \quad (3.8)$$

where

$$|m_{ee}| = |\sum_i (U^{ei}_{PMNS})^2 m_i| \quad (3.9)$$

Although experimentally this process has never been observed, there are mutliple experiments underway to try to observe this process as it would shed light on, the nature of the neutrinos and the structure of the PMNS matrix.

3.2 GUTs

We have seen in Chapter 2 that augmenting the Standard Model with supersymmetry leads to a high degree of convergence. Additionally, the inclusion of right handed neutrino states could modify the RGEs for even better convergence. Grand Unified Theories (GUTs) take this curiosity and formalise it.

Physics has a history of unification: electronic forces and magnetic forces were unified into electromagnetism; space and time were unified into spacetime. Given this history of success, it seems well motivated to try to unify further. In particular, GUTs aim to unify the three Standard Model forces into one by embedding the symmetry groups of the Standard Model, G_{SM}, into a larger group, G_{GUT}.

$$SU(3)_C \times SU(2)_L \times U(1)_Y \subset G_{GUT} \tag{3.10}$$

This parent force would exist only at very high scales, M_{GUT}, below which the symmetry is broken.

Although formalising the convergence of the coupling is rather aesthetically appealing and continuing in a tradition of unification seems like a good strategy for progressing physics, is this enough to motivate the study of such models? There is another critical motivation. The electric charges of the proton and the electron, somewhat miraculously, cancel each other perfectly. Given that the leptons and the quarks do not belong to the same representation of the $U(1)_Y$ group, and the charges under $U(1)_Y$ are not inherently quantised this seems like a strange coincidence. However, if the entire Standard Model originates from the same representation of some parent symmetry group the common ancestry of these seemingly disparate particles would explain their connection.

In order to contain the symmetries of the Standard Model we need a symmetry group of at least rank 4 (number of commuting generators in a lie algebra). It turns out that the simplest such representation, introduced with the Georgi-Glashow model, is $SU(5)$ [71]. Another popular choice is $SO(10)$ which has the additional benefit of encompassing right handed neutrinos in a non-trivial representation [72]. I will now give a brief introduction to $SU(5)$ GUTs for their pertinence to later chapters.

3.2.1 SU(5)

$SU(5)$ is the most minimal GUT symmetry. It is composed of five by five unitary matrices with transformations given by $U = e^{i/2\alpha^a\lambda^a}$ where λ^a are the generators. As always, the gauge boson must be in the adjoint representation. This has $N^2 - 1 = 24$ degrees of freedom. We can embed the Standard Model bosons into this representation as follow

$$\frac{1}{\sqrt{2}}\begin{pmatrix} & & & X_1 & Y_1 \\ & [G \cdot \frac{2B}{\sqrt{30}}]^{\beta}_{\alpha} & & X_2 & Y_2 \\ & & & X_3 & Y_3 \\ \overline{X_1} & \overline{X_2} & \overline{X_3} & \frac{W^3}{\sqrt{2}} + \frac{3B}{\sqrt{30}} & W^+ \\ \overline{Y_1} & \overline{Y_2} & \overline{Y_3} & W^- & \frac{-W^3}{\sqrt{2}} + \frac{3B}{\sqrt{30}} \end{pmatrix} \tag{3.11}$$

where, α and β run from 1 to 3, G are the gluons, W are the $SU(2)$ bosons, and B is the U(1) boson. Additionally, we have two new characters, X and Y. These twelve new gauge bosons are a charged under both $SU(2)$ and $SU(3)$. They can therefore be considered a type of leptoquarks. Their presence in the model could serve to induce baryon and lepton number violation which would thereby predict some proton decay. This can be solved if they have masses of $\mathcal{O}(M_{GUT})$ thereby suppressing operators associated with them and giving the nucleons a longer life time.

Then all of the Standard Model fermions can be packed into the antifundamental representation $\overline{\mathbf{5}}$ and the **10** representation.

$$\overline{\mathbf{5}} = \begin{pmatrix} d^{c1} \\ d^{c2} \\ d^{c3} \\ e^{-} \\ -\nu_e \end{pmatrix}, \mathbf{10} = \begin{pmatrix} 0 & u^{c3} & -u^{c2} & u^1 & d^1 \\ -u^{c3} & 0 & u^{c1} & u^2 & d^2 \\ u^{c2} & -u^{c1} & 0 & u^3 & d^3 \\ -u^1 & -u^2 & -u^3 & 0 & e^c \\ -d^1 & -d^2 & -d^3 & -e^c & 0 \end{pmatrix} \tag{3.12}$$

where the superscript, c, denotes the charge conjugation, 1,2, and 3 superscripts refer to colour, and all the fermionic states are Weyl fermions. With these representations we can now understand the charge quantisation in the SM. If we take two of the SU(5) generators as the hypercharge and third component isospin generators, then applying them to either of our fermionic representations should be traceless (as can be verified). But if both the components of Q are traceless, then Q itself must be traceless when applied to the representations. This, ofcourse, fixes the charges of the electric charges of the fermions and thus naturally explains the quantised nature of the electric charge and hypercharge.

Finally, we must consider the Higgs boson. When breaking SU(5) directly to the SM, we place it in the **5** representation. If SUSY is incorporated in the model then there are two Higgs doublets, H_u and H_d, that go in the **5** and the $\overline{\mathbf{5}}$ respectively.

Now, having constructed our SU(5) GUT symmetry containing all of the Standard Model (and SUSY) content, we must break it. As with electroweak symmetry breaking, this is done with the introduction of a new Higgs. In particular, we take the adjoint **24** representation. This then acquires a vev such that $< H >= v_5 diag(2, 2, 2 - 3, -3)$ thus leaving SU(2) and SU(3) unbroken. This will break the $SU(5)$ to the Standard Model leaving us with some extra physical Higgs-like degrees of freedom; H_8 who is an octet under $SU(3)$, H_3 who is a triplet under $SU(2)$, and H_0 who is a singlet under both. All of these states have masses, after symmetry breaking, proportional to v_5 and are therefore very massive and hidden from modern experiment. Additionally there are the twelve goldstone bosons, H_X and H_Y, who are eaten by the X and Y gauge bosons. Again these masses will be proportional to v_5 solving the nucleon decay problem.

It should be noted that there is an important short coming of $SU(5)$. If our model is to explain neutrino oscillations, then it must include right handed neutrinos. But there is

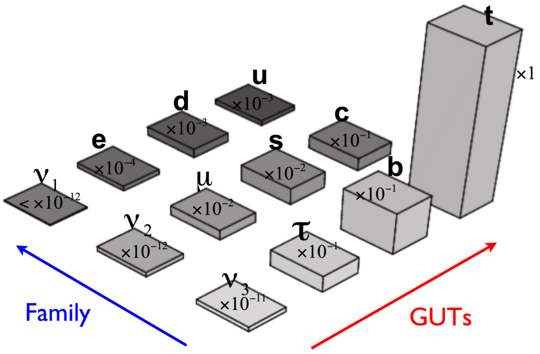

FIGURE 3.1: The different effects of the symmetries are represented with the family symmetry acting intra particle type and the GUT symmetry acting extra particle type. The re scaled column heights represent the hierarchy of masses. This figure was produced by [47].

no natural way to accommodate these right handed fields. Instead, one must resort to the same approach used in the neutrino mass augmented SM and simply include an additional singlet, in this case a singlet of $SU(5)$, and store the neutrinos there.

3.2.2 Flavoured GUTs

The application of GUT symmetries can be very effective in explaining the differing relations the quark and lepton types have with the fundamental forces. But these GUT symmetries do not act within each generation and yet we see greatly diverging masses and mixing patterns. Indeed, there is no explanation for the existence of the three generations within each family. Having learned the utility of applying symmetries to problems in particle physics, applying a similar strategy here is well motivated. Figure 3.1 shows the utility of a family symmetry in explaining the hierarchy within each type of fermion.

By applying spontaneous symmetry breaking, it has been shown that one can satisfy the low scale flavour mixing and CP-violation [59]. In order to achieve this, the introduction of yet another set of Higgs-like scalar fields must be introduced (known as flavons) in order to break the symmetry. Again, this occurs at some scale well above electroweak symmetry breaking.

These models are of particular interest for neutrino mass as leptonic mixing angles are relatively large and discrete symmetry groups which tend to give large values in the resultant mixing matrices [47]. In addition, family symmetry can influence flavour structure in the soft SUSY Lagrangian thus controlling the non-minimal flavour violating tendencies of SUSY.

There are many choices of GUT symmetries and many choices of family symmetries. However, I have focussed $SU(5) \times S_4$ where S_4 is the rigid rotation group of a cube.

3.3 Cosmic Inflation

As already discussed in Chapter 1, the CMB shows remarkable homogeneity and isotropy. However, small temperature fluctuations are present. Some dynamical means of explaining both of these phenomena is required. Inflation provides such a mechanism.

Inflation, first introduced by Guth [73] is a process in the early universe in which the universe underwent super rapid expansion some time in the first $10^{-36}s$. This process explains the seeming connection between disparate parts of the CMB. What ever the initial conditions of causally disconnected regions of the CMB, they appear to be in equilibrium as the process of inflation smooths out the inhomogeneities and anisotropies. Furthermore, small quantum fluctuations during the inflationary period explain the small temperature fluctuations in CMB.

Indeed, inflation does not just address the horizon problem; many problems are solved by the introduction of this theory. In particular, the "flatness problem" and the "magnetic monopoles problem". According to modern experiment, the universe is very close to have the critical density such that the curvature of the universe is flat. This condition requires fine tuning in the early universe as any curvature is exaggerated over the evolution of the universe. Inflation dynamically solves this problem as small curvature in the early universe is inflated away. The magnetic monopole problem questions the lack of experimental evidence for magnetic monopoles. If such particles do exist but their mass is above the inflation scale, their relic density would be washed out during inflation.

In QFT an inflation mechanism is provided by slow-roll inflation [74]. We introduce a new scalar field, the inflaton. If this inflaton has significantly more potential energy than kinetic, it will roll down its potential towards the minimum driving the inflationary expansion. As this is a quantum field theory, it undergoes some quantum fluctuations in its field value. Therefore, different regions reach the end of their inflation at different times. This variation causes the temperature fluctuations in the CMB.

Starobinsky inflation is a special case for inflation [89, 97] which is particularly well suited to current observed phenomena. It is a modification of general relativity that gives rise to a characteristic exponential potential leading to predictions consistent with the latest measurements. Additionally, it can arise from the special case of "no-scale" supergravity as we shall see later.

Chapter 4

Muon g-2, Dark Matter and the Higgs mass in No-Scale Supergravity

4.1 Introduction

As discussed in Chapter 1.8.4, recent experimental results have propelled the anomalous muon magnetic moment $g-2$ back into the centre stage of particle physics. Following the original Brookhaven National Laboratory measurements [75], the Fermilab Muon collaboration has recently affirmed these findings [76], with the combined results now showing a 4.2σ discrepancy with the Standard Model (SM) calculation as shown in Equation 1.45. In Chapter 2.4.6 we see the mechanisms SUSY can supply, due to loops of light sleptons, $\widetilde{\mu}$, $\widetilde{\nu}_{\mu}$, and light electroweak gauginos [77]. These days such an explanation must be made consistent with the measurement of the Higgs boson mass, and LHC constraints on superpartners, both of which point towards rather heavy squarks and gluinos, and such studies have been recently performed in various SUSY models [78–85].

Here we shall be interested in the phenomenology of no-scale supergravity (SUGRA) (for a review and early references see [86]), focussing on the interplay between the muon $g-2$, dark matter and the Higgs boson mass in particular. No-scale SUGRA is an ultraviolet (UV) completion of the minimal supersymmetric standard model (MSSM), in which the scalar masses are zero at the high scale and are subsequently generated by renormalisation group (RG) running via couplings to the non-zero gaugino masses. Apart from its minimality, it is motivated by string theory and more recently by the fact that the hidden sector contains the ingredients for inflation. However, its phenomenological viability is not straightforward given the fact that the

Higgs mass requires large stop masses, while the muon g-2 requires light slepton masses, and dark matter is known to be non-trivial to achieve in the general MSSM, and all this must be achieved in no-scale SUGRA starting from zero scalar masses at the high scale. This provides the main motivation for a detailed phenomenological study of no-scale SUGRA. In our approach, there will be an important constraint coming from inflation, to which we now turn.

In Chapter 3.3, we discuss why inflation is one of the key concepts in modern cosmology [87–92]. Not only does it explain the vast size of the universe (the flatness problem), it also explains the extreme homogeneity and isotropy of the universe on cosmological scales (the horizon problem), as well as diluting cosmological relics (the monopole problem). Furthermore, the slow rolling inflaton provides small quantI fluctuations which eventually lead to large scale structure [93, 94]. However, despite its successes, the precise mechanism that causes inflation is unknown. Clues to the theory behind inflation, may come from current observational data [95], where the spectral index is measured to be $n_s \approx 0.96 \pm 0.007$ with a low tensor-to-scalar ratio $r < 0.08$. These data exclude the simplest chaotic models with inflaton potentials ϕ^2 or ϕ^4 [96]. Amongst the successful models which are consistent with these data is Starobinsky inflation [89, 97], which may have a link to SUSY models [98–100]. Since inflation is sensitive to ultraviolet (UV) scales, one must also consider SUGRA when dealing with inflation, and the no-scale SUGRA models [101] in particular are well suited for maintaining the flatness of the inflaton potential (thereby solving the η problem), although other approaches have also been discussed [102–106]. Also the Lyth bound [107] on the tensor-to-scalar ratio also suggests a scale of inflation below the Planck scale, leading to testable at collider tests of inflation.

Ellis, Nanopoulos, Olive (ENO) have shown that no-scale SUGRA can behave like the successful Starobinsky inflationary model [108–110]. However, in the ENO approach, a term with constant modular weight is used to break SUSY, and there is no connection between inflation and SUSY breaking. Subsequently one of us has considered the above ENO model, but with a linear Polonyi term added to the superpotential [111]. The purpose of adding this term was to provide an explicit mechanism for breaking SUSY in order to provide a link between inflation and SUSY breaking. Indeed they showed that inflation requires a strict upper bound for the gravitino mass $m_{3/2} < 10^3$ TeV [111]. It was subsequently shown [112] how the model in [111] may be generalised to include the fields in the visible sector of the minimal supersymmetric standard model (MSSM). In such a framework the soft-SUSY breaking parameters depend on the modular weights in the superpotential and lead to new phenomenological possibilities for supersymmetry (SUSY) breaking, based on generalisations of no-scale SUSY breaking and pure gravity mediated SUSY breaking. The strict upper limit on the gravitino mass $m_{3/2} < 10^3$ TeV provides an important phenomenological constraint, bearing in mind that the gaugino masses are typically suppressed by a loop factor $1/(16\pi^2)$ in gravity mediated scenarios.

In this chapter, motivated by the desire to relate inflation to collider physics, including dark matter and the muon $g-2$ measurement, I study the phenomenology of the no-scale SUGRA inflation model in [112]. Although related phenomenological studies of similar works have been undertaken [108–110] a full phenomenological study of the model in [112], which is subject to the upper bound on the gravitino mass, has not yet been undertaken. Here I shall present a phenomenological study of two of the simplest cases suggested in [112]: the first case consisting of no-scale SUGRA with zero soft scalar masses $m_0 = 0$ and zero trilinear soft parameter $A_0 = 0$, where the only source of SUSY breaking in the visible sector is via the gaugino masses M_i; the second case switches on a small soft trilinear mass $A_0 \neq 0$, while maintaining zero soft scalar masses $m_0 = 0$. In both cases I assume that the gaugino masses M_i (which are not fixed by the Kahler potential and are therefore independent of the details of inflation) to arise from a hybrid of anomaly mediated and universal sources [113]. Such gaugino masses M_i at the high scale will act as the seed of all soft squark and slepton masses at low energy via renormalisation group (RG) running effects. Given the small number of input parameters, I shall use a Monte Carlo scan over parameter space, using the `SPheno` [114, 115] package linked to `FeynHiggs` [116], `MicrOmegas` [117–121] and `CheckMATE` [122, 123]. For each case above, I display viable regions of parameter space displaying the results in terms of a Likelihood function, including the requirement of successful dark matter relic density. I then consider a set of representative benchmark points from viable regions of parameter space, and discuss the prospects for discovering the resulting SUSY spectrum at colliders. In particular I show that the no-scale SUGRA case allows for dark matter while satisfying all phenomenological constraints, including the correct Higgs mass and dark matter relic density, leading to the prospect that SUSY may be discovered at the LHC or FCC.

The layout of this Chapter is as follows. In section 4.2, I summarise the basic parameters of the no-scale SUGRA models that I analyse. In section 4.1 I describe our calculational approach and numerical tools and algorithms that I employ in the analysis. In section 4.4 I present our results for non-scale SUGRA case I, with all soft parameters equal to zero at the high scale apart from the gaugino masses. In section 4.5 I present our results for non-scale SUGRA case II, where I allow in addition (small) non-zero values of A_0, which relaxes the collider constraints somewhat. Section 4.6 concludes the chapter.

4.2 The no-scale SUGRA model parameters

In the considered model [112], the soft supersymmetry breaking parameters are well approximated by

$$\begin{aligned} m_0 &= 0 \\ \frac{A_0}{m_{\frac{3}{2}}} &= -6\alpha, \\ \frac{B_0}{m_{\frac{3}{2}}} &= 2(1-\beta) \end{aligned} \tag{4.1}$$

where α, β are undetermined modular weights in the Kähler potential.

Turning to the gauginos, the model does not constrain the gaugino mass parameters. We therefore examine a general breaking scenario where the gaugino mass parameters are partly derived from "anomaly mediated" susy breaking giving three mass parameters. Each one is determined partly by loop corrections given below [124] and partly by a universal term parameterised below by the dimensionless coefficient k [125],

$$\begin{aligned} M_1 &= (\frac{33}{5}\frac{g_1^2}{16\pi^2} + k)m_{\frac{3}{2}}, \\ M_2 &= (\frac{g_2^2}{16\pi^2} + k)m_{\frac{3}{2}}, \\ M_3 &= (-3\frac{g_3^2}{16\pi^2} + k)m_{\frac{3}{2}} \end{aligned} \tag{4.2}$$

Note that the sign of k plays an important phenomenological role in determining the gaugino mass spectrum. For small and positive k the electroweak gaugino masses $M_{1,2}$ are enhanced while the magnitude of the gluino mass M_3 is reduced due to the partial cancellation against the negative anomaly mediated contribution. This yields a spectrum with a relatively light gluino and heavy winos and binos. On the other hand, for small and negative k, the electroweak gaugino masses $M_{1,2}$ are reduced due to a partial cancellation, while the magnitude of the gluino mass M_3 is increased. This yields a spectrum with relatively light winos and binos which is more suited to explaining the muon $g-2$.

The supersymmetric theory produced by this model gives a very small set of high scale parameters; the scalar mass scale, m_0, the bilinear coupling, B_0, and the trilinear coupling, A_0. In turn the two unified coupling parameters are determined by the gravitino scale $m_{\frac{3}{2}}$ and our choice of the modular weights α and β. Furthermore, m_0 is determined by our choice of Kähler potential [112]. In addition we choose a suitable value of $tan(\beta)$ and μ to minimise the broken higgs potential and thus satisfy the higgs potential minimisation conditions given in [126]. We are therefore left with just five input parameters; α, β, $tan(\beta)$, $m_{\frac{3}{2}}$ and μ, that must be selected in order to fully characterise the high scale model and its spontaneously broken characteristics. We shall mainly focus on the simplest cases $\alpha = 0$ and $\beta = 1$ which lead to zero soft parameters $A_0 = 0$ and $B_0 = 0$ at the high scale.

4.3 Method

The aim of this project is to Monte-Carlo scan over the small set of input parameters for the two cases given above. We do not use the Metropolis-Hastings algorithm [127]. This is simply because the input parameter set is so small that a random scan on the IRIDIS computer cluster will be suffice to cover the parameter landscape. We then calculate various experimental outcomes including collider phenomenology, mass spectrum, and dark matter relic density to calculate a likelihood associated with each parameter point. The likelihood is defined as follows,

$$L = e^{\sum_i - \frac{(x_i - x_i')^2}{2\sigma_i^2}} \tag{4.3}$$

where x_i is the calculated value of the constraint, x_i' is the experimentally observed value, and σ_i is the standard deviation. We assume a Gaussian distribution around the mean value for our experimental constraints. The relevant constraints can be found in Table 4.3.

By calculating the likelihood we will gain a greater understanding of the model and its physical viability by finding the regions that maximise the likelihood. We aim to place some lower bound on the gravitino mass scale thus constraining the model from above, via inflation constraints, and below, via Collider phenomenology. Furthermore, we hope to find some best fit parameter points that might satisfy the latest $g - 2$ results.

Instead of performing a global fit and maximising the likelihood, we split the parameter space up into smaller regions. This helps optimise parameter searches with limited computer resources and helps with our intuition as different cases are explicitly separated. The different regions we selected are summarised in Table 4.2 and Table 4.1. We start with the simplest possible case, and subsequently increase its complexity. Therefore, initially we fix $\alpha = 0$ such that $A_0 = 0$. As B_0 is determined by electroweak symmetry breaking, we leave β and $tan(\beta)$ as free parameters. `SPheno` also requires the $sign(\mu)$ to be prescribed. Although previous analyses suggest positive μ is more in-keeping with modern results, we chose to allow for both signs.

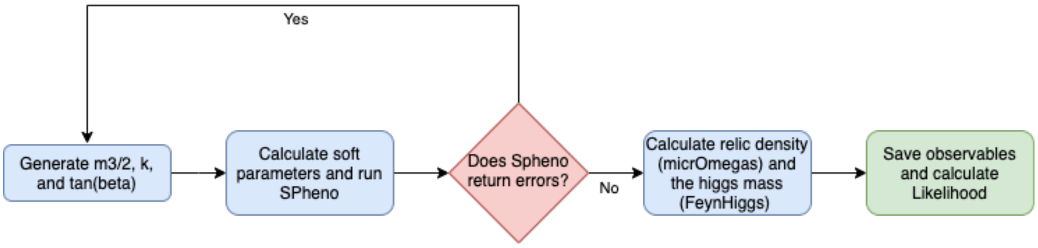

FIGURE 4.1: Shows the algorithm flow used for this analyses.

Generally speaking, the algorithm works as shown in Fig. 4.1. Four primary open source softwares were used to perform the calculations. For calculating the SUSY spectrum, $g-2$, and a number of other observables, we chose to use a modified version of `SPheno` that printed the value of B_0. In brief this program solves RG equations to two loop numerically and outputs various phenomenological constraints. Initially it calculates the gauge and Yukawa couplings at tree level at m_Z. This are used as input for the one loop formulas and run to the high scale where the gauge couplings unify. Here, user defined soft breaking boundary conditions are applied. These are then run down to the electroweak breaking scale where important electroweak parameters are calculated as well as the sparticle pole masses. Radiative corrections are then applied to the gauge and Yukawa couplings which are subsequently run up to the high scale where this whole process is repeated iteratively until convergence occurs (the sparticle masses receive corrections smaller than a user defined δ on the previous iteration. For all of our calculations, we use the default value of δ.

Although for the most part our use of this software was very standard, we encountered a technical problem regarding the $\overline{DR}$ renormalisation scheme. Large values of the gluino mass induce large logs in the top mass that must be re-summed. This has an effect for the Higgs mass whose value can be vastly inflated. To solve this we use `FeynHiggs` to renormalise the top mass on-shell and calculate the Higgs mass. The `FeynHiggs` output is then passed to `MicrOmegas` in order to calculate the relic density. The SUSY contribution to the anomalous magnetic moment as well as some other BSM observables are calculated by `SPheno`.

For post data collection analysis we simulate collider effects using `CheckMATE` [123]. This software combines a number of subsidiary packages to simulate the events in a collider and exclude any given model to a 95% confidence level. We chose to use $13 TeV$ and $8 TeV$ pp collision data with the ATLAS detector in a variety of signal regions. Many different regions played a critical role in assessing the validity of our benchmark points depending on the particular make-up of the input parameters.

Instead of predefining β, as we did with α, and therefore fixing a value of B_0, we decided to leave $tan(\beta)$ as a free parameter to be scanned over. This affords us some flexibility in understanding the parameter space. Furthermore, with the results in hand it is simple to solve Equation 4.1 and find the relevant β parameter.

case	m_0	A_0	B_0	Section
I	0	0	$2(1-\beta)m_{\frac{3}{2}}$	4.4
II	0	$-6\alpha m_{\frac{3}{2}}$	$2(1-\beta)m_{\frac{3}{2}}$	4.5

TABLE 4.1: Table showing the two cases considered in this work. Gaugino mass terms (with a value for k), $tan(\beta)$, the sign of μ, and the gravitino mass scale are also generated depending on the model being considered.

In order to fully explore the parameter space, a number of scans (and accordant parameter limits) were initialised. Each scan is assigned to a subsection and summarised in Table 4.2. Note that each scan is performed twice; once for $\mu > 0$ and again for $\mu < 0$.

	$m_{\frac{3}{2}}$ (TeV)	α	$tan(\beta)$	k	Subsection
Scan 1	$[1, 1000]$	0	$[1.5, 30]$	$[0, 0.1]$	4.4.1
Scan 2	$[1, 400]$	0	$[1.5, 50]$	$[-0.01, -0.04]$	4.4.2
Scan 3	$[1, 1000]$	$[-0.166, 0.166]$	$[1.5, 50]$	$[0, 0.1]$	4.5.1
Scan 4	$[1, 200]$	$[-0.005, 0.005]$	$[1.5, 50]$	$[-0.014, -0.035]$	4.5.2

TABLE 4.2: Show the parameters for the 4 primary scans conducted in this study. Links to the subsections in which each scan is presented are also included. In general, parameter ranges were chosen by trial an error so as to be representative of the parameter scape without losing excessive efficiency.

In each section, a different set of constraints is pertinent to the objectives of this work and therefore we modify our likelihood calculation to reflect this. Table 4.3 shows a summary of the experimental values and deviations of the constraints used.

Observable	Constraint	Ref
m_h	$(125 \pm 2) GeV$	[10, 11]
Ωh^2	(0.12 ± 0.012)	[117–121]
Δa_μ	$(2.51 \pm 0.59) \times 10^{-9}$	[75]

TABLE 4.3: Table gives the constraints used to calculate the likelihood. In all sections the Higgs mass is considered. However, Ωh^2 only contributes to the likelihood in Sections 4.4.1 and 4.5.1 and Δa_μ contributes to the likelihood in Sections 4.4.2 and 4.5.2.

4.4 No-scale SUGRA with $A_0 = 0$ (Case I)

Completely no-scale SUGRA with $A_0 = 0$ represents a fascinating scheme for this model. Previously thought to be ruled out, such scale-less supersymmetry has seen something of a resurrection motivated by inflationary model building [128]. As shown in Table 4.1, $\alpha = 0$, and therefore $A_0 = 0$, precludes trilinear terms from the model. Although we allow variance in β in order to understand the parameter space, we shall see a strong preference for $\beta \approx 1$ implying $B_0 = 0$ bilinear coupling. With $m_0 = 0$, the scalar masses are all zero at the high scale. However, the gauginos get mass terms by Equation 4.3 and generate non-zero low energy scalar masses via the RGEs. Remarkably, it turns out that such a scheme is phenomenologically viable, as we shall see.

We begin by analysing the results of Scan 1 in Table 4.2, which assumes positive universal gaugino masses k, and allows the gravitino mass $m_{\frac{3}{2}}$ to vary up to its upper bound from inflation of 1000 TeV.

4.4.1 Positive k (Scan 1)

As discussed earlier, positive universal gaugino mass parameter k will tend to yield a spectrum with a relatively light gluino and relatively heavy winos and binos, so we do not expect this choice to explain the muon $g-2$, so we will focus mainly on the Higgs mass and dark matter in this case. Figure 4.2 shows a scatter plot between the two most influential scan variables, k and $m_{\frac{3}{2}}$. It should be noted that, although $tan(\beta)$ is a scan parameter, its influence on the overall likelihood is limited.

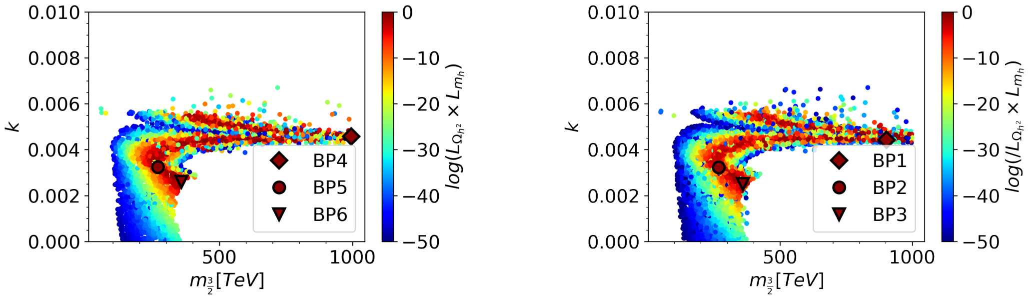

(A) $\mu < 0$, case I

(B) $\mu > 0$, case I

FIGURE 4.2: Shows k against $m_{\frac{3}{2}}$ for case I, $\alpha = 0$ data from a Monte-Carlo scan with parameter ranges ranges $tan(\beta) \in [1.5, 30], k \in [0, 0.1]$, and $m_{\frac{3}{2}} \in [10^3 GeV, 10^6 GeV]$. Colour denotes likelihood, with hotter colours corresponding with high likelihoods. The likelihood is dominated by the relic density calculation. The range of k is naturally restricted to $k \lesssim 0.006$ due to $|\mu|^2 < 0$. Two bands of high likelihood points; one from above, one from below, converge at $(1000 TeV, 0.0044)$ in $(m_{\frac{3}{2}}, k)$ space. The 6 benchmarks that are presented in Table 4.4 are also marked. The central colour of the benchmark denotes its likelihood.

As points that failed to produce correct electroweak symmetry breaking or a suitable dark matter candidate have been excluded from these plots, a fascinating structure of allowed, disallowed, and high likelihood points emerges. Firstly, for values of $k \gtrsim 0.006$ electroweak symmetry breaking cannot be satisfied (except for some anomalous points that, due to numeric instability, achieve electroweak symmetry breaking). Secondly, for values of $k \lesssim 0.004$ with $m_{\frac{3}{2}} \gtrsim 400$ TeV the LSP becomes charged. This can be seen in Figure 4.3 where cold-coloured points tend to 0 mass difference and therefore, a charged LSP for large $m_{\frac{3}{2}}$ values.

In addition to the structure of excluded points, a band of hot-coloured points in the $(m_{3/2}, k)$ plane from (350 TeV, 0.0025) up to (250 TeV, 0.004) and across to (1000 TeV, 0.0045) where the relic density likelihood is maximised. An additional strip of high likelihood points begins at (400 TeV, 0.0055) and tracks down to (1000 TeV, 0.0046). We speculate that there could be some symmetry about $k \approx 0.0045$ that is broken above $k \approx 0.006$ due to electroweak symmetry breaking.

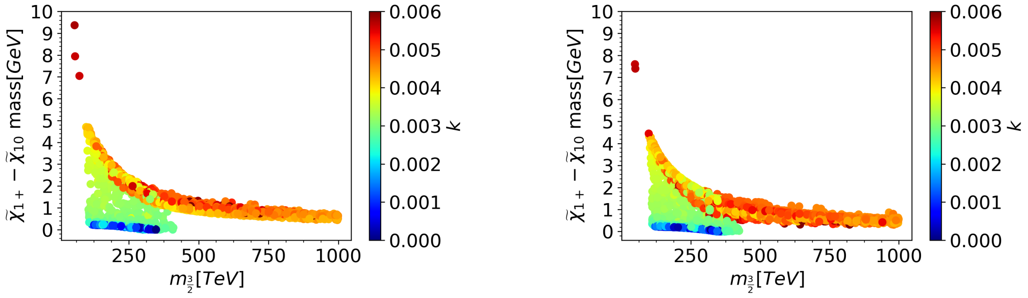

(A) $\mu < 0$, case I,

(B) $\mu > 0$, case I,

FIGURE 4.3: Shows the mass difference between the LSP and the nLSP for case I, $\alpha = 0$. The colour denotes the value of k. Small values of k lead to a negative difference between the $\widetilde{\chi}_{1+}$ and $\widetilde{\chi}_{10}$ at $400 TeV$ implying a charged LSP.

The masses of the first two neutralinos [36] are given by

$$\begin{aligned} m_{\widetilde{\chi}_{10}} &= M_1 - \frac{m_W^2(M_1 + \mu sin(2\beta))}{\mu^2 - M_1^2} + ... \\ m_{\widetilde{\chi}_{20}} &= M_2 - \frac{m_W^2(M_2 + \mu sin(2\beta))}{\mu^2 - M_2^2} + ... \end{aligned} \tag{4.4}$$

and the first chargino by,

$$m_{\widetilde{\chi}_{1+}} = M_2 - \frac{m_W^2(M_2 + \mu sin(2\beta))}{\mu^2 - M_2^2} + ... \tag{4.5}$$

From Table 4.6 we can see that as k reduces, the LSP becomes increasingly "wino-like". Therefore, the mass of the lightest neutralino is dominated by the mass of $m_{\widetilde{\chi}_{20}}$ (Equation 4.4). In turn, the mass of lightest chargino is given, to leading order, by the same expression (Equation 4.5). Therefore, their masses are exceptionally close. Although this can be helpful in reducing the relic density by some co-annihilation processes, for high $m_{\frac{3}{2}}$ the contributing factors can lead to a switch in hierarchy between the two mass states. This is further confirmed in Figure 4.3 where the mass difference between the LSP and the nLSP tends to 0 for small k.

In this case $m_0 = 0$ and thus the susy scale is relatively low. Therefore, it is important to consider the spectrum masses, their potential collider signature, and the effect new SUSY diagrams could have on certain branching ratios. We begin by looking at the mass distributions of the SUSY spectrum.

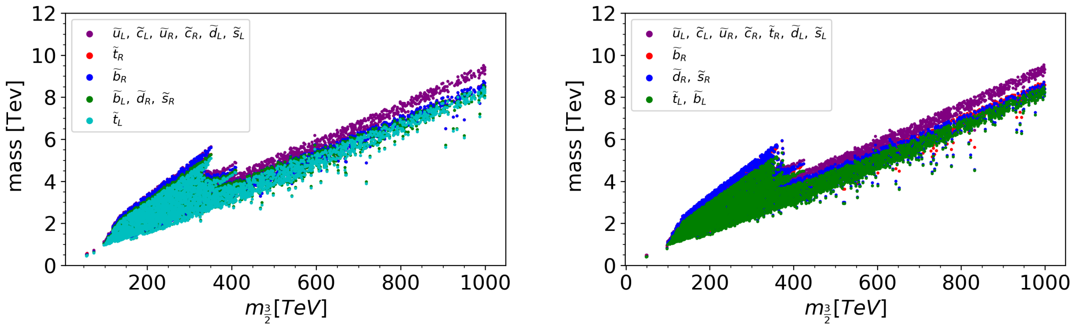

(A) $\mu < 0$, case I

(B) $\mu > 0$, case I

FIGURE 4.4: Shows the squark mass spectrum for case I, $\alpha = 0$. Particles are plotted in the same colour if they are sufficiently mass degenerate as to be indistinguishable in this plot. Typically, this would entail masses within 15GeV of each other. Increasing k increases the mass of the squarks. Low k points cut-off just below $400 TeV$.

From Fig 4.4, we see the mass distribution of the squarks with respect to $m_{\frac{3}{2}}$. Although it is not explicitly plotted we can see the effect of k variance as a part of the mass distribution cuts-off just below $400 TeV$. This is a reflection of the point demonstrated in Figure 4.3, where low k points tend to having a charged LSP for large $m_{\frac{3}{2}}$. This same dependance of k can also be seen in Figures 4.5 and 4.6.

We see that a reduction in k increases the overall scale of the squarks. Their mass is given predominantly by M_3 contributions. Therefore, a reduction of k will lead to an increase in the absolute value of M_3 as, by Equation 4.3, the anomaly mediated term is negative. This increase in mass scale leads to an increase in the mass scale of the squarks. We also note that the left handed $\widetilde{t}$ tends to be the the lightest squark with the first generation squarks making up the heaviest squarks as is typical in such models without flavour mixing.

Unlike the squarks, a reduction in k decreases the mass scale of the sleptons. As they are uncharged under $SU(3)$, they receive their mass from contribution from M_1 and M_2. Furthermore, their anomaly mediated terms are positive, so a reduction in k leads to a reduction in their absolute scale and thus a reduction in the slepton masses. Analogously to the squarks, the left handed $\widetilde{\tau}$ states tend to be the lightest sleptons.

Perhaps predictably, given the scaleless nature of the model, Figure 4.6 shows the most interesting structure with regard to the mass spectrum. Firstly, as $m_{\frac{3}{2}}$ increases,

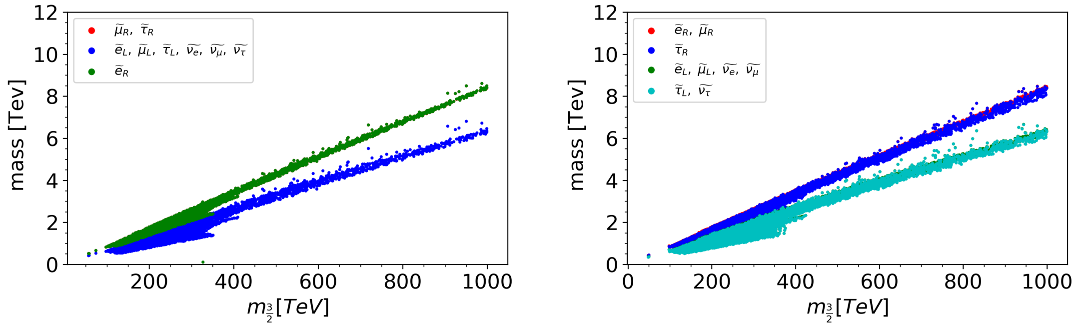

(A) $\mu < 0$, case I

(B) $\mu > 0$, case I

FIGURE 4.5: As in Figure 4.4 but showing the slepton masses. Increasing k decreases the mass of the sleptons. Low k points cut-off just below 400TeV.

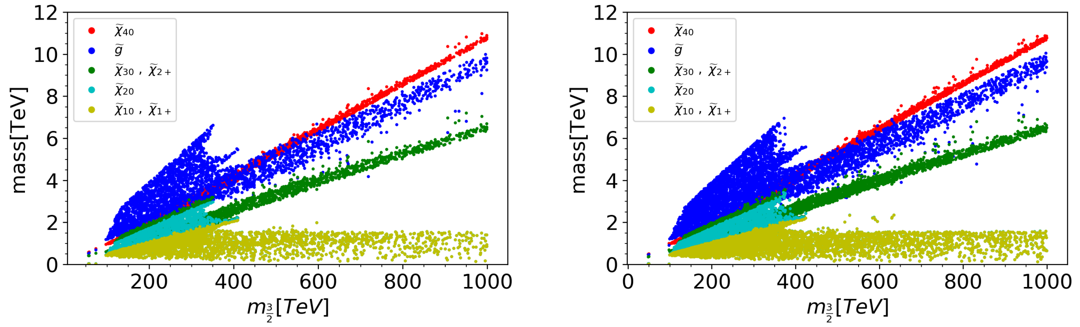

(A) $\mu < 0$, case I

(B) $\mu > 0$, case I

FIGURE 4.6: As in Figure 4.4 but showing the gaugino masses. Increasing k decreases the mass of the gauginos. Low k points cut-off just below 400TeV.

the hierarchy of the heaviest neutralino and the gluino reverse. Furthermore, as k increases, the gluino mass increases significantly. This can be understood by a similar argument to that of the squarks; an increase in k leads to a decrease in the absolute scale of M_3 and thus a decrease in the gluino mass.

Furthermore, for large values of k the first neutralino mass, χ_{10}, does not depend on $m_{\frac{3}{2}}$. The large values of k increase the proportion of the first neutralino that is "higgsino-like". As this mass depends predominantly on μ, this stabilises the mass of the neutralino with respect to $m_{\frac{3}{2}}$. Conversely, small k creates a "wino-like" neutralino whose mass is proportional to M_2 and thus to $m_{\frac{3}{2}}$.

Due to the different natures of the model weights, we decided to allow $tan(\beta)$, and therefore B_0 and β^1, to vary as a free parameter but keep α fixed. Therefore, it is interesting to see the implications of the scan for the free β parameter. Looking at Fig 4.7 we find a striking prediction for the model. For both signs of μ this model predicts that $\beta \approx 0.998$ (excluding some anomalous points). Recall that, by Eq. 4.1, β is

---

[1] β is used both as the inverse tangent of the ratio of the higgs vevs, and as the modular weight. From context it should be clear which is being referred to.

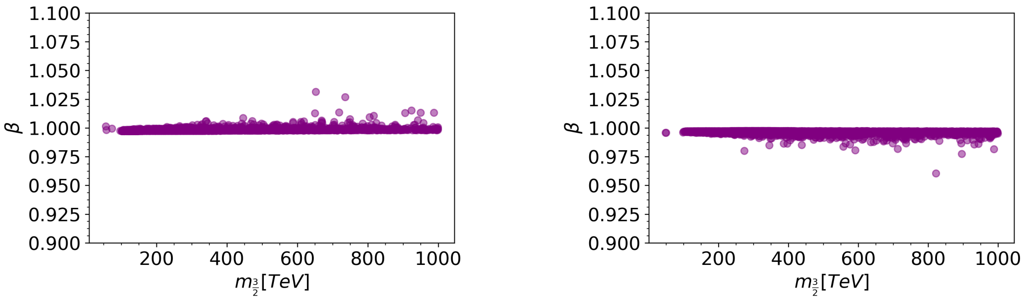

(A) $\mu < 0$, case I

(B) $\mu > 0$, case I

FIGURE 4.7: Shows the values of the modular weight, β, produced for case I, $\alpha = 0$. There is a natural tendency for values very close to 1. According to Eq. 4.1, this suggests $B_0 \approx 0$, in-keeping with scale-less supersymmetry or no-scale SUGRA.

connected to the bilinear coupling such that if $\beta = 1 \implies B_0 = 0$. As can be seen, the model clearly favours a bilinear coupling very close to 0 making a fully scale-less model.

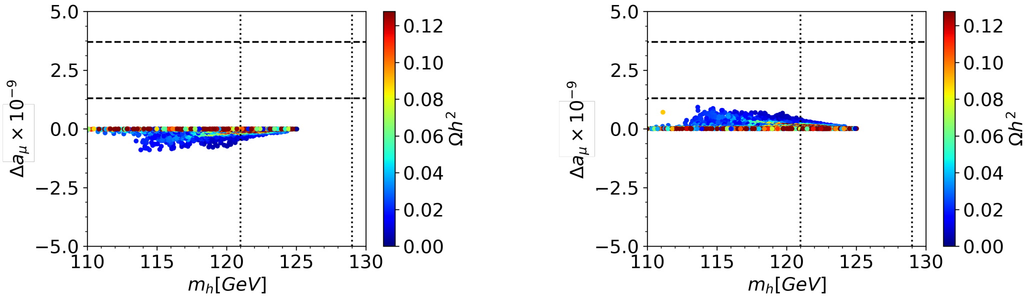

(A) $\mu < 0$, case I

(B) $\mu > 0$, case I

FIGURE 4.8: Shows a scatter plot of the higgs mass against the anomalous muon magnetic moment for a scan with ranges $tan(\beta) \in [1.5, 30], k \in [0, 0.1]$, and $m_{\frac{3}{2}} \in [10^3 GeV, 10^6 GeV]$. The 2σ region of a_μ is marked with dotted lines while the 2σ region of m_h is marked with dashed lines. The colour denotes the relic density. No point satisfies the observed values of the muon $g - 2$.

From Figure 4.8 we see that this model cannot satisfy this condition for either sign of μ. In the $\mu < 0$ case, we see that the contributions are in fact negative. The contributions generally take the form $\Delta a_\mu \propto \text{sign}[\mu] \frac{1}{(m_{\tilde{\mu},\tilde{\nu}_\mu})^2}$. Therefore, a change in the sign of μ reverses the sign of these contributions. In general, large $m_{\frac{3}{2}}$ leads to a large mass spectrum which in turn suppresses the $g - 2$ contributions. From Figure 4.5 we can see that the masses of the $\tilde{\mu}$s and $\tilde{\nu}_\mu$s grow linearly with $m_{\frac{3}{2}}$ leading to quadratic suppression of Δa_μ. Although in the positive μ case, the contributions are themselves positive, no point can satisfy the measured discrepancy.

To gain further insight into this model, a set of benchmark points is presented. Table 4.4 shows the input parameters for each benchmark point selected. The benchmark points were selected to reflect a variety of viable regions in the model.

Quantity	BP1	BP2	BP3	BP4	BP5	BP6
α	0	0	0	0	0	0
β	0.996	0.997	0.997	0.998	0.998	0.998
$m_{\frac{3}{2}}$ [TeV]	903	268	359	995	269	358T
k	0.00443	0.00323	0.00251	0.00457	0.00324	0.0026
SPheno:						
m_0 [GeV]	0	0	0	0	0	0
$tan(\beta)$	18.1	23.9	19.6	29.3	20.0	29.6
$sign(\mu)$	1	1	1	-1	-1	-1
A_0 [GeV]	0	0	0	0	0	0
M_1 [GeV]	20800	5700	7600	23000	5900	7600
M_2 [GeV]	6800	1700	2000	7600	1700	2000
M_3 [GeV]	-4400	-1600	-2400	-4700	-1600	-2400

TABLE 4.4: Shows six benchmark points representing six different areas of interest in the parameter where case I, $\alpha = 0$. We present the model parameters and the resultant SPheno input parameters. BP1 and BP4 show the highest likelihood points for $\mu > 0$ and $\mu < 0$ respectively. BP2 and BP5 show points where $m_{\frac{3}{2}}$ is minimised whilst still satisfying our main constraints for $\mu > 0$ and $\mu < 0$ respectively. BP3 and BP6 show points for minimal values of k whilst still satisfying our main constraints for $\mu > 0$ and $\mu < 0$ respectively. Dimensions of the parameters are given. $m_{\frac{3}{2}}$ is given in units of TeV, and m_0, A_0, M_i are given in GeV.

Benchmark points 1,2, and 3 all have their sign of μ positive while the reverse is true for points 4,5, and 6. BP1 and BP4 are the highest likelihood points of the model for their respective signs of μ. BP4 comes from the second band of high likelihood points at $k > 0.0045$. They both have very high $m_{\frac{3}{2}}$ values existing just below the cut-off set by the CMB in the context of inflation [112]. BP2 and BP5 have the lowest values of $m_{\frac{3}{2}}$ whilst staying in a high likelihood range and BP3 and BP6 have the lowest values of k whilst staying in a high likelihood range.

Table 4.5 shows the resultant SUSY mass spectrum for the 6 benchmark points presented so far. As changing the sign of μ plays little role, we will refer to the combination of BP1 and BP4 as BP1,4, and similarly for the other benchmark points. Many points do not achieve the precise value for the Higgs mass. However, there is a relatively large theoretical uncertainty on this parameter leaving all these points with relatively high likelihoods.

BP1,4 shows a hugely inflated mass spectrum for the squarks and sleptons. Furthermore, we see huge masses for the heaviest gauginos. However, although much of the spectrum is high in mass, the lighter gauginos are only about 1TeV. These could leave a tell tale signature in current or future colliders. We also see a relatively low μ value. This causes the high "higgsino-like" proportions of the LSP. $\widetilde{\nu}_{\tau L}$ is the smallest supersymmetric scalar (excluding the Higgs boson).

BP2,5 shows a significantly reduced SUSY spectrum due to the reduced scale of $m_{\frac{3}{2}}$

Masses	BP1	BP2	BP3	BP4	BP5	BP6
$\widetilde{e}_L$	5690	1540	1900	6340	1540	1910
$\widetilde{e}_R$	7590	2160	2790	8400	2170	2790
$\widetilde{\nu}_{eL}$	5690	1530	1890	6340	1540	1910
$\widetilde{\mu}_L$	5690	1540	1900	6340	1540	1910
$\widetilde{\mu}_R$	7590	2160	2790	8400	2170	2790
$\widetilde{\nu}_{\mu L}$	5690	1530	1890	6330	1540	1910
$\widetilde{\tau}_1$	5690	1490	1860	6100	1510	1820
$\widetilde{\tau}_2$	7460	2100	2740	8040	2130	2680
$\widetilde{\nu}_{\tau L}$	5610	1490	1860	6100	1510	1820
$\widetilde{d}_L$	8580	3190	4500	9260	3190	4450
$\widetilde{d}_R$	7780	3060	4390	8310	3060	4330
$\widetilde{u}_L$	8580	3190	4500	9260	3190	4450
$\widetilde{u}_R$	8920	3300	4680	9620	3310	4630
$\widetilde{s}_L$	8580	3190	4500	9260	3190	4450
$\widetilde{s}_R$	7780	3060	4390	8310	3060	4330
$\widetilde{c}_L$	8580	3190	4500	9260	3190	4450
$\widetilde{c}_R$	8920	3300	4680	9620	3310	4630
$\widetilde{b}_1$	7670	2910	4160	8040	2940	4090
$\widetilde{b}_2$	7870	2980	4320	8420	3020	4230
$\widetilde{t}_1$	7600	2840	4050	8190	2840	4010
$\widetilde{t}_2$	7880	2940	4170	8420	2960	4110
$\widetilde{g}$	8940	3510	5080	9540	3510	5010
$\widetilde{\chi}_{10}$	1110	1370	1750	1110	1370	1770
$\widetilde{\chi}_{20}$	1111	1410	2170	1110	1400	2110
$\widetilde{\chi}_{30}$	5810	1500	2170	6520	1500	2110
$\widetilde{\chi}_{40}$	9650	2620	3440	10800	2640	3440
$\widetilde{\chi}_{1+}$	1110	1370	1750	1110	1370	1770
$\widetilde{\chi}_{2+}$	5810	1500	2180	6520	1500	2110
h_0	124.5	120	122	125	121	123
H_0	5510	1860	2690	5410	1970	2520
A_0	5510	1860	2690	5410	1970	2520
$H_\pm$	5520	1870	2700	5410	1970	2520
μ	1100	1400	2100	-1070	-1390	-2090
B_0	7610	1510	1970	3890	1240	1700

TABLE 4.5: Shows the spectrum of SUSY masses for the benchmark points given in Table 4.4. The difference between the mass of $\widetilde{\chi}_{1+}$ and $\widetilde{\chi}_{10}$ is also given as this pertains to the production of dark matter. We also include the highscale bilinear coupling value B_0 for its relevance to the high scale parameters of the model. All massses are given in GeV.

Quantity	BP1	BP2	BP3	BP4	BP5	BP6
$\Omega_{DM}h^2$	0.119	0.124	0.115	0.119	0.119	0.124
$\widetilde{\chi}_{10}$ [GeV]	1109.5	1372.7	1748.3	1110.5	1372.1	1767.0
$\widetilde{\chi}_{1+} - \widetilde{\chi}_{10}$ [GeV]	0.48072	1.5	0.0329	0.59656	1.699	0.03567
$\lvert\alpha_1\rvert^2$	0.000016	0.000441	0.000004	0.000009	0.0004	0.000004
$\lvert\alpha_2\rvert^2$	0.000144	0.312481	0.982081	0.0001	0.228484	0.976144
$\lvert\alpha_3\rvert^2$	0.499849	0.352836	0.011025	0.499849	0.394384	0.014161
$\lvert\alpha_4\rvert^2$	0.499849	0.335241	0.007396	0.499849	0.375769	0.009604
$\sigma^{SI} \times 10^9 [pb]$	0.03	34.29	2.12	0.01	19.05	1.80

TABLE 4.6: Shows the relic density of the LSP for each benchmark point. The difference between the LSP and the nLSP is also given. Finally, we give the probability of finding the given LSP in a particular flavour state. That is to say; we give $|\alpha_i|^2$ where $\widetilde{\chi}_{10} = \alpha_1 \widetilde{B} + \alpha_2 \widetilde{W} + \alpha_3 \widetilde{H}_1 + \alpha_4 \widetilde{H}_2$ and $\sum |\alpha_i|^2 = 1$. Dimensionful parameters are given in GeV except for the spin independent cross-section which is given in pb. The experimental limit for $\sigma^{SI}_{BP1,4} = 0.96 \times 10^{-9} pb$, $\sigma^{SI}_{BP2,5} = 1.19 \times 10^{-9} pb$, $\sigma^{SI}_{BP3,6} = 1.52 \times 10^{-9} pb$. Therefore, BP2,5 and BP3,6 exceed the experimental limits.

and therefore the reduction in $M_{1,2,3}$. Although the majority of the spectrum is still mostly out of range of modern detectors, the model still produces low mass light gauginos. Although the mass gap between $\widetilde{\chi}_{10}$ and $\widetilde{\chi}_{1+}$ is still small, the gap between the first two charged states has increased due to a change in the mixing of the gauginos. Again, $\widetilde{\nu}_{\tau L}$ is the smallest supersymmetric scalar.

Finally, BP3,6 shows a slight increase in the overall SUSY scale in comparison to the BP2,5. Although the mass gap between the heavy and light gaugino states has increased, the overall scale for the states has increased significantly as the LSP becomes almost exclusively "wino-like". In general, a high wino-like state can lead to excessive co-annihilation with the first chargino; especially when, as can be seen in Table 4.6, the mass gap between said states is so low. However, for sufficiently high mass neutralinos, the freeze out temperature is high thus ending these problematic processes early in the universes cosmological past and thereby preventing the excessive annihilation of the candidate. Although $\widetilde{\chi}_{1+}$ is still the second lowest mass particle, the $\widetilde{\nu}_{\tau L}$ is lighter than the $\widetilde{\chi}_{20}$ unlike in the other benchmark points where a clear hierarchy existed between the fermionic and scalar states.

Table 4.6 shows information specifically regarding the relic density for the benchmarks points. In all cases we see a very compressed gaugino mass spectrum inducing the requisite co-annihilarion processes. BP3,6 shows an exceptionally compressed mass gap. As was previously argued, the high mass leads to an early freeze out temperature preventing these co-annihilartion processes eradicating the dark matter too efficiently. We also present the proportion of bino, wino, and higgsino for the given particle. We see a very interesting shift between the respective benchmark points with BP1,4 being mostly higgsino, BP2,5 being evenly split between higgsino and wino, and BP3,6 being majority wino.

In addition to the relic density, we consider the spin-independant nucleon scattering cross-section, σ^{SI}, in order to compare the benchmark points with direct detection experiments. The authors have done work in [59] to extrapolate XENON1T limits for a range of dark matter candidate masses (further details of this extrapolation can be found there-in). We also consider the spin-dependant limits but, as these are much less stringent and are easily satisfied by the model, we do not present them here. Although BP1,4 easily satisfies the spin-independent limits, BP2,5 and BP3,6 have cross-sections that exceed them as they have significant wino content .

Tables 4.7, 4.8, 4.9 show phenomenological information regarding potential constraints and collider physics. BP1 and BP4, BP2 and BP5 , and BP3 and BP6 are paired together as they belong to similar regions of parameter space. We implemented a checkmate analysis for both 8, 13, and 14 TeV ATLAS and CMS analyses. However, we chose not to include 14TeV analysis in our tables as they are not based on LHC runs but rather Monte-Carlo simulations. Instead, where appropriate, we have simply noted the r_{max} value (defined below) produced as suggestive of the type of the effects future colliders could have. We use MadGraph_2.6.7 [129, 130] to generate events with SUSY final states. Pythia_8.2.45 [131, 132] is then used to shower and hadronise the events. Finally, Delphes_3.4.2 [133] and some subsidiary tools [134–137] are used to perform event and detector analysis. This approach allows us to assess a given benchmark points viability in comparison with experimental data. We find that all presented benchmark points cannot be ruled out by the LHC at $\sqrt{s} \leq 13TeV$. We include a quantity r_{max} defined by

$$r_{max} = \frac{S - 1.64 \cdot \Delta S}{S95} \tag{4.6}$$

where S is the number of signal events, ΔS is its uncertainty, and $S95$ is the experimental upper limit on the number of signal events. This quantity indicates whether a point is ruled out by the analyses or not. Points with $r_{max} \geq 1$ are ruled out; those with $r_{max} < 1$ are not. Finally, the most important signal regions analysed by CheckMATE are given. We find a variety of different analyses are important due to the changing mixing matrices and SUSY spectrum.

We include a number important beyond the standard model constraints; Δa_μ, BR $(B_s \to \mu^+ \mu^-)$, the relic density, and BR $(b \to s\, \gamma)$. We find that the two branching ratios agree with experimental data very well. However, the lack of light $\widetilde{\mu}$s and $\widetilde{\nu}_\mu$s lead to insufficient contributions to the Δa_μ loop diagrams as these are suppressed by the propagator mass squared. Indeed, BP4, 5, and 6 have negative contributions to the anomalous muon magnetic moment. This is due to the reversal of sign of the μ parameter, and the dependancy on μ in the gaugino mediated diagrams that contribute to Δa_μ. As the relic density is our strongest constraint, all points have been chosen to satisfy modern cosmological constraints on the production of dark matter.

Finally, we include the decay width and branching ratios of the two lightest particles (excluding the LSP who is stable). In BP1,4 and BP2,5 these are light gaugino states. However, in BP3,6, the $\widetilde{\nu}_\tau$ is lighter than the χ_{20}. Only branching ratios that contribute by more than 1% are included.

Although BP1,4 shows a long lifetime it is drastically insufficient for the particle to escape the detector. Therefore, the particles decay products are very important in assessing the signature of this model. The analysis region of most significance is one that focuses on mono-jets. This analysis has a very large luminosity. It should be noted that, unlike BP2,5 and BP3,6, 14TeV analysis yields an r_{max} value of 0, perhaps due to the lack of significance at such high energy scales. The branching ratios for both the two lightest non-LSP particles are dominated by $\widetilde{\chi}_{10}$ decays. This would suggest large corresponding missing momenta. We find an excellent fit for the BSM constraints as well as dark matter. However, Δa_μ cannot be satisfied.

The most constraining region for BP2,5 focuses on squarks and gluinos, with 0 leptons, and 2-6 jets at 13Tev. This is due to the relatively low mass of the strongly coupled particles. We see the highest value of r_{max} of all the benchmark points due to the abundance of these lighter particles. $\widetilde{\chi}_{20}$ shows a huge variety in decay channels as the mass gap is too small for the squark pairs to hadronise. We find that 14TeV analysis yields very high r_{max} values of 0.276 in the positive μ case. This suggests that future colliders could probe regions of interest in this model. Again, the relic and BSM branching ratios can be fitted well, but Δa_μ cannot.

As previously eluded to, BP3,6 shows a change in the spectrum hierarchy. From Table 4.6, the mass difference between $\widetilde{\chi}_{10}$ and $\widetilde{\chi}_{1+}$ is the smallest. Therefore, a smaller phase space is available leading to fewer decay channels. In contrast to $\widetilde{\nu}_\tau$, whose lifetime is very small, the lifetime of χ_{1+} is sufficiently long that the particle could escape the detector. As it is a charged particle, this would appear as a charge track in the calorimeter. As was the case for BP2,5, 14TeV analysis gives a whole order of magnitude increase in r_{max} hinting at the exciting prospects for physics to come. Again, the BSM constraints and the relic are satisfied; however, Δa_μ is not.

Quantity	BP1	BP4
$\Gamma\chi_{1+}$ [GeV]	8.4×10^{-14}	1.7×10^{-13}
BR $(\chi_{1+} \to \chi_{10}\, \pi^{+})$ [%]	92.9	89.3
BR $(\chi_{1+} \to \chi_{10}\, e^{+}\, \nu_e)$ [%]	4.00	5.71
BR $(\chi_{1+} \to \chi_{10}\, \mu^{+}\, \nu_\mu)$ [%]	3.14	4.90
$\Gamma\chi_{20}$ [GeV]	5.12×10^{-12}	2.9×10^{-12}
BR $(\chi_{20} \to \chi_{10}\, \pi^{0})$ [%]	63.8	74
BR $(\chi_{20} \to \chi_{1+}\, \pi^{-})$ [%]	6.1	2.64
BR $(\chi_{20} \to \chi_{1-}\, \pi^{+})$ [%]	6.1	2.64
BR $(\chi_{20} \to \chi_{10}\, \gamma)$ [%]	4.9	5.79
BR $(\chi_{20} \to \chi_{10}\, e^{-}\, e^{+})$ [%]	2.0	1.81
BR $(\chi_{20} \to \chi_{10}\, \mu^{-}\, \mu^{+})$ [%]	2.0	1.72
BR $(\chi_{20} \to \chi_{10}\, \nu_e\, \overline{\nu_e})$ [%]	2.0	10.8
BR $(b \to s\, \gamma)$ [%]	0.032	0.032
BR $(B_s \to \mu^{+}\, \mu^{-})$ [%]	2.9×10^{-7}	2.9×10^{-7}
Δa_μ	8.39×10^{-12}	-1.15×10^{-11}
$\Omega_{DM} h^2$	0.119	0.119
χ_{10} [GeV]	1110	1110
$\sigma_{q\bar{q}\to\chi_{10}\chi_{10}}$ [pb]	0	0
r_{max}	3.72×10^{-4}	2.03×10^{-4}
$\sqrt{s}$ [TeV]	13	13
Analysis	atlas_conf_2017_060	atlas_conf_2017_060
Signal Region	EM7	IM6
Ref.	[138]	[138]

TABLE 4.7: Shows branching ratios for lightest supersymmetric particles in the spectrum for the benchmarks points with highest likelihood, BP1 and BP4. Only branching ratios greater than 1% are included. We also include some the the beyond the standard model observables BR $(b \to s\, \gamma)$, BR $(B_s \to \mu^{+}\, \mu^{-})$, Δa_μ, and $\Omega_{DM} h^2$, where Δa_μ is a calculation of the SUSY contribution beyond the standard model. The model successfully predicts the b decays discrepancy as well as the relic density. However, the anomalous muon magnetic moment cannot be satisfied. CheckMATE runs using 13TeV and 8TeV analyses cannot rule out these points. Decay widths and masses are given in GeV and branching ratios are given in %.

Quantity	BP2	BP5
$\Gamma\chi_{1+}$ [GeV]	8.9×10^{-12}	1.4×10^{-11}
BR $(\chi_{1+} \to \chi_{10}\, \bar{d}\, u)$ [%]	60.0	58.9
BR $(\chi_{1+} \to \chi_{10}\, \bar{s}\, c)$ [%]	0.34	2.02
BR $(\chi_{1+} \to \chi_{10}\, e^{+}\nu_e)$ [%]	20.1	19.7
BR $(\chi_{1+} \to \chi_{10}\, \mu^{+}\nu_\mu)$ [%]	19.6	19.4
$\Gamma\chi_{20}$ [GeV]	2.45×10^{-4}	6.1×10^{-5}
BR $(\chi_{20} \to \chi_{10}\, u\, \bar{u})$ [%]	3.92	4.22
BR $(\chi_{20} \to \chi_{10}\, c\, \bar{c})$ [%]	3.90	4.18
BR $(\chi_{20} \to \chi_{10}\, d\, \bar{d})$ [%]	5.09	5.49
BR $(\chi_{20} \to \chi_{10}\, s\, \bar{s})$ [%]	5.09	5.49
BR $(\chi_{20} \to \chi_{10}\, b\, \bar{b})$ [%]	4.68	4.74
BR $(\chi_{20} \to \chi_{10}\, e^{-}\, e^{+})$ [%]	1.17	1.26
BR $(\chi_{20} \to \chi_{10}\, \mu^{-}\, \mu^{+})$ [%]	1.17	1.26
BR $(\chi_{20} \to \chi_{10}\, \tau^{-}\, \tau^{+})$ [%]	1.16	1.24
BR $(\chi_{20} \to \chi_{10}\, \nu_e\, \overline{\nu_e})$ [%]	7.03	7.57
BR $(\chi_{20} \to \chi_{1+}\, d\, \bar{u})$ [%]	11.2	10.8
BR $(\chi_{20} \to \chi_{1-}\, \bar{d}\, u)$ [%]	11.2	10.8
BR $(\chi_{20} \to \chi_{1+}\, s\, \bar{c})$ [%]	11.1	10.7
BR $(\chi_{20} \to \chi_{1-}\, \bar{s}\, c)$ [%]	11.1	10.7
BR $(\chi_{20} \to \chi_{1+}\, e^{-}\, \overline{\nu_e})$ [%]	3.72	3.60
BR $(\chi_{20} \to \chi_{1-}\, e^{+}\, \nu_e)$ [%]	3.72	3.60
BR $(\chi_{20} \to \chi_{1+}\, \mu^{-}\, \overline{\nu_\mu})$ [%]	3.72	3.60
BR $(\chi_{20} \to \chi_{1-}\, \mu^{+}\, \nu_\mu)$ [%]	3.72	3.60
BR $(\chi_{20} \to \chi_{1+}\, \tau^{-}\, \overline{\nu_\tau})$ [%]	3.68	3.54
BR $(\chi_{20} \to \chi_{1-}\, \tau^{+}\, \nu_\tau)$ [%]	3.68	3.54
BR $(b \to s\, \gamma)$ [%]	0.033	0.033
BR $(B_s \to \mu^{+}\, \mu^{-})$ [%]	2.9×10^{-7}	3.0×10^{-7}
Δa_μ	1.15×10^{-10}	-9.6×10^{-11}
$\Omega_{DM}h^2$	0.124	0.119
χ_{10} [GeV]	1370	1370
$\sigma_{q\bar{q}\to\chi_{10}\chi_{10}}$ [pb]	8.629×10^{-8}	2.718×10^{-8}
r_{max}	1.12×10^{-2}	8.10×10^{-3}
$\sqrt{s}$ [TeV]	13	13
Analysis	atlas_1712_02332	atlas_1712_02332
Signal Region	2j-3600	2j-3600
Ref.	[139]	[139]

TABLE 4.8: As in Table 4.7 but for BP2 and BP5; points with low $m_{\frac{3}{2}}$.

Quantity	BP3	BP6
$\Gamma\chi_{1+}$ [GeV]	7.2×10^{-20}	1.0×10^{-19}
BR $(\chi_{1+} \to \chi_{10}\, \overline{d}\, u)$ [%]	72	72
BR $(\chi_{1+} \to \chi_{10}\, e^{+}\, \nu_e)$ [%]	28	28
$\Gamma\widetilde{\nu_\tau}$ [GeV]	2.9×10^{-1}	7.7×10^{-2}
BR $(\widetilde{\nu_\tau} \to \chi_{10}\, \nu_\tau)$ [%]	33.3	33.0
BR $(\widetilde{\nu_\tau} \to \chi_{1+}\, \tau^{-})$ [%]	66.7	67.0
BR $(b \to s\, \gamma)$ [%]	0.032	0.032
BR $(B_s \to \mu^{+}\, \mu^{-})$ [%]	2.9×10^{-7}	3.0×10^{-7}
Δa_μ	5.50×10^{-11}	-8.30×10^{-11}
$\Omega_{DM}h^2$	0.115	0.124
χ_{10} [GeV]	1750	1750
$\sigma_{q\bar{q}\to\chi_{10}\chi_{10}}$ [pb]	7.805×10^{-8}	6.467×10^{-8}
r_{max}	3.458×10^{-3}	3.189×10^{-3}
$\sqrt{s}$ [TeV]	13	13
Analysis	atlas_conf_2017_060	atlas_conf_2017_060
Signal Region	EM10	EM10
Ref.	[138]	[138]

TABLE 4.9: As in Table 4.7 but for BP3 and BP6; points with low k.

4.4.2 Negative k (Scan 2)

In this case we expect a negative universal gaugino mass parameter k to tend to yield a spectrum with a heavy gluino and relatively light winos and binos, possibly suitable to explain the muon $g-2$, as well as the Higgs mass and dark matter. Moreover, in order to explain the measured Δa_μ, small values of the $\widetilde{\mu}$ mass are required. As seen in Figures 4.4, 4.5, and 4.6, a reduction in k reduces the slepton masses, whilst increasing the gluon and squark masses. Further reductions in k reduce the $\widetilde{\mu}$ mass sufficiently but keep the mass of the higgs boson high as this is dependant on the SU(3) charged squarks and sleptons.

In Scan 2, the k parameter is varied from 0 to -0.04. As noted, negative values of k will increase the absolute scale of M_3 but reduce the scale of M_2. This will further contribute to the effect described above, increasing squark masses whilst decreasing slepton masses. As previously argued, the Δa_μ contributions depend on $m_{\widetilde{\mu}}^{-2}$ and therefore large values of $m_{\frac{3}{2}}$ will lead to a suppression of the contributions. We therefore scan for lower values of $m_{\frac{3}{2}}$ between 0 and 400 TeV.

Fig 4.9 shows the distribution of k against $m_{\frac{3}{2}}$ for both signs of μ. As we are now focussing on a_μ we redefine the likelihood as $L = L_{a_\mu} \times L_{m_h}$. However, we do not want relic particles whose abundance would rule out the model entirely. Therefore, we impose the condition that $\Omega h^2 < 0.12 + 2 \times 0.0078$ such that no point can be ruled out by leaving a non-phenomenologically large relic abundance.

From Fig 4.9, we see two distinct areas of points that give viable results; $k \approx -0.016$ and $k \approx -0.023$. However we find that $k \approx -0.023$ with $\mu < 0$ is phenomenologically preferred. In this region, we also find $30TeV < m_{\frac{3}{2}} < 100TeV$ to be preferred.

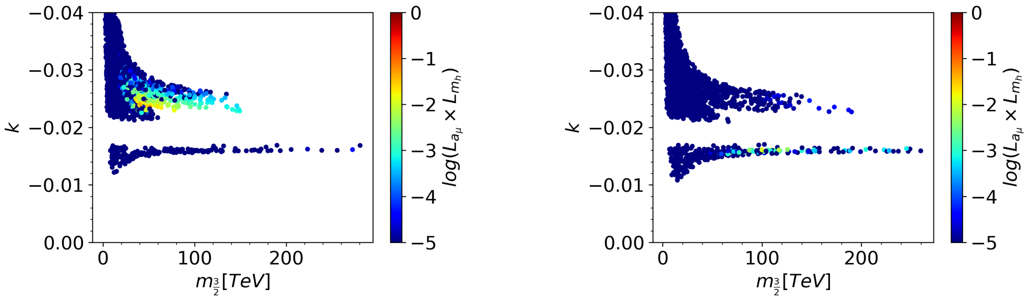

(A) $\mu < 0$, case I

(B) $\mu > 0$, case I

FIGURE 4.9: Shows the distribution of k against $m_{\frac{3}{2}}$ with a_μ and m_h log likelihood for $m_{\frac{3}{2}} \in [0TeV, 400TeV]$, $\alpha = 0$ and $k \in [-0.035, -0.014]$. A region with $\mu < 0$, $k \approx -0.023$ and $m_{\frac{3}{2}} \in [40TeV, 60Tev]$ is preferred.

Finally, we present the results of a scan focussing on the good region as seen in Figure 4.10 where k varies between -0.022 and -0.027 and the sign of μ is fixed as negative.

Negative results for Δa_μ are now ruled out as the absolute value of the gaugino mass parameters is large, suppressing some key SUSY contributions to $(g-2)$ that involve these particles. This leaves us with one first order loop diagram that contributes to this result whose sign is fixed by the sign of μ.

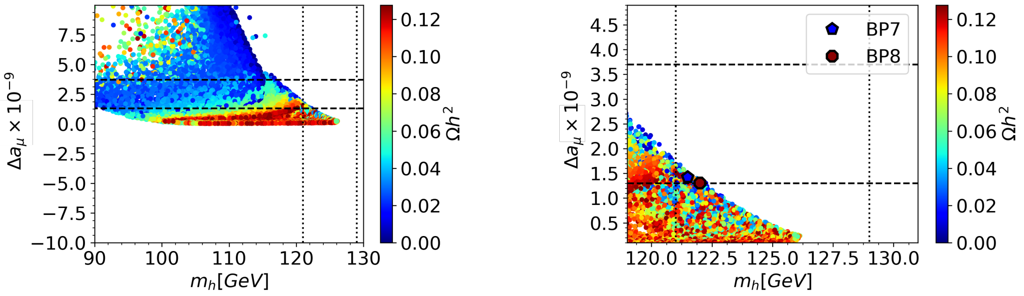

(A) $\mu < 0$, case I

(B) $\mu < 0$, case I, zoomed

FIGURE 4.10: Shows a scatter plot of a_μ and m_h for a focussed scan with ranges $m_{\frac{3}{2}} \in [0TeV, 160TeV]$, $k \in [-0.022, -0.027]$ and $tan(\beta) \in [2, 12]$. The 2σ region of a_μ is marked with dotted lines while the 2σ region of m_h is marked with dashed lines. The colour denotes the relic density.

Figure 4.10 shows the distribution of Δa_μ against the higgs mass. We see many points sit within the 2σ region. Furthermore, we find that many of these points have excellent dark matter relic densities. Two benchmark points are marked on Figure 4.10 who are presented later.

Until now, the relic abundance of dark matter has played a pivotal role in assessing the veracity of any given point. However, we find large parts of the parameter space give the right handed stau state as the lightest sparticle. In all preceding plots and in Figure 4.10 we present results where the neutralino is the LSP. However, it is also interesting to consider potential R-parity violating models in which these light, charged particles decay into standard model particles. Although a detailed discussion of the viability of such points is beyond the scope of this work, we include Figure 4.11 as these states can lead to excellent fits for a_μ and m_h.

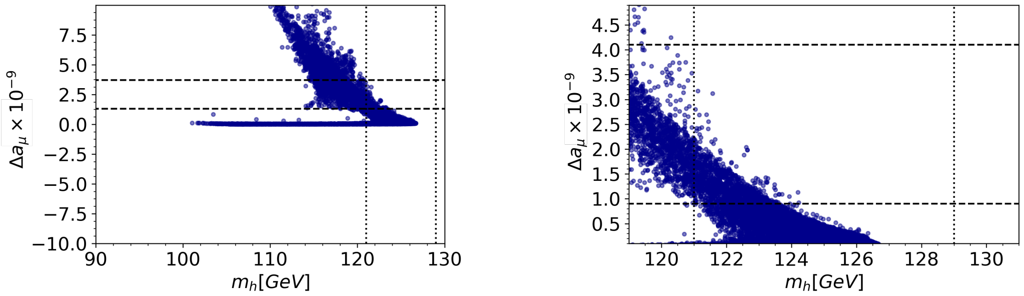

(A) $\mu < 0$, case I

(B) $\mu < 0$, case I, zoomed

FIGURE 4.11: As for Fig 4.10 but where points that have charged LSP states are shown. Such states are marked in blue to indicate that no relic density could be calculated.

Continuing our analysis, we took a number of points from the allowed region and ran them through `CheckMATE`. Finding that a sample of points were excluded we wrote a code to systematically check points in the allowed region. We found that all points were either excluded by `CheckMATE` or in a region near exclusion (allowing for uncertainties in the analysis). We include some of the more promising benchmark points below. It should be noted that we ran `CheckMATE` using the default 5000 points. However, if a warning was presented speculating that more data could exclude the point in question we increased the number of events by the specified amount.

In Table 4.10 we present the input parameters for two benchmarks points from Case I with negative k values. One point was selected for its relatively high values of Δa_μ whilst the other was selected for it's relatively high value of Ωh^2. Both points are $k = -0.023$ in accordance with the highest likelihood region. Indeed, both points are very similar in a variety of ways suggesting a small input deviations can give large variance in output; particularly for the LSP relic abundance.

Table 4.11 shows the SUSY spectrum for benchmark points 7 and 8. Strikingly, we see that the lightest stau state is the nLSP behind the usual neutralino LSP. This ofcourse has implications for the most powerful diagrams for the relic density. Furthermore, the nnLSP is given by $\widetilde{\mu}_R$ as anticipated by our efforts to generate a high Δa_μ value using diagrams involving this particle. Unlike the sleptons, the squarks are very high in mass contributing to the phenomenologically viable Higgs mass. In both cases $\widetilde{\tau}_1 - \widetilde{\chi}_{10} \approx 10 GeV$. This is important for critical co-annihilation diagrams for the relic density. Again we see that B_0 is very small in comparison with $m_{\frac{3}{2}}$ suggesting a fully scale-less model.

Both benchmarks produce a completely bino-like LSP state caused by the large scale difference between M_1 and M_2 and have very similar dark matter physics in general. Although BP7 has a dark matter relic density within the allowed region, BP8 gives an excellent value. We see a much larger mass gap between the LSP and the nLSP than for Benchmark points 1 to 6. This is because the points produce a much smaller mass

Quantity	BP7	BP8
α	0	0
β	1	1
$m_{\frac{3}{2}}$ [TeV]	51	57
k	-0.023	-0.023
SPheno:		
m_0 [GeV]	0	0
$tan(\beta)$	9.72	9.37
$sign(\mu)$	-1	-1
A_0 [GeV]	0	0
M_1 [GeV]	-263	-263
M_2 [GeV]	-1058	-1152
M_3 [GeV]	-1694	-1863

TABLE 4.10: Shows two benchmark points representing two different areas of interest in the parameter space. We present the model parameters and the resultant SPheno input parameters. BP7 shows a point with high a_μ and BP8 shows a point with high Ω. $m_{\frac{3}{2}}$ is given in TeV and all other dimensionful parameters are given in GeV.

LSP. Therefore, the freeze out temperature is low and as such, there is more cosmological time for co-annihilation to occur. A larger mass gap reduces the strength of these co-annihilation channels allowing for the phenomenological Higgs boson mass. Both points have spin-independent cross-sections less than the experimental limits of $0.09 \times 10^{-9} pb$ as they are exclusively bino and thus will not interact with the nucleus in direct detection experiments.

Table 4.13 shows some key observables for the given benchmark points. As previously stated, both points are at the borderline of exclusion by Checkmate analysis, since, both points still have relatively low $r_{max} \sim 1$ values, suggesting that both points might be viable within the uncertainties of the analysis, as we discuss further below.

We see short life times for $\widetilde{\tau}_1$ with only one decay channel therefore potentially leaving a strong collider signature. Both points get their strongest constraints from the CMS analysis [140] that focuses on direct electroweak production of charginos and neutralinos leading to final state leptons, little hadronic activity, and a large missing momentum. As the colour charged particles are far more massive than the leptons and gauginos, the latter will represent the dominant production mechanism for the sparticles. The signal region focuses on a final state with three light leptons where two of the three are either e or μ and as we have a light gaugino LSP with light sleptons for $g-2$ this is likely to be constraining. Furthermore this region focuses on states where the leptonic pair have invariant mass greater than $105 GeV$ and transverse mass of the third lepton greater than $160 GeV$. $\widetilde{\chi}_{20}$ has a 32% branching ratio into $\widetilde{\mu}^{\pm}\mu^{\mp}$ / $\widetilde{e}^{\pm}e^{\mp}$ combined with $\widetilde{\chi}_{1+}$'s tendency to decay into $\widetilde{\tau}\nu_\tau$ pairs creates a strong signal in this region placing the parameter point on the edge of exclusion. Furthermore, the relatively large mass of $\widetilde{\chi}_{20}$ means that the resultant lepton pair will exceed the

Masses	BP7	BP8
$\widetilde{e}_L$	661	717
$\widetilde{e}_R$	133	138
$\widetilde{\nu}_{eL}$	656	712
$\widetilde{\mu}_L$	661	717
$\widetilde{\mu}_R$	133	137
$\widetilde{\nu}_{\mu L}$	656	712
$\widetilde{\tau}_1$	104	109
$\widetilde{\tau}_2$	661	717
$\widetilde{\nu}_{\tau L}$	654	710
$\widetilde{d}_L$	3110	3390
$\widetilde{d}_R$	3050	3330
$\widetilde{u}_L$	3110	3390
$\widetilde{u}_R$	3050	3320
$\widetilde{s}_L$	3110	3390
$\widetilde{s}_R$	3050	3330
$\widetilde{c}_L$	3110	3390
$\widetilde{c}_R$	3050	3320
$\widetilde{b}_1$	2890	3150
$\widetilde{b}_2$	3040	3310
$\widetilde{t}_1$	2580	2820
$\widetilde{t}_2$	2910	3170
$\widetilde{g}$	3560	3890
$\widetilde{\chi}_{10}$	100	99
$\widetilde{\chi}_{20}$	855	933
$\widetilde{\chi}_{30}$	1890	2060
$\widetilde{\chi}_{40}$	1890	2060
$\widetilde{\chi}_{1+}$	855	933
$\widetilde{\chi}_{2+}$	1890	2060
h_0	121.5	122
H_0	1990	2170
A_0	1990	2170
$H_\pm$	2000	2170
μ	-1777	-1931
B_0	-12	-26.5
$\widetilde{\tau}_1 - \widetilde{\chi}_{10}$	4.2	9.6

TABLE 4.11: Shows the spectrum of SUSY masses for the benchmark points given in Table 4.10. The difference between the mass of $\widetilde{\tau}_1$ and $\widetilde{\chi}_{10}$ is also given as this pertains to the production of dark matter. We also include the high scale bilinear coupling value B_0 for its relevance to the high scale parameters of the model. All parameters are given in GeV.

Quantity	BP7	BP8
$\Omega_{DM}h^2$	0.020	0.112
$\widetilde{\chi}_{10}$ [GeV]	100	99
$\widetilde{\tau}_1 - \widetilde{\chi}_{10}$ [GeV]	4.2	9.6
$\|\alpha_1\|^2$	1	1
$\|\alpha_2\|^2$	0	0
$\|\alpha_3\|^2$	0	0
$\|\alpha_4\|^2$	0	0
$\sigma^{SI} \times 10^9 [pb]$	0.004	0.003

TABLE 4.12: Shows the relic density of the LSP for each benchmark point. The difference between the LSP and the nLSP is also given. Finally, we give the probability of finding the given LSP in a particular flavour state. That is to say; we give $|\alpha_i|^2$ where $\widetilde{\chi}_{10} = \alpha_1 \widetilde{B} + \alpha_2 \widetilde{W} + \alpha_3 \widetilde{H}_1 + \alpha_4 \widetilde{H}_2$ and $\sum |\alpha_i|^2 = 1$. Dimensionful parameters are given in GeV except for the spin independent cross-section which is given in pb. The experimental limit for both of these points is $0.09 \times 10^{-9} pb$. Therefore, these points do not exceed the experimental limits.

required 105 GeV invariant mass and the production of the τ are on the edge of exclusion of the transverse mass limit. The b-type decays satisfy the experimental constraints for both points.

Quantity	BP7	BP8
$\Gamma\widetilde{\tau}_1$ [GeV]	3.30×10^{-3}	1.63×10^{-2}
BR $(\widetilde{\tau}_1^- \to \chi_{10}\tau^-)$ [%]	100	100
$\Gamma\widetilde{\mu}_R$ [GeV]	1.32×10^{-1}	1.67×10^{-1}
BR $(\widetilde{\mu}_R^- - \to \chi_{10}\mu^-)$ [%]	100	100
BR $(b \to s\,\gamma)$ [%]	0.032	0.032
BR $(B_s \to \mu^+\,\mu^-)$ [%]	2.97×10^{-7}	2.96×10^{-7}
$\Delta\frac{(g-2)_\mu}{2}$	1.42×10^{-9}	1.30×10^{-9}
$\Omega_{DM}h^2$	0.020	0.112
χ_{10} [GeV]	100	99
$\sigma_{q\bar{q}\to\chi_{10}\chi_{10}}$ [pb]	1.796×10^{-14}	3.562×10^{-14}
r_{max}	1.22	1.04
$\sqrt{s}$ [TeV]	13	13
Analysis	cms_sus_16_039	cms_sus_16_039
Signal Region	SR_A44	SR_A44
Ref.	[140]	[140]

TABLE 4.13: Shows branching ratios for lightest supersymmetric particles in the spectrum for BP7 and BP8. Only branching ratio greater than 1% are included. We also include some beyond the standard model observables BR $(b \to s\,\gamma)$, BR $(B_s \to \mu^+\,\mu^-)$, $\Delta\frac{(g-2)_\mu}{2}$, and $\Omega_{DM}h^2$, where $\Delta\frac{(g-2)_\mu}{2}$ is a calculation of the SUSY contribution beyond the standard model. The model successfully predicts the b decays discrepancy and satisfies the anomalous muon magnetic moment to 2σ. The relic density is too small and is therefore not ruled out phenomenologically. CheckMATE runs using 13 TeV and 8 TeV analyses rule out these points. Decay widths and masses are given in GeV and branching ratios are given in %.

4.5 No-scale SUGRA with non-zero A_0 (Case II)

In order to fully explore the parameter space we can also allow for non-zero values of A_0. Indeed, non-zero A_0 will serve to increase the Higgs boson mass, encouraging a better fit to the current experimental results. We therefore present a subsequent scan where we vary α between -0.016 and 0.016. These values were chosen by trial and error such that computer time would not be wasted by producing many points with large A_0 values breaking colour charge symmetry.

Analogously to the previous, we start by analysing the positive k values. Further to this analogy, we revert to the previous definition of the likelihood to emphasise the relic density as key constraint in this paradigm and highlight the fact that $g-2$ will not be satisfied for positive values of k.

4.5.1 Positive k (Scan 3)

Fig 4.12 shows the distribution of A_0 against k for both signs of μ. Interestingly, the shape of the two plots for the two signs of μ is quite different, with the $\mu < 0$ sign

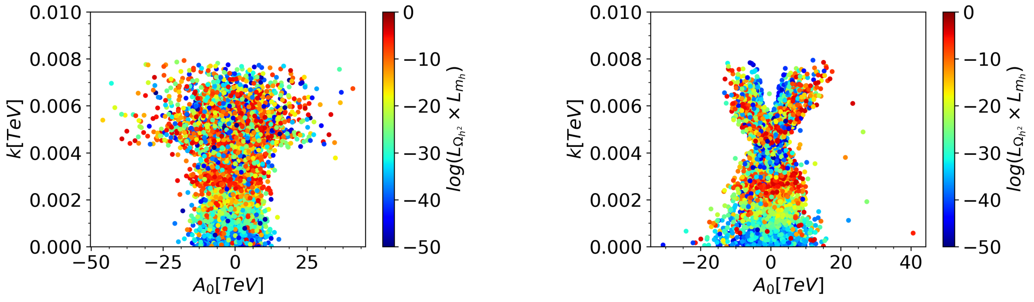

(A) $\mu < 0$, case II

(B) $\mu > 0$, case II

FIGURE 4.12: Shows the distribution of A_0 where case I data from a Monte-Carlo scan with parameter ranges $tan(\beta) \in [1.5, 50], k \in [0, 0.1]$, $\alpha \in [-0.166, 0.166]$, and $m_{\frac{3}{2}} \in [10^3 GeV, 10^6 GeV]$. Colour denotes likelihood, with hotter colours corresponding with high likelihoods. As before, the likelihood is dominated by the relic density calculation.

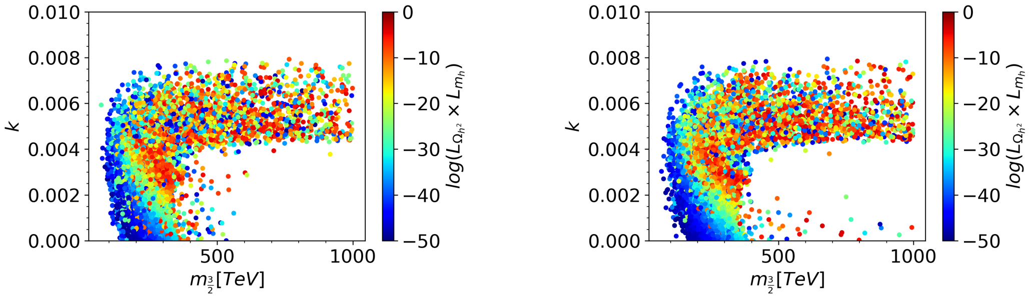

(A) $\mu < 0$, case II

(B) $\mu > 0$, case II

FIGURE 4.13: Shows k against $m_{\frac{3}{2}}$ where case II data from a Monte-Carlo scan with parameter ranges ranges $tan(\beta) \in [1.5, 50], k \in [0, 0.1]$, $\alpha \in [-0.166, 0.166]$, and $m_{\frac{3}{2}} \in [10^3 GeV, 10^6 GeV]$. Colour denotes likelihood, with hotter colours corresponding with high likelihoods. As before, the likelihood is dominated by the relic density calculation.

yielding a mushroom shaped distribution of points, while the $\mu > 0$ sign results in a wigwam shaped plot. However, there are some key features of both that are shared. In neither do we see any particular likelihood increase for non-0 A_0. This suggests that moving to case II will not give significant improvement compared to the previous case. Furthermore, in both we observe a preferred region of $k \approx 0.003$.

Fig 4.13 closely mirrors the structure of Fig 4.7b; with A_0 variation causing some spread in the likelihoods. The structure of LSP make-up as well as spectrum is generally similar. For this reason we refer you to the previous for detailed analysis. Furthermore, the density of points is greatly reduced as variation in A_0 produces many low-likelihood points. This does support claims of naturalness for the exclusively scaleless model previously presented. Although this scan was not truly exhaustive, no gains were made in terms of the overall likelihood.

As in case I with positive k, we see that no point can satisfy the higgs mass and $g-2$ simultaneously. The same is true of $g-2$ and the relic density. In order to achieve the correct higgs mass, $m_{\frac{3}{2}}$ must be at least 200TeV. This has the effect of increasing the slepton masses and thus decreasing Δa_μ. We therefore, turn our attention to $k < 0$ values.

4.5.2 Negative k (Scan 4)

As was previously argued, the inclusion of negative k values should allow for larger Higgs boson masses while keeping slepton masses low; thus incorporating a mechanism for generating the anomalous muon magnetic moment. As was done previously, we loosen the relic density constraint insisting only that the relic density is sufficiently small so as not to completely rule out the given point. Furthermore, we find large parts of the parameter space give the right handed stau state as the lightest sparticle. In Figures 4.14 to 4.16 we present results where the neutralino is the LSP. However, it is also interesting to consider potential R-parity violating models in which these light, charged particles decay into standard model particles. As was previously stated, a detailed discussion of the viability of such points is beyond the scope of this work, but we do include Figures 4.17 and 4.18 as these states can lead to excellent fits for a_μ.

Below we present the results of two scans (over positive and negative μ values). We limit the range of $m_{\frac{3}{2}}$ under the upper limit set by the starobinsky-like inflation limits previously discussed. This eliminates particularly massive gaugino states and thus large slepton mass states.

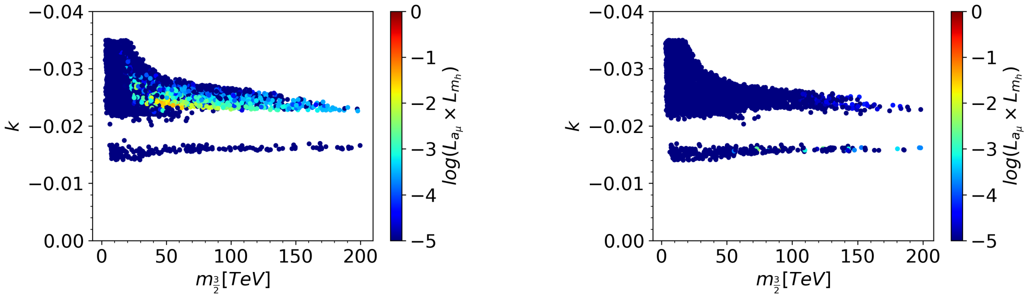

(A) $\mu < 0$, case II

(B) $\mu > 0$, case II

FIGURE 4.14: Shows the distribution of k against $m_{\frac{3}{2}}$ with a_μ and m_h log likelihood for $m_{\frac{3}{2}} \in [0TeV, 200TeV]$, $\alpha \in [-0.005, 0.005]$ and $k \in [-0.035, -0.014]$.

In both cases, two values of k are favoured by the scan. Analogously to case I, $k \approx -0.016$ and $k \approx -0.0023$ with the latter snf $\mu < 0$ representing a greater likelihood region of parameter space. This gives an approximate ratio of the high scale gaugino mass parameters as $|M_1| : |M_2| : |M_3| \approx 1 : 4 : 7$.

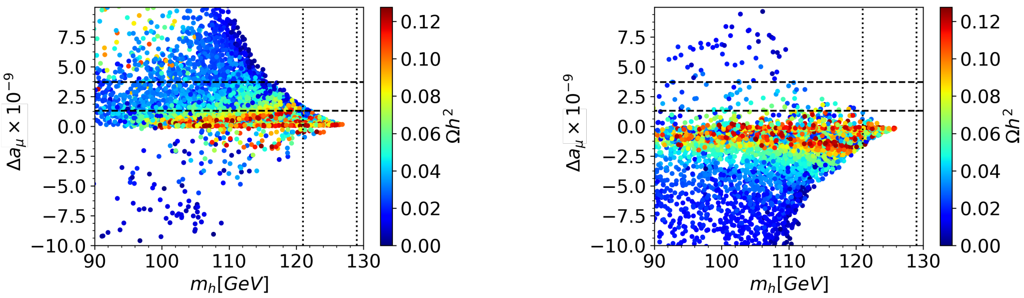

(A) $\mu < 0$, case II

(B) $\mu > 0$, case II

FIGURE 4.15: Shows a scatter plot of the higgs mass against the anomalous muon magnetic moment for a scan with ranges $m_{\frac{3}{2}} \in [0TeV, 200TeV]$, $\alpha \in [-0.005, 0.005]$ and $k \in [-0.035, -0.014]$. The 2σ region of a_μ is marked with dotted lines while the 2σ region of m_h is marked with dashed lines. The colour denotes the relic density.

From Fig. 4.15 and 4.16 we again see that $\mu < 0$ is favoured with a proportion of points sitting well within the 2σ range. We also observe that some points have a remarkably high relic density almost satisfying the 1σ region. This is a tantalising suggestion that this effectively scaleless model may be able to satisfy the higgs mass, relic density, and a_μ simultaneously. Having said this, the inclusion of A_0 does not give any discernible improvement in the allowed values of the Higgs boson mass due to the previously discussed natural tendency toward a scale-less model. However, these results are still included as the inclusion of a small A_0 parameter can modify the SUSY parameters sufficiently such that some points pass the `CheckMATE` collider constraints as presented in benchmark points 9 and 10 (Table 4.14).

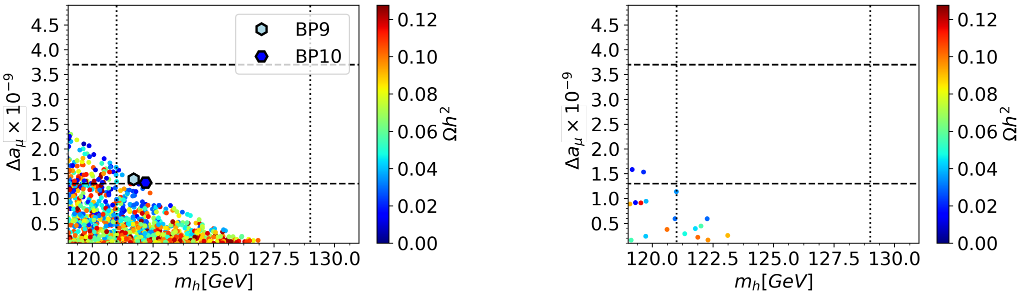

(A) $\mu < 0$, case II

(B) $\mu > 0$, case II

FIGURE 4.16: As for Fig 4.15 but zoomed in on the 3σ region for both a_μ and m_h. Two benchmark points (presented below are marked)

From Fig 4.17 we can see that allowing for these RPV parameter points slightly increases the a_μ values. Conversely to the previous, $\mu < 0$ now represents the higher likelihood points. As the stau is the lightest particle in the cases, no relic density can be calculated, and therefore we mark all points in blue to indicate this issue. Having said this, some parameter points perfectly attain the higgs mass and a_μ. For a discussion of the phenomenology of such points see [113].

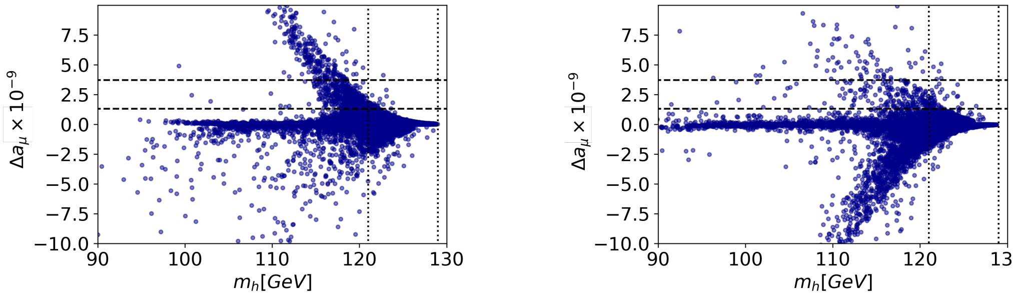

(A) $\mu < 0$, case II

(B) $\mu > 0$, case II

FIGURE 4.17: As for Fig 4.15 but where points that have charged LSP states are shown. Such states are marked in blue to indicate that no relic density could be calculated.

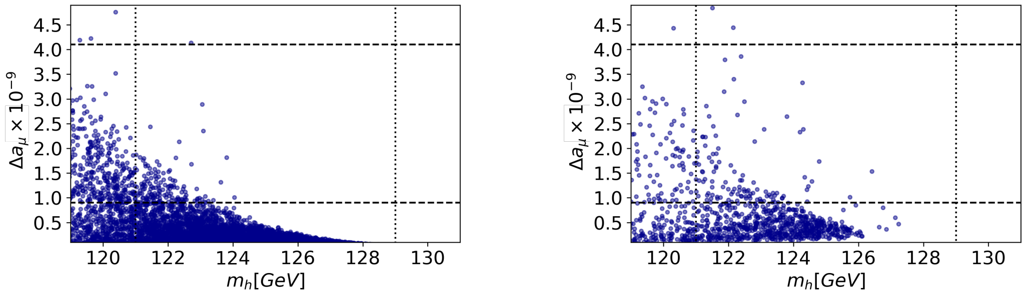

(A) $\mu < 0$, case II

(B) $\mu > 0$, case II

FIGURE 4.18: As for Fig 4.17 but zoomed in on the 3σ region for both a_μ and m_h.

We now present the two benchmark points plotted on Fig 4.16. Both were selected to represent a particularly high value of a_μ as well as interesting collider results.

Both benchmarks 9,10 have the same value of k as shown in Fig 4.12 where $k = -0.23$ had clear phenomenological advantages. Furthermore, the values of $m_{\frac{3}{2}}$ and $tan(\beta)$ are also approximately similar. They are both selected from the $\mu < 0$ scan due to its more promising phenomenology. In both cases $\beta \approx 1$ and α is very small. This is consistent with the no-scale model we are examining. The high scale gaugino mass parameters are also presented. After running to the low scale the ratio becomes far more extreme causing a great hierarchical divergence between the colour charged and the non-colour charged sparticles as can be seen below.

Table 4.15 shows the mass spectrum for the two benchmark points BP9, BP10. Large values of M_3 give large values of squark and gluon masses and contribute to the relatively large Higgs mass. Conversely, the smaller values of the other two gaugino mass parameters, in combination with the absence of m_0, gives the requisite small slepton states. Furthermore, the hierarchy between M_1 and M_2 gives a notable disparity between the right and left handed states. Due to the small value of $tan(\beta)$ and the negative sign of μ, $\widetilde{\tau}_1$ is predominantly right handed. We note the very light

Quantity	BP9	BP10
α	0.0007	0.0003
β	1	1
$m_{\frac{3}{2}}$ [TeV]	56	57
k	-0.023	-0.023
SPheno:		
m_0 [GeV]	0	0
$tan(\beta)$	10.5	10.0
$sign(\mu)$	-1	-1
A_0 [GeV]	-227	-109
M_1 [GeV]	-271	-271
M_2 [GeV]	-1144	-1163
M_3 [GeV]	-1841	-1877

TABLE 4.14: Shows two benchmark points representing two different areas of interest in the parameter space. We present the model parameters and the resultant SPheno input parameters. BP9 shows a point with high a_μ and BP10 shows a point with high Ω. Dimensions of the parameters are given. $m_{\frac{3}{2}}$ is given in units of TeV, and m_0, A_0, M_i are given in GeV.

smuon states that give key contributions to a_μ. Finally, the small value of M_1 leads to predominantly bino-like, light dark matter candidate.

Table 4.16 shows the key parameters for the relic density calculation for the two points BP9, BP10. As the stau is the nLSP, the mass difference between it and $\widetilde{\chi}_{10}$ is presented. As its mass gap is so small, the $\widetilde{\tau}$ plays a critical role in the mechanism for dark matter annihilation. Indeed the dominant decay channels contributing to the relic density calculation are $\widetilde{\tau}_1\,\widetilde{\tau}_1 \to \tau\,\tau$ and $\widetilde{\tau}_1\,\widetilde{\chi}_{10} \to \tau\,\gamma$. As the mass gap is especially small in the BP9, dark matter is over-annihilated by these channels leading to a relic density below the desired value. Both points have spin-independent cross-sections less than the experimental limits of $0.09 \times 10^9 pb$ as they are exclusively bino-like.

Table 4.17 shows the key collider and phenomenological findings resulting from these parameter points BP9, BP10. Both the nnLSP, $\widetilde{\mu}_R$, and the LSP $\widetilde{\tau}_1$, have short lifetimes with only one decay channel perhaps suggesting a strong collider signature. Indeed, the strongest signal region for both BP9 and BP10 is one that focuses on dileptonic final states with missing transverse energy in the context of "electroweakinos". Both b-type branching ratios are very well fitted in both cases. Furthermore, a_μ is within the 2σ region for BP9 and BP10. We see relatively high values of r calculated by CheckMATE due to the low mass sleptons.

Masses	BP9	BP10
$\widetilde{e}_L$	712	724
$\widetilde{e}_R$	139	140
$\widetilde{\nu}_{eL}$	708	719
$\widetilde{\mu}_L$	712	724
$\widetilde{\mu}_R$	139	140
$\widetilde{\nu}_{\mu L}$	708	719
$\widetilde{\tau}_1$	107	110
$\widetilde{\tau}_2$	712	724
$\widetilde{\nu}_{\tau L}$	706	717
$\widetilde{d}_L$	3360	3420
$\widetilde{d}_R$	3290	3350
$\widetilde{u}_L$	3360	3420
$\widetilde{u}_R$	3290	3350
$\widetilde{s}_L$	3360	3420
$\widetilde{s}_R$	3290	3350
$\widetilde{c}_L$	3360	3420
$\widetilde{c}_R$	3290	3350
$\widetilde{b}_1$	3120	3180
$\widetilde{b}_2$	3280	3340
$\widetilde{t}_1$	2800	2840
$\widetilde{t}_2$	3140	3190
$\widetilde{g}$	3850	3920
$\widetilde{\chi}_{10}$	103	103
$\widetilde{\chi}_{20}$	926	942
$\widetilde{\chi}_{30}$	2000	2050
$\widetilde{\chi}_{40}$	2000	2060
$\widetilde{\chi}_{1+}$	926	943
$\widetilde{\chi}_{2+}$	2009	2060
h_0	122	122
H_0	2110	2160
A_0	2110	2160
$H_\pm$	2110	2170
μ	-1870	-1930
B_0	-68	-46
$\widetilde{\tau}_1 - \widetilde{\chi}_{10}$	3.87	6.77

TABLE 4.15: Shows the spectrum of SUSY masses for the benchmark points given in Table 4.14. The difference between the mass of $\widetilde{\tau}_1$ and $\widetilde{\chi}_{10}$ is also given as this pertains to the production of dark matter. We also include the high scale bilinear coupling value B_0 for its relevance to the high scale parameters of the model. All parameters are given in GeV.

Quantity	BP9	BP10
$\Omega_{DM}h^2$	0.0397	0.020
$\widetilde{\chi}_{10}$ [GeV]	103	103
$\widetilde{\tau}_1 - \widetilde{\chi}_{10}$ [GeV]	3.87	6.77
$\lvert\alpha_1\rvert^2$	1	1
$\lvert\alpha_2\rvert^2$	0	0
$\lvert\alpha_3\rvert^2$	0	0
$\lvert\alpha_4\rvert^2$	0	0
$\sigma^{SI} \times 10^9 [pb]$	0.003	0.003

TABLE 4.16: Shows the relic density of the LSP for each benchmark point. The difference between the LSP and the nLSP is also given. Finally, we give the probability of finding the LSP in a particular flavour state. That is to say; we give $|\alpha_i|^2$ where $\widetilde{\chi}_{10} = \alpha_1 \widetilde{B} + \alpha_2 \widetilde{W} + \alpha_3 \widetilde{H}_1 + \alpha_4 \widetilde{H}_2$ and $\sum |\alpha_i|^2 = 1$. Dimensionful parameters are given in GeV except for the spin independent cross-section which is given in pb. The experimental limit for both of these points is $0.09 \times 10^9 pb$. Therefore, these points do not exceed the experimental limits.

Quantity	BP9	BP10
$\Gamma\widetilde{\tau}_1$ [Gev]	2.61×10^{-3}	8.18×10^{-3}
BR $(\widetilde{\tau}_1^- \to \chi_{10}\tau^-)$ [%]	100	100
$\Gamma\widetilde{\mu}_R$ [Gev]	1.47×10^{-1}	1.57×10^{-1}
BR $(\widetilde{\mu}_R^- - \to \chi_{10}\mu^-)$ [%]	100	100
BR $(b \to s\,\gamma)$ [%]	0.032	0.032
BR $(B_s \to \mu^+\,\mu^-)$ [%]	2.96×10^{-7}	2.95×10^{-7}
$\Delta\frac{(g-2)_\mu}{2}$	1.39×10^{-9}	1.32×10^{-9}
$\Omega_{DM}h^2$	0.0397	0.020
χ_{10} [Gev]	103	103
$\sigma_{q\bar{q}\to\chi_{10}\chi_{10}}$ [pb]	3.982×10^{-14}	2.290×10^{-14}
r_{max}	0.40	0.57
$\sqrt{s}$ [TeV]	13	13
Analysis	cms_sus_16_039	cms_sus_16_039
Signal Region	SR_A44	SR_A44
Ref.	[140]	[140]

TABLE 4.17: Shows branching ratios for lightest supersymmetric particles in the spectrum for BP7 and BP8. Only branching ratio greater than 1% are included. We also include some beyond the standard model observables BR $(b \to s\,\gamma)$, BR $(B_s \to \mu^+\,\mu^-)$, $\Delta\frac{(g-2)_\mu}{2}$, and $\Omega_{DM}h^2$, where $\Delta\frac{(g-2)_\mu}{2}$ is a calculation of the SUSY contribution beyond the standard model. The model successfully predicts the b decays discrepancy and satisfies the anomalous muon magnetic moment to $2/3\sigma$. The relic density is too small and is therefore not ruled out phenomenologically. CheckMATE runs using 13TeV and 8TeV analyses do not rule out these points. Decay widths and masses are given in GeV and branching ratios are given in %.

4.6 Conclusion

Inflation represents a very attractive solution to a number of cosmological problems and, in combination with supersymmetry, a very attractive model for Beyond the Standard Model physics emerges based on no-scale SUGRA. We have focussed on the particular case where the Polonyi term in the superpotential acts as a slow roll inflaton for Starobinsky inflation, leading to an upper bound on the gravitino mass $m_{3/2} < 1000$ TeV.

The recent Fermilab muon $g-2$ result further motivates a no-scale model, where all the dimensionful parameters the model are zero (except the gaugino masses which arise via mixed modulus and anomaly mediation), naturally leading to light slepton masses for certain gaugino masses. For negative universal gaugino masses, $k < 0$, we find relatively light bino/wino masses together with light sleptons, as suggested by the muon $g-2$ measurement. In general, such a model is also capable of providing a good dark matter candidate whilst satisfying constraints from collider physics, as well as yielding the correct Higgs boson mass, but it turns out to be non-trivial to achieve this while satisfying the desired muon $g-2$ constraints.

We have conducted a Monte Carlo parameter scan over the given model in two conditions: case I and case II, corresponding to zero or non-zero trilinear soft parameter A_0. We show that case I with $k > 0$ can give excellent fits for the Higgs boson mass and relic density whilst easily satisfying the collider and flavour constraints. Furthermore, with a reversal in the sign of k we show that $g-2$ can be satisfied to 2σ, as exemplified by BP7 and BP8, where BP8 also satisfies the desired relic density. Since BP7 and BP8 are on the edge of exclusion, with r_{max} values slightly above unity, this motivates the study of case II where we allow a non-zero A_0 trilinear soft parameter. By including a small A_0 parameter at the high scale, we find that muon $g-2$ can be satisfied whilst satisfying the collider constraints that threaten case I. However we find, while the case II benchmark points BP9 and BP10 satisfy the collider constraints and the muon $g-2$, they both predict a relic density which is below the desired value, which does not exclude these points of course, but is somewhat disappointing from the point of view of dark matter. Interestingly, we find that, in both cases, a large part of parameter space is dominated by RPV-style points, where the LSP becomes the lightest $\widetilde{\tau}$ state. Although such states are beyond the scope of this work, a detailed discussion of these kind of points can be found [113].

In general, we find that the lightest neutralino $\widetilde{\chi}_{10}$ should be a purely bino-like state with a mass of around 100 GeV for parameter points BP7-BP10 that satisfy the muon $g-2$ constraint. We highlight in particular the fully no-scale SUGRA point with zero A_0, B_0 and m_0, namely BP8, which can explain not only the recent Fermilab muon $g-2$ measurement, and has the correct Higgs boson mass, but also yields the desired dark matter relic density, albeit with $r_{max} = 1.04$ on the edge of exclusion. We remark that current LHC limits are more easily evaded due to right handed sleptons being almost degenerate with the neutralino LSP, while the left handed counterparts are much higher in mass, suppressing chargino decay channels into first and second generation sleptons. However, even for BP9 and BP10, the r_{max} value is not too far from unity, suggesting that future LHC runs are capable of discovering such SUSY particles for all the interesting benchmarks that satisfy the muon $g-2$.

In conclusion, no-scale SUGRA is not only well motivated theoretically from string theory and provides an elegant framework for accounting for cosmological Starobinsky inflation, but also has very interesting phenomenological implications as well. Ignoring the muon $g-2$ to begin with, and assuming positive universal gaugino mass contributions, in addition to the anomaly mediated contributions, we show that no-scale SUGRA can readily satisfy the dark matter and Higgs boson mass requirements, consistently with all other phenomenological constraints. We then show that the recent Fermilab measurement of the muon $g-2$ may be accommodated, together with the correct Higgs boson mass, for no-scale SUGRA with negative universal gaugino mass contributions in addition to the anomaly mediated contributions. For the fully no-scale SUGRA case, with all soft parameters equal to zero at the high scale, apart from gaugino masses, we find that successful points which satisfy the muon $g-2$, and can sometimes yield the desired relic density, although such points tend to be near the edge of LHC collider exclusion. Analysing no-scale SUGRA with a non-zero A_0, we find that the muon $g-2$ can still be explained, with the collider constraints somewhat relaxed. However, even in this case, light sleptons and charginos are still predicted, with good prospects for discovering these SUSY particles in LHC Run 3.

Chapter 5

Data-driven analysis of a SUSY GUT of flavour

5.1 Introduction

The Minimal Supersymmetric Standard Model (MSSM), introduced in Chapter 2.4, remains an appealing extension of the Standard Model of particle physics, as it provides solutions to the most prominent shortcomings of the latter. In addition to solving the hierarchy problem related to the mass of the Higgs boson [141, 142], the model includes a viable candidate for the observed Cold Dark Matter (CDM) in the Universe, namely the lightest of the four neutralinos. Furthermore, I discussed in Chapter 3.1 how the masses of the Standard Model neutrinos can be generated through the Seesaw mechanism [61–65] by including heavy right-handed neutrinos which can easily be implemented in the MSSM.

While collider searches for new physics have remained unsuccessful so far, additional information can be obtained from examining precision observables involving flavour transitions. For example, in the hadronic sector, the branching ratios of rare decays such as $b \to s\gamma$ are sensitive to new physics contributions, especially if they involve the NMFV paradigm discussed in Chapter 2.4.5, i.e. sources of flavour violation beyond the Cabbibo Kobayashi Maskawa (CKM) matrix [40, 41]. The same holds for the lepton sector [68, 69], where NMFV contributions can induce the branching ratios like $\mu \to e\gamma$ and $\mu \to 3e$, or $\mu - e$ conversion rates in nuclei. Flavour precision observables therefore provide an interesting handle towards the new physics spectrum, and in particular towards the underlying flavour structure.

Extensive studies have shown that the MSSM parameter space can accommodate NMFV in both the squark and the slepton sectors despite the numerous experimental and theoretical constraints [143–145]. In addition, NMFV may lead to specific collider signatures [146–156], weaken the current mass limits derived from the non-observation of superpartners [157–159], and, although to some lesser extend, affect the dark matter phenomenology [160–163].

As shown in Chapter 2.4.4 and, SUSY has great utility in the context of GUTs. Such a framework allows a unification of the gauge couplings at a scale of about 10^{16} GeV with better precision than the Standard Model alone [164]. In the same spirit, the soft breaking parameters related to squarks and sleptons stem from a common origin. In the most simple realisations this allows for the reduction of the number of parameters of the model. Starting from the imposed values at the GUT scale, the phenomenological aspects are obtained through renormalisation group running to the TeV scale, where the physical masses and related observables are computed.

The two aforementioned aspects are introduced in Chapter 3.2.2 where I address them by considering SUSY-GUTs including flavour symmetries, such as $SU(5) \times A_4$ [165] or $SU(5) \times S_4$ [166, 167], to cite only two examples. In such a situation, the flavour structure of the theory is defined at the GUT scale by the imposed symmetry. Renormalization group running then translates the GUT-scale structure into the observable mass spectrum at the TeV scale. The TeV-scale phenomenology thus inherits a footprint of the imposed flavour structure at the GUT scale.

In a previous study [168], some of the authors have explored the phenomenology of NMFV within a $SU(5) \times A_4$ implementation of the MSSM suggested first in Ref. [165]. Based on the variation of the NMFV parameters around a MFV reference scenario taken from Ref. [165], it has been shown that these parameters need to be varied simultaneously in order to cover all phenomenological aspects, in particular since cancellations between different contributions may occur. Moreover, it has been demonstrated that a model may feature a reasonable amount of flavour violation while satisfying the stringent constraints of rare decays such as $b \to s\gamma$ or $\mu \to e\gamma$. It is therefore interesting to pursue the study of GUT implementations of flavour violation, e.g., via flavour symmetries, in the context of low-energy and precision constraints as well as TeV-scale phenomenology.

In the present document, I shall focus on the case of $SU(5)$ unification combined with an S_4 flavour symmetry, as suggested by one of the authors in Refs. [166, 167]. In a similar way as in Ref. [168], I will explore in detail the TeV-scale aspects of this model, including observables related to flavour violation and dark matter phenomenology. More precisely, in this study, we aim at a complete exploration of the associated parameters, i.e. including a variation of all relevant parameters at the GUT scale. For the sake of an efficient exploration, I make use of the Markov Chain Monte Carlo technique [169–171].

The Chapter is organised as follows. In Section 5.2, I review the assumed model. Section 5.3 is dedicated to the discussion of the Markov Chain Monte Carlo algorithm that I employ to efficiently explore the model parameter space. Results are then presented in Section 5.4. Our conclusions are given in Section 5.5.

5.2 The Model

5.2.1 Fields and symmetries

The model developed in Refs. [166, 167, 172, 173] is based on the grand unifying group $SU(5)$ combined with an S_4 family symmetry, and supplemented by a $U(1)$ symmetry. The left-handed quarks and leptons are unified into the representations $\bar{\mathbf{5}}$, $\mathbf{10}$ of $SU(5)$ and $\mathbf{1}$ for the right-handed neutrino as given in Equation 3.12. The three families are controlled by a family symmetry S_4, with F and N each forming a triplet and the first two families of T forming a doublet, while the third family T_3 (containing the top quark) is a singlet, as summarised in Table 5.1. The choice of the third family T_3 being a singlet, permits a renormalisable top quark Yukawa coupling to the singlet Higgs discussed below.

The S_4 singlet Higgs fields $H_{\mathbf{5}}$, $H_{\bar{\mathbf{5}}}$ and $H_{\overline{\mathbf{45}}}$, each contain a doublet $SU(2)_L \times U(1)_Y$ representation that eventually form the standard up (H_u) and down (H_d) Higgses of the MSSM (where the H_d emerges as a linear combination of doublets from the $H_{\bar{\mathbf{5}}}$ and $H_{\overline{\mathbf{45}}}$) [174].[1] The VEVs of the two neutral Higgs fields are

$$v_u = \frac{v}{\sqrt{1+t_\beta^2}}\, t_\beta, \qquad v_d = \frac{v}{\sqrt{1+t_\beta^2}}, \tag{5.2.1}$$

where $t_\beta \equiv \tan(\beta) = \frac{v_u}{v_d}$ and $v = \sqrt{v_u^2 + v_d^2} \approx 246$ GeV.

Just below the $SU(5)$ breaking scale to the usual SM gauge group, the flavour symmetry is broken by the VEVs of some new fields: the flavons, Φ_ρ^f, which are

---

[1] As $H_{\bar{\mathbf{5}}}$ and $H_{\overline{\mathbf{45}}}$ transform differently under $U(1)$, it is clear that the mechanism which spawns the low energy Higgs doublet H_d must necessarily break $U(1)$. Although the discussion of any details of the $SU(5)$ GUT symmetry breaking (which, e.g., could even have an extra dimensional origin) are beyond the scope of our work, I remark that a mixing of $H_{\bar{\mathbf{5}}}$ and $H_{\overline{\mathbf{45}}}$ could be induced by introducing the pair $H_{\mathbf{24}}^{\pm}$ with $U(1)$ charges ±1 in addition to the standard $SU(5)$ breaking Higgs $H_{\mathbf{24}}^0$.

Field	T_3	T	F	N	H_5	$H_{\bar{5}}$	$H_{\overline{45}}$	Φ_2^u	$\widetilde{\Phi}_2^u$	Φ_3^d	$\widetilde{\Phi}_3^d$	Φ_2^d	$\Phi_{3'}^\nu$	Φ_2^ν	Φ_1^ν	η
$SU(5)$	**10**	**10**	$\bar{\mathbf{5}}$	**1**	**5**	$\bar{\mathbf{5}}$	$\overline{\mathbf{45}}$	**1**	**1**	**1**	**1**	**1**	**1**	**1**	**1**	**1**
S_4	**1**	**2**	**3**	**3**	**1**	**1**	**1**	**2**	**2**	**3**	**3**	**2**	$\mathbf{3}'$	**2**	**1**	$\mathbf{1}'$
$U(1)$	0	5	4	-4	0	0	1	-10	0	-4	-11	1	8	8	8	7

TABLE 5.1: Field content of the model and associated charges and representations.

labelled by the corresponding S_4 representation ρ as well as the fermion sector f to which they couple at leading order (LO). Two flavons, Φ_2^u and $\tilde{\Phi}_2^u$, generate the LO up-type quark mass matrix. Three flavon multiplets, Φ_3^d, $\tilde{\Phi}_3^d$ and Φ_2^d, are responsible for the down-type quark and charged lepton mass matrices. Finally, the right-handed neutrino mass matrix is generated from the flavon multiplets $\Phi_{3'}^\nu$, Φ_2^ν and Φ_1^ν as well as the flavon η which is responsible for breaking the tri-bimaximal pattern of the neutrino mass matrix to a trimaximal one at subleading order. An additional $U(1)$ symmetry must be introduced in order to control the coupling of the flavon fields to the matter fields in a way which avoids significant perturbations of the flavour structure by higher-dimensional operators.

5.2.2 Flavon alignments

The vacuum alignment of the flavon fields is achieved by coupling them to a set of so-called driving fields and requiring the F-terms of the latter to vanish. These driving fields, whose transformation properties under the family symmetry are discussed in Refs. [166, 167, 172, 173], are SM gauge singlets and carry a charge of $+2$ under a continuous R-symmetry. The flavons and the GUT Higgs fields are uncharged under this $U(1)_R$, whereas the supermultiplets containing the SM fermions (or right-handed neutrinos) have charge $+1$. As the superpotential must have a $U(1)_R$ charge of $+2$, the driving fields can only appear linearly and cannot have any direct interactions with the SM fermions or the right-handed neutrinos.

Using the driving fields, the flavour superpotential may be constructed, resulting in the following vacuum alignments (for details see Refs. [172, 173]),

$$\frac{\langle\Phi_2^u\rangle}{M} = \begin{pmatrix} 0 \\ 1 \end{pmatrix} \phi_2^u\,\lambda^4, \qquad \frac{\langle\tilde{\Phi}_2^u\rangle}{M} = \begin{pmatrix} 0 \\ 1 \end{pmatrix} \tilde{\phi}_2^u\,\lambda^4, \tag{5.2.2}$$

$$\frac{\langle\Phi_3^d\rangle}{M} = \begin{pmatrix} 0 \\ 1 \\ 0 \end{pmatrix} \phi_3^d\,\lambda^2, \qquad \frac{\langle\tilde{\Phi}_3^d\rangle}{M} = \begin{pmatrix} 0 \\ -1 \\ 1 \end{pmatrix} \tilde{\phi}_3^d\,\lambda^3, \qquad \frac{\langle\Phi_2^d\rangle}{M} = \begin{pmatrix} 1 \\ 0 \end{pmatrix} \phi_2^d\,\lambda\,, \tag{5.2.3}$$

$$\frac{\langle\Phi_{3'}^\nu\rangle}{M} = \begin{pmatrix} 1 \\ 1 \\ 1 \end{pmatrix} \phi_{3'}^\nu\,\lambda^4, \qquad \frac{\langle\Phi_2^\nu\rangle}{M} = \begin{pmatrix} 1 \\ 1 \end{pmatrix} \phi_2^\nu\,\lambda^4, \qquad \frac{\langle\Phi_1^\nu\rangle}{M} = \phi_1^\nu\,\lambda^4, \qquad \frac{\langle\eta\rangle}{M} = \phi^\eta\,\lambda^4 \tag{5.2.4}$$

where $\lambda = 0.22$ is approximately equal to the Wolfenstein parameter [175] and the ϕ's are dimensionless order one parameters. Imposing CP-symmetry of the underlying theory [176], all coupling constants can be taken real, so that CP is broken spontaneously by generally complex values for the ϕs. M denotes a generic messenger scale which is common to all the non-renormalisable effective operators and assumed to be around the scale of grand unification.

5.2.3 Yukawa matrices

Because of the non-trivial structure of the Kähler potential, non-canonical kinetic terms are generated. For a proper analysis of the flavour structure, one needs to perform a canonical normalisation (CN) operation, swapping the misalignment of the kinetic terms to the superpotential. Therefore, in the model proposed in Refs. [166, 167, 172, 173], contributions to the flavour texture from both the superpotential and the Kähler potential are taken into account. In this subsection, I shall begin by ignoring such corrections, and also only consider the leading order Yukawa operators, in order to clearly illustrate the origin of the flavour structure in the model. However, all such corrections are taken into account in the phenomenological treatment of the Yukawa matrices in the following subsection. I remark that the model is highly predictive, as the parameters entering the flavour structure are expected to be of $O(1)$ but the overall flavour texture is provided as a function of the expansion parameter $\lambda = 0.22$.

5.2.3.1 Up-type quarks

The Yukawa matrix of the up-type quarks can be constructed by considering all the possible combinations of a product of flavons with TTH_5 for the upper-left 2×2 block, with TT_3H_5 for the $(i3)$ elements, and with $T_3T_3H_5$ for the (33) element. The most important operators which generate a contribution to the Yukawa matrix of order up to and including λ^8 are

$$y_t T_3 T_3 H_5 + \frac{1}{M} y_1^u TT\Phi_2^u H_5 + \frac{1}{M^2} y_2^u TT\Phi_2^u \tilde{\Phi}_2^u H_5 \,, \tag{5.2.5}$$

where the parameters y_t and y_i^u are real order one coefficients. Inserting the flavon VEVs and expanding the S_4 contractions of Eq. (5.2.5), with TT and $\Phi_2^u\tilde{\Phi}_2^u$ each combined into a doublet using the Clebsch-Gordan coefficients [172, 173], yields the up-type Yukawa matrix at the GUT scale

$$\mathcal{Y}^u_{\mathrm{GUT}} \approx \begin{pmatrix} y_u e^{i\theta_u^y}\lambda^8 & 0 & 0 \\ 0 & y_c e^{i\theta_c^y}\lambda^4 & 0 \\ 0 & 0 & y_t \end{pmatrix} , \tag{5.2.6}$$

where the relation to the flavon VEVs, see Eqs. (5.2.2) – (5.2.4), is given by

$$y_u e^{i\theta_u^y} = y_2^u \phi_2^u \tilde{\phi}_2^u \,, \qquad y_c\, e^{i\theta_c^y} = y_1^u \phi_2^u \,. \tag{5.2.7}$$

5.2.3.2 Down-type quarks and charged leptons

The Yukawa matrices of the down-type quarks and the charged leptons can be deduced from the leading superpotential operators

$$y_1^d \frac{1}{M} F T_3 \Phi_3^d H_{\bar{5}} + y_2^d \frac{1}{M^2} (F \tilde{\Phi}_3^d)_{\mathbf{1}} (T \Phi_2^d)_{\mathbf{1}} H_{\overline{45}} + y_3^d \frac{1}{M^3} (F (\Phi_2^d)^2)_{\mathbf{3}} (T \tilde{\Phi}_3^d)_{\mathbf{3}} H_{\bar{5}} \,, \tag{5.2.8}$$

where the y_i^d are real order one coefficients. For the operators proportional to y_2^d and y_3^d, specific S_4 contractions indicated by $(\cdots)_{\mathbf{1}}$ and $(\cdots)_{\mathbf{3}}$ have been chosen (justified by messenger arguments) such that the Gatto-Sartori-Tonin (GST) [177] and Georgi-Jarlskog (GJ) [178] relations are satisfied. Separating the contributions of $H_{\bar{\mathbf{5}}}$ and $H_{\overline{\mathbf{45}}}$, the S_4 contractions give rise to

$$\mathcal{Y}_{\bar{\mathbf{5}}} \approx \begin{pmatrix} 0 & \tilde{x}_2 e^{i\theta_2^{\tilde{x}}} \lambda^5 & -\tilde{x}_2 e^{i\theta_2^{\tilde{x}}} \lambda^5 \\ -\tilde{x}_2 e^{i\theta_2^{\tilde{x}}} \lambda^5 & 0 & \tilde{x}_2 e^{i\theta_2^{\tilde{x}}} \lambda^5 \\ 0 & 0 & y_b e^{i\theta_b^y} \lambda^2 \end{pmatrix} , \quad \mathcal{Y}_{\overline{\mathbf{45}}} \approx \begin{pmatrix} 0 & 0 & 0 \\ 0 & y_s e^{i\theta_s^y} \lambda^4 & -y_s e^{i\theta_s^y} \lambda^4 \\ 0 & 0 & 0 \end{pmatrix} . \tag{5.2.9}$$

The parameters in these expressions are related to the flavon VEVs as defined in Eqs. (5.2.2)–(5.2.4) via

$$y_b e^{i\theta_b^y} = y_1^d \phi_3^d \,, \quad y_s e^{i\theta_s^y} = y_2^d \phi_2^d \tilde{\phi}_3^d, \,, \quad \tilde{x}_2 e^{i\theta_2^{\tilde{x}}} = y_3^d (\phi_2^d)^2 \tilde{\phi}_3^d \,. \tag{5.2.10}$$

The Yukawa matrices of the down-type quarks and the charged leptons are linear combinations of the two structures in Eq. (5.2.9). Following the construction proposed by Georgi and Jarlskog, we have $\mathcal{Y}^d_{\text{GUT}} = \mathcal{Y}_{\bar{5}} + \mathcal{Y}_{\overline{45}}, \quad \mathcal{Y}^e_{\text{GUT}} = (\mathcal{Y}_{\bar{5}} - 3\mathcal{Y}_{\overline{45}})^T$. CKM mixing is dominated by the diagonalisation of the down-type quark Yukawa matrix. Note that in some models it is possible to go beyond the simple case $m_b = m_\tau$ at the GUT scale, by including larger Higgs representations [179, 180].

5.2.3.3 Neutrinos

The neutrino masses originate from a standard Supersymmetric Type I Seesaw mechanism, where the heavy right-handed fields, N, are turning the tiny observed neutrino effective Yukawa couplings into natural parameters. The Lagrangian for the neutrino sector is therefore given by

$$\mathcal{L}_\nu \supset (\mathcal{Y}^\nu)_{ij} \overline{L}_i H_u N_j + (\mathcal{M}_R)_{ij} N_i N_j \,, \tag{5.2.11}$$

where $\mathcal{Y}_\nu$ is the Dirac Yukawa coupling and $\mathcal{M}_R$ is the right-handed Majorana mass matrix.

The Dirac coupling of the right-handed neutrinos N to the left-handed SM neutrinos is dominated by the superpotential term

$$y_D F N H_5 \tag{5.2.12}$$

where y_D is a real order one parameter. The corresponding Yukawa matrix is determined as

$$\mathcal{Y}^\nu \approx \begin{pmatrix} y_D & 0 & 0 \\ 0 & 0 & y_D \\ 0 & y_D & 0 \end{pmatrix}, \tag{5.2.13}$$

The mass matrix of the right-handed neutrinos is obtained from the superpotential terms

$$w_{1,2,3} N N \Phi^\nu_{1,2,3'} + w_4 \frac{1}{M} N N \Phi^d_2 \eta \,, \tag{5.2.14}$$

where w_i denote real order one coefficients. This results in a right-handed Majorana neutrino mass matrix $\mathcal{M}_R$ of the form

$$\frac{\mathcal{M}_R}{M} \approx \begin{pmatrix} A+2C & B-C & B-C \\ B-C & B+2C & A-C \\ B-C & A-C & B+2C \end{pmatrix} e^{i\theta_A}\lambda^4 + \begin{pmatrix} 0 & 0 & D \\ 0 & D & 0 \\ D & 0 & 0 \end{pmatrix} e^{i\theta_D}\lambda^5 \tag{5.2.15}$$

with

$$A e^{i\theta_A} = w_1 \phi^\nu_1 \,, \quad B e^{i\theta_A} = w_2 \phi^\nu_2 \,, \quad C e^{i\theta_A} = w_3 \phi^\nu_{3'} \,, \quad D e^{i\theta_D} = w_4 \, \eta \, \phi^d_2 \,. \tag{5.2.16}$$

The first matrix of Eq. (5.2.15) arises from terms involving only $\Phi^\nu_{1,2,3'}$. As their VEVs respect the tri-bimaximal (TB) Klein symmetry $Z_2^S \times Z_2^U \subset S_4$, this part is of TB form. The second matrix of Eq. (5.2.15), proportional to D, is due to the operator $w_4 \frac{1}{M} N N \Phi^d_2 \eta$ which breaks the Z_2^U at a relative order of λ, while preserving the Z_2^S. The resulting trimaximal TM_2 structure can accommodate the sizable value of the reactor neutrino mixing angle θ^l_{13}.

It is instructive to show the effective light neutrino mass matrix which arises via the type I seesaw mechanism, and has the form

$$m^{\rm eff}_\nu \approx \frac{y_D^2 v_u^2}{\lambda^4 M} \left[\begin{pmatrix} b^\nu + c^\nu - a^\nu & a^\nu & a^\nu \\ a^\nu & b^\nu & c^\nu \\ a^\nu & c^\nu & b^\nu \end{pmatrix} e^{-i\theta_A} + \begin{pmatrix} 0 & 0 & d^\nu \\ 0 & d^\nu & 0 \\ d^\nu & 0 & 0 \end{pmatrix} \lambda \, e^{i(\theta_D - 2\theta_A)} \right] \tag{5.2.17}$$

with a^ν, b^ν, c^ν and d^ν being functions of the real parameters A, B, C and D. The deviation from tri-bimaximal neutrino mixing is controlled by $d^\nu \propto D$. Due to the three independent input parameters ($w_1 \propto A$, $w_2 \propto B$, $w_3 \propto C$), any neutrino mass spectrum can be accommodated in this model. Note that this expression, while generally providing a good estimation of the effective neutrino mass matrix, is only an approximation valid at order λ. Therefore, it does not strictly hold when considering a potential $O(10)$ D-parameter as we do in the numerical analysis which requires a more rigorous treatment.

5.2.4 Phenomenological Yukawa couplings at the GUT scale

The true model predictions at the high scale differ from those shown previously, since they also involve other higher order corrections to the Yukawa terms, and one must also include the effects of canonical normalisation (CN) leading to the matrices in Ref. [167]. For simplicity, while keeping the phenomenology indistinguishable from the constructed model, we allow for minor approximations, and here we summarise the form of the Yukawa matrices that we actually assume at the GUT scale.

Concerning the up-type quark Yukawa matrix, we shall continue to take it to be diagonal as the off-diagonal entries are much more λ suppressed than the diagonal ones. We may also absorb the phases into a redefinition of the fields.

Since the CKM matrix is controlled by the down-type quark Yukawa matrix, we shall include some of the higher-order terms and some of the effects of CN, in order to obtain a perfect fit to quark data. Therefore there are some corrections to the GST relations.

The charged lepton Yukawa matrix is, like in any standard $SU(5)$ model, closely related to the down-quark Yukawa matrix as per $Y_\ell \simeq Y_d^T$, together with a modified via the GJ mechanism through the incorporation of $\mathbf{\bar{45}}$ and $\mathbf{\bar{5}}$ Higgs representations in order to generate a more reasonable relation between m_s and m_μ.

The explicit Yukawa matrices we will use for the charged fermionic sector are therefore provided by the following expressions:

$$
\begin{aligned}
Y_u &= \begin{pmatrix} y_u\lambda^8 & 0 & 0 \\ 0 & y_c\lambda^4 & 0 \\ 0 & 0 & y_t \end{pmatrix} , \\
Y_d &= \begin{pmatrix} z_1^d\lambda^8\, e^{-i\delta} & x_2\lambda^5 & -x_2\lambda^5\, e^{i\delta} \\ -x_2\lambda^5 & y_s\lambda^4\, e^{-i\theta_2^d} & -y_s\lambda^4\, e^{2i(\theta_2^d+\theta_3^d)} + x_2\lambda^5 e^{3i(\theta_2^d+\theta_3^d)} \\ (z_3^d\, e^{-i\theta_2^d} - \frac{1}{2}K_3 y_b\, e^{-i\delta})\lambda^6 & (z_2^d\, e^{-i\theta_2^d} - \frac{1}{2}K_3 y_b\, e^{-i\delta})\lambda^6 & y_b\lambda^2 \end{pmatrix} , \\
Y_\ell &= \begin{pmatrix} -3z_1^d\lambda^8\, e^{-i\delta} & -x_2\lambda^5 & (z_3^d\, e^{-i\theta_2^d} - \frac{1}{2}K_3 y_b\, e^{-i\delta})\lambda^6 \\ x_2\lambda^5 & -3y_s\lambda^4\, e^{-i\theta_2^d} & (z_2^d\, e^{-i\theta_2^d} - \frac{1}{2}K_3 y_b\, e^{-i\delta})\lambda^6 \\ -x_2\lambda^5\, e^{i\delta} & 3y_s\lambda^4\, e^{2i(\theta_2^d+\theta_3^d)} + x_2\lambda^5 e^{3i(\theta_2^d+\theta_3^d)} & y_b\lambda^2 \end{pmatrix} ,
\end{aligned}
\tag{5.2.18}
$$

where $\delta = 2\theta_2^d + 3\theta_3^d$, and θ_ρ^d ($\rho = 2, 3$) corresponds to the phase of a ρ-representation flavon in the original model. Note that our analysis, including the soft masses discussed below, relies only on the two phases θ_2^d and θ_3^d. The up-type quark Yukawa has been approximated with respect to Ref. [167].

In the neutrino sector, the effects of CN are negligible, and we therefore take these matrices to have the same form as given previously,

$$
\frac{M_R}{M_{GUT}} = \begin{pmatrix} A+2C & B-C & B-C \\ B-C & B+2C & A-C \\ B-C & A-C & B+2C \end{pmatrix} \lambda^4\, e^{-2i\theta_3^d} + \begin{pmatrix} 0 & 0 & D \\ 0 & D & 0 \\ D & 0 & 0 \end{pmatrix} \lambda^5\, e^{i(4\theta_2^d-\theta_3^d)} . \tag{5.2.19}
$$

The Dirac neutrino coupling, neglecting the $O(\lambda^4)$ terms, compared to the original paper [167], that is also of the form given in the previous subsection,

$$
Y_\nu = \begin{pmatrix} y_D & 0 & 0 \\ 0 & 0 & y_D \\ 0 & y_D & 0 \end{pmatrix} . \tag{5.2.20}
$$

5.2.5 SUSY breaking terms

We now consider the SUSY breaking sector of the low energy scale MSSM generated after integrating out the heavy degrees of freedom. In the context of the standard phenomenological R-parity conserving MSSM, the soft Lagrangian is parametrised as in Equation 2.8, but with an additional neutrino soft mass term of the form $-\tilde{\nu}^\dagger m_\nu^2 \tilde{\nu}$. Assuming that the SUSY breaking is controlled by some hidden sector mediated by a superfield X, the soft parameters described in Equation 2.8 are generated when X

develops a VEV in its F-term at the SUSY breaking scale. Furthermore, we consider that the SUSY breaking mechanism is independent of the flavour breaking one.

The new flavour structure arising from the SUSY breaking sector is also controlled by the flavour symmetry, in a similar fashion as the SM texture is. Extracting the results from Ref. [167], we first summarise the predictions for the soft trilinear terms A_f,

$$
\begin{aligned}
\frac{A^u_{GUT}}{A_0} &\simeq \begin{pmatrix} a_u\lambda^8 & 0 & 0 \\ 0 & a_c\lambda^4 & \\ 0 & 0 & a_t \end{pmatrix} , \\
\frac{A^d_{GUT}}{A_0} &\simeq \begin{pmatrix} z_1^{d_a}\lambda^8 & \widetilde{x}_2^a\lambda^5 & -\widetilde{x}_2^a\lambda^5 \\ -\widetilde{x}_2^a\lambda^5 & a_s\lambda^4 & -a_s\lambda^4 \\ (z_3^{d_a} - \frac{K_3 a_b}{2})\lambda^6 & (z_2^{d_a} - \frac{K_3 a_b}{2})\lambda^6 & a_b\lambda^2 \end{pmatrix} , \\
\frac{A^e_{GUT}}{A_0} &\simeq \begin{pmatrix} -3a_d\lambda^8 & -\widetilde{x}_2^a\lambda^5 & (z_3^{d_a} - \frac{K_3 a_b}{2})\lambda^6 \\ \widetilde{x}_2^a & -3a_s\lambda^4 & (z_2^{d_a} - \frac{K_3 a_b}{2})\lambda^6 \\ -\widetilde{x}_2^a\lambda^5 & 3a_s\lambda^4 & a_b\lambda^2 \end{pmatrix} , \\
\frac{A^\nu_{GUT}}{A_0} &\simeq \begin{pmatrix} a_D & 0 & 0 \\ 0 & 0 & a_D \\ 0 & a_D & 0 \end{pmatrix} .
\end{aligned}
\tag{5.2.21}
$$

The trilinear soft couplings exhibits the same structure as the Yukawa terms, except that the $O(1)$ parameters and phases are now different. This is expected since the trilinear terms are projected out from the Yukawa terms when the superfield X acquires its VEV, breaking the different supermultiplets. Therefore, we can use the same approximations as the ones considered for the Yukawa couplings. Furthermore, for simplicity, we neglect all additional CP-violating phases that may appear in the soft terms.

Similarly, we summarise the results on the soft scalar mass matrices,

$$
\begin{aligned}
M_T^2 &\simeq m_0^2 \begin{pmatrix} b_{01} & (b_2 - b_{01}k_2)\lambda^4 & (b_4 - \frac{k_4(b_{01}-b_{02})}{2})e^{-i\theta_{4k}}\lambda^6 \\ \cdot & b_{01} & (b_3 - \frac{k_3(b_{01}-b_{02})}{2})e^{-i\theta_{3k}}\lambda^5 \\ \cdot & \cdot & b_{02} \end{pmatrix} , \\
M_{F(N)}^2 &\simeq m_0^2 \begin{pmatrix} B_0^{(N)} & (B_3^{(N)} - K_3^{(N)})\lambda^4 & (B_3^{(N)} - K_3^{(N)})\lambda^4 \\ \cdot & B_0^{(N)} & (B_3^{(N)} - K_3^{(N)})\lambda^4 \\ \cdot & \cdot & B_0^{(N)} \end{pmatrix} ,
\end{aligned}
\tag{5.2.22}
$$

where N is the right handed sneutrino term, $\theta_{3k} = -5\theta_2^d$ and $\theta_{4k} = \theta_3^d - \theta_2^d$. Because of the unification, all the sfermion soft matrices are linked to the soft matrix of the $SU(5)$

representation they belong to.

5.3 Data-driven model exploration

5.3.1 Algorithm

The full analysis of the parameter space relies on a Markov-Chain Monte Carlo technique [171], and more specifically the Metropolis-Hastings algorithm [169, 170]. This technique allows one to perform a sophisticated data-driven exploration of an high-dimension parameter space. The idea behind the algorithm is to estimate the likelihood $\mathcal{L}$ of a given set of parameter values $\vec{\theta}$ with respect to the set of observables $\vec{O}$. For simplicity and the rest of the analysis we assume that the observables are not correlated, i.e.

$$\mathcal{L}(\vec{\theta},\vec{O},\vec{\sigma}) = \prod_i \mathcal{L}_i(\vec{\theta},O_i,\sigma_i), \tag{5.3.23}$$

where σ_i is the uncertainty associated to the observable O_i.

Successively, random values of the parameters, picked around the previous ones, are evaluated at each iteration. In our implementation, the new proposed parameter value θ^{n+1} is obtained through a Gaussian jump,

$$\theta_i^{n+1} = \mathcal{G}\left(\theta_i^n,\, \kappa(\theta_i^{\max} - \theta_i^{\min})\right)\,, \tag{5.3.24}$$

where $\mathcal{G}\,(a,b)$ is a Gaussian distribution centered around a with width b, κ is a parameter that needs to be tuned empirically for the algorithm and $\theta_i^{\max}$ and $\theta_i^{\min}$ stands for the extrema values of the θ_i considered range.

If $\mathcal{L}^{n+1}(\vec{\theta}^{n+1},\vec{O},\vec{\sigma}) > \mathcal{L}^n(\vec{\theta}^n,\vec{O},\vec{\sigma})$, the point is accepted and the chain continues from this point. Otherwise, the new point is accepted with probability

$$p = \frac{\mathcal{L}^{n+1}(\vec{\theta}^{n+1},\vec{O},\vec{\sigma})}{\mathcal{L}^n(\vec{\theta}^n,\vec{O},\vec{\sigma})} \tag{5.3.25}$$

This avoids falling into local minima, and thus ensures complete parameter space exploration. In practice, we randomly choose a number $\mu \in [0,1]$ such that the test succeeds if $\mu < p$. Otherwise, the point is rejected, and we reevaluate the step $n+1$ for another proposal set of parameters deduced from step n. Within this framework, the algorithm can move across larger regions while still converging to highest likelihood regions.

In high-dimensional parameter space, the quality of the exploration relies more on the total of chain numbers than the length of the chain themselves. Indeed, different

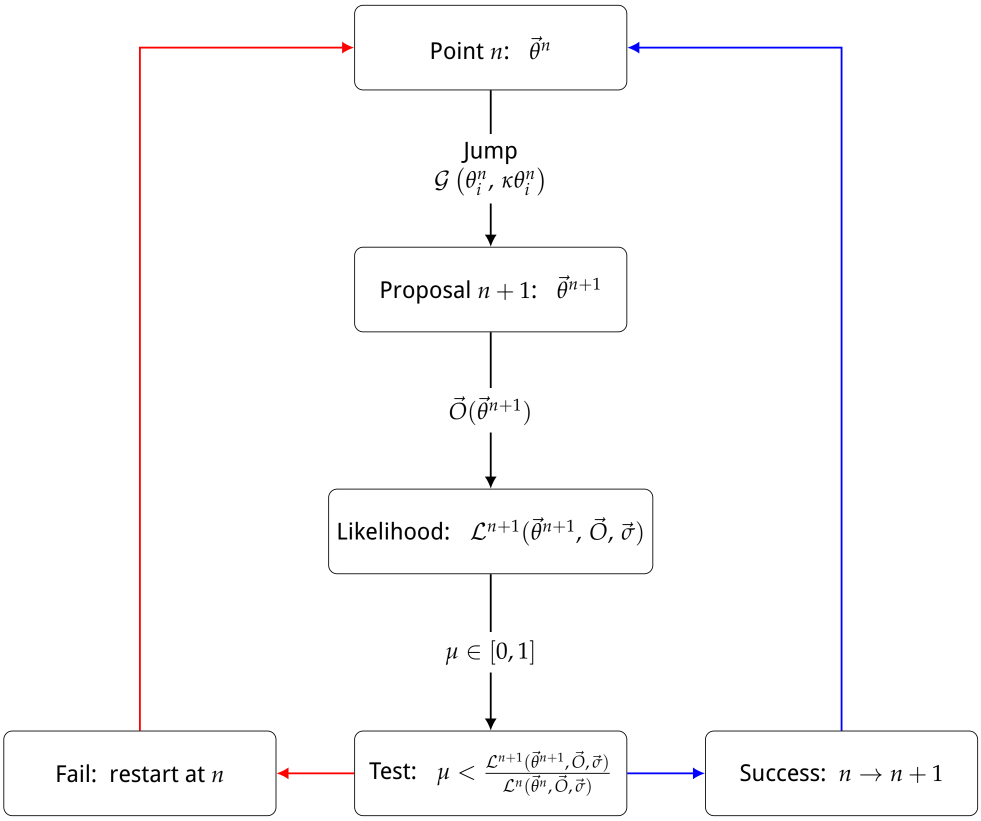

FIGURE 5.1: Illustration of the MCMC algorithm utilisation.

starting points (chosen randomly) can lead to different likelihood maximums. A summary of the algorithm is given in Figure 5.1.

5.3.2 Constraints, tools and setup

We now develop on the numerical tools and constraints employed in our analysis. As the model is defined at the GUT scale, we first perform the evolution of the renormalisation group equations (RGEs) to the low scale, to derive low energy observables. For this purpose we employed the `SARAH v4.14.1` Mathematica package [181–185] in order to generate a type I Seesaw GUT MSSM model based on `SPheno v4.0.4` [114, 115]. Right handed Majorana neutrinos, which typically live near the GUT scale are therefore consistently integrated out at their mass scale. Furthermore, the `Flavour kit` [186] available within `SARAH` / `SPheno` computes a wide range of flavour observables, simplifying our framework as both one-loop masses and flavour observables are evaluated within a single executable.

However, modifications of this model have been realised: In the usual `SPheno` instances, SM fermion masses are enforced to match the experimental data by several runs up and down between the GUT scale and the low scale, rendering our model predictions impossible to estimate. To overcome this, we have removed the SM fermions from this iterative convergence process while keeping the massive gauge bosons. To consistently implement such restrictions, attention must be payed concerning several features. An extended discussion regarding our modified `SPheno` version can be found in Appendix A.

We have also decided to include dark matter constraints in our analysis. Restricting ourselves to neutralino dark matter, we imposed a step dark matter candidate likelihood (1 if the LSP is the lightest neutralino, 0 otherwise). In order to derive relic density and direct detection constraints, we have used `micrOMEGAs v5.2`, which accepts the spectrum files generated by `SPheno` through the SUSY Les Houches Accord (SLHA) [187, 188] interface.

It should be noted that `SARAH` generated `micrOMEGAs` models are in general limited to real Lagrangian parameters, that is all couplings need to be real. This caused problems in our relic density calculations due to the presence of phases in multiple sectors. To overcome this, we maintained a full calculation including phases within `SPheno` but recast the model with real valued couplings for the relic density calculation. As, in general, the CP-violating contribution to relevant (co-)annihilation channels are limited, and our CP-violating parameters are also numerically rather small, this is a valid approximation. We have verified for a few cases, that the effect of the phases had little impact on the amplitudes squared of the relevant processes.

Linking these tools together, we are able to investigate a wide range of constraints. The list of the Standard Model parameters to be fitted is given in Table 5.3 while the flavour and dark matter constraints are listed in Table 5.4. We give the list of input parameters and their respective scanning range in Table 5.2.

In all tables, the upper bounds constraints are given at the 90% confidence level and in order to help the process of chain convergence and initialization, we postulate a smoothing step function for the upper limits constraints

$$\mathcal{L}_{\text{upper}}(\vec{\theta}, O_i, \sigma_i) = \begin{cases} 1 & \text{for } O_i(\vec{\theta}) \leq O_i^{\text{bound}} \\ e^{-\frac{\left(O_i(\vec{\theta}) - O_i^{\text{bound}}\right)^2}{2\sigma_i^2}} & \text{for } O_i(\vec{\theta}) > O_i^{\text{bound}} \end{cases} \tag{5.3.26}$$

where we chose, somehow arbitrarily, a common value of $\sigma_i = 10\% \cdot O_i^{\text{bound}}$.

On the other hand, we associate a Gaussian likelihood function for all experimentally measured observables

$$\mathcal{L}_{\text{measured}}(\vec{\theta}, O_i, \sigma_i) = e^{-\frac{\left(O_i(\vec{\theta}) - O_i^{\text{exp}}\right)^2}{2\sigma_i^2}}, \tag{5.3.27}$$

σ_i being the uncertainty given in Tables 5.3 and 5.4.

Parameter	Range	Parameter	Range	Parameter	Range
A_0	$[-1000, 1000]$	y_d	$[-2, 2]$	k_2	$[-8, 8]$
m_0^2	$[2 \cdot 10^5, 7 \cdot 10^6]$	z_1^d	$[-2, 2]$	k_3	$[-8, 8]$
$m_{H_u}^2$	$[2 \cdot 10^5, 7 \cdot 10^6]$	x_2	$[-1.2, 1.2]$	k_4	$[-8, 8]$
$m_{H_d}^2$	$[2 \cdot 10^5, 7 \cdot 10^6]$	y_s	$[-1, 1]$	$B_0^{(N)}$	$[0, 8]$
M_1	$[500, 1500]$	z_3^d	$[-2, 2]$	$B_3^{(N)}$	$[-8, 8]$
M_2	$[500, 1500]$	z_2^d	$[-2, 2]$	$K_3^{(N)}$	$[-8, 8]$
M_3	$[800, 3000]$	y_b	$[-2.5, 2.5]$	a_u	$[-8, 8]$
$\tan(\beta)$	$[6, 15]$	A	$[-8, 8]$	a_c	$[-8, 8]$
y_u	$[0.1, 1.5]$	B	$[-8, 8]$	a_t	$[-8, 8]$
y_c	$[0.1, 1.5]$	C	$[-8.8]$	a_s	$[-8, 8]$
y_t	$[0.4, 0.7]$	D	$[-8, 8]$	a_b	$[-8, 8]$
θ_3^d	$[0, 2\pi]$	b_{01}	$[0, 8]$	$\tilde{x}_2^a$	$[-8, 8]$
θ_2^d	$[0, 2\pi]$	b_{02}	$[0, 8]$	z_3^{da}	$[-8, 8]$
z_1^{da}	$[-8, 8]$	b_2	$[-8, 8]$	z_2^{da}	$[-8, 8]$
α_D	$[-8, 8]$	b_3	$[-8, 8]$		
y_D	$[-1.5, 1.5]$	b_4	$[-8, 8]$		

TABLE 5.2: GUT scale input parameters for the model and their scanning range. For all parameters, the step size for a Markov chain iteration is given as 0.5% of the total range length of the allowed values. This step size was procured by trial and error in order to balance scan efficiency and a search of the parameter space. In addition, we set a fixed value for the following parameters: $\text{sign}(\mu) = -1$; and $\lambda = 0.22$ and $M_{\text{GUT}} = 2 \cdot 10^{16}$ which enters as parametrization of Yukawa, trilinear and mass matrices as stated in Eqs. (5.2.18), (5.2.19) and (5.2.22).

Observable	Constraint	Refs.
m_u	$(2.2 \pm 0.5) \cdot 10^{-3}$	[189]
m_c	1.275 ± 0.0035	[189]
m_t	172.76 ± 0.9	[189]
m_d	$(4.7 \pm 0.5) \cdot 10^{-3}$	[189]
m_s	$(93 \pm 9) \cdot 10^{-3}$	[189]
m_b	4.18 ± 0.04	[189]
m_e	$0.511 \cdot 10^{-3}$	[189]
m_μ	$105.66 \cdot 10^{-3}$	[189]
m_τ	1.7769	[189]
m_h	125	[189]

Observable	Constraint	Refs.
$(\Delta m_{21}^\nu)^2$	$(7.42 \pm 0.2) \cdot 10^{-23}$	[48]
$(\Delta m_{31}^\nu)^2$	$(2.514 \pm 0.028) \cdot 10^{-21}$	[48]
$\sin(\theta_{12}^{\text{CKM}})$	0.225 ± 0.0010	[190]
$\sin(\theta_{13}^{\text{CKM}})$	$(0.003675 \pm 9.5) \cdot 10^{-5}$	[190]
$\sin(\theta_{23}^{\text{CKM}})$	0.042 ± 0.00059	[190]
δ^{CKM}	1.168 ± 0.04	[190]
$\sin(\theta_{12}^{\text{PMNS}})$	0.55136 ± 0.012	[48]
$\sin(\theta_{13}^{\text{PMNS}})$	0.1490 ± 0.0022	[48]
$\sin(\theta_{23}^{\text{PMNS}})$	0.7550 ± 0.0134	[48]
δ^{PMNS}	3.86 ± 1.2	[48]

TABLE 5.3: νSM parameters, masses and EWSB constraints for our model exploration. All masses are given in GeV and are pole masses, except for the bottom and light quarks: the bottom (light quarks) one is the $\overline{\text{MS}}$ mass given at the scale $Q = m_b$ ($\mu = 2$ GeV). Theoretical uncertainties of 1% are assumed for the different masses and are added in quadrature with the experimental ones. Note that the charged lepton and Higgs boson mass experimental uncertainties are negligible with respect to the theoretical ones and are therefore omitted.

Observable	Constraint	Refs.
$\mathrm{BR}(\mu \to e\gamma)$	$< 4.2 \cdot 10^{-13}$	[189]
$\mathrm{BR}(\tau \to e\gamma)$	$< 3.3 \cdot 10^{-8}$	[189]
$\mathrm{BR}(\tau \to \mu\gamma)$	$< 4.4 \cdot 10^{-8}$	[189]
$\mathrm{CR}(\mu - e, Ti)$	$< 4.3 \cdot 10^{-12}$	[189]
$\mathrm{CR}(\mu - e, Au)$	$< 7 \cdot 10^{-13}$	[189]
$\mathrm{CR}(\mu - e, Pb)$	$< 4.6 \cdot 10^{-11}$	[189]
$\mathrm{BR}(\mu \to 3e)$	$< 1 \cdot 10^{-12}$	[189]
$\mathrm{BR}(\tau \to 3e)$	$< 2.7 \cdot 10^{-8}$	[189]
$\mathrm{BR}(\tau \to 3\mu)$	$< 2.1 \cdot 10^{-8}$	[189]
$\mathrm{BR}(\tau - \to e^- \mu^+ \mu^-)$	$< 2.7 \cdot 10^{-8}$	[189]
$\mathrm{BR}(\tau - \to \mu^- e^+ \mu^-)$	$< 1.8 \cdot 10^{-8}$	[189]
$\mathrm{BR}(\tau - \to e^+ \mu^- \mu^-)$	$< 1.7 \cdot 10^{-8}$	[189]
$\mathrm{BR}(\tau - \to \mu^+ e^- e^-)$	$< 1.5 \cdot 10^{-8}$	[189]

Observable	Constraint	Refs.
$\mathrm{BR}(Z \to e\mu)$	$< 7.5 \times 10^{-7}$	[189]
$\mathrm{BR}(Z \to e\tau)$	$< 9.8 \times 10^{-6}$	[189]
$\mathrm{BR}(Z \to \mu\tau)$	$< 1.2 \times 10^{-5}$	[189]
$\mathrm{BR}(h \to e\mu)$	$< 6.1 \times 10^{-5}$	[189]
$\mathrm{BR}(h \to e\tau)$	$< 4.7 \times 10^{-3}$	[189]
$\mathrm{BR}(h \to \mu\tau)$	$< 2.5 \times 10^{-3}$	[189]
$\mathrm{BR}(\tau \to e\pi)$	$< 8 \times 10^{-8}$	[189]
$\mathrm{BR}(\tau \to e\eta)$	$< 9.2 \times 10^{-8}$	[189]
$\mathrm{BR}(\tau \to e\eta')$	$< 1.6 \times 10^{-7}$	[189]
$\mathrm{BR}(\tau \to \mu\pi)$	$< 1.1 \times 10^{-7}$	[189]
$\mathrm{BR}(\tau \to \mu\eta)$	$< 6.5 \times 10^{-8}$	[189]
$\mathrm{BR}(\tau \to \mu\eta')$	$< 1.3 \times 10^{-7}$	[189]
Ωh^2	0.12 ± 0.012 th.	[117, 191–193]
Direct detection	cf. Figure 5.2	[194, 195]

TABLE 5.4: Leptonic flavour and dark matter constraints. These upper limits numbers are given at the 90% confidence level. For the dark matter relic density we assume 10% theoretical uncertainties because of cosmological assumptions.

From Table 5.2, this model has 46 parameters. On the other hand, there are only 20 standard model constraints in Table 5.3 and 26 further constraints in Table 5.4 (although these are often only upper limits. Naively, this could be interpreted to imply that this model will inherently be sufficient to fit all the data as the number of constraints matches the number of parameters. However, the precise nature of the model in question and the precise nature of the symmetry breaking schema are critical in the phenomenological realisation of the parameters into observables. Indeed, as we shall see later, only by directly tackling these phenomenological implications can we make any claims as to the viability of a given model as it is not trivial to satisfy the set of experimental results simultaneously.

Regarding the dark matter direct detection constraints, we extracted and extrapolated the curves from Refs. [194, 195] as shown in Figure 5.2, while for the relic density we have used the results from Ref. [191] adding a 10% uncertainty due to `micrOMEGAs` precision in combination with underlying cosmological assumptions. For the other constraints we are using the current experimental uncertainties associated to the values given in the different tables while adding in quadrature a theoretical constraints on the different standard model masses. The theory uncertainty on the Higgs mass is fixed at 2 GeV [196] while we assume a common 1% uncertainty on the different fermion masses because of RGE fixed order precision and changes from the $\overline{\mathrm{DR}}$ to the on-shell renormalisation scheme. If no experimental constraints is present for a given value in the tables it is understood that theoretical uncertainties are by far dominant with respect to the experimental ones. Finally, the different quark masses are extracted at different scales, i.e. $Q = 2$ GeV for $q = (u, d, c, s)$ and $Q = m_b$ for $q = b$.

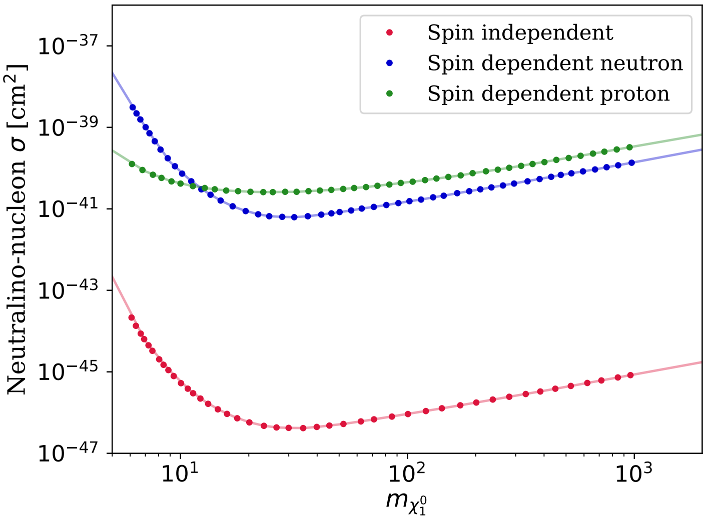

FIGURE 5.2: Dark matter direct detection limits in plane of dark matter mass and spin-(in)dependent nucleon scattering cross section. The dots correspond to data extracted from Xenon1T experiments presented in Refs. [194, 195], while the solid line is the extrapolation we performed.

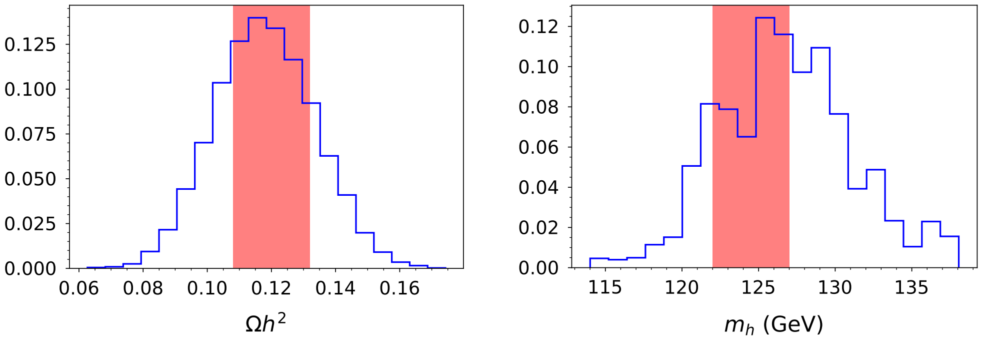

FIGURE 5.3: Distribution of the Higgs mass and dark matter relic density predictions, normalised to one. The 1σ region is marked in red. The MCMC displays an approximate Gaussian fit around the experimental values.

Having implemented and executed the above, 197 chains were recovered. As the parameter space was so vast and such a large number of very precise constraints were used, the efficiency of these scans was very low, requiring weeks of computer time to complete. Therefore, the scans were allowed 2000 Markov chain steps each. After this process we collect the data and applied a likelihood cutoff such that only points with relatively high likelihood are left in the final data set. This was in order to prevent the distributions presented here-in from misleading the reader into thinking some parts of parameter space were viable when, in fact, they produce excessively low likelihoods. The likelihood cutoff applied was 10^{-150}. Although this is tiny, much of the poor likelihood comes from poor convergence of the fermion masses (see discussion in Section 5.4.1). In general, the remaining constraints converged very well to the observed values. As an example of two constraints, see Figure 5.3, which shows how the Higgs boson mass and relic density are centered around the expected value.

5.4 Results

The subsequent results are based on the Markov Chain Monte Carlo (MCMC) study following the methods elucidated previously. Having already presented two illustrative plots showing the constraints used to guide the MCMC, we now present the resultant spectra and phenomena. We begin with a discussion of the fermion masses, mixing, and a general discussion of the model's success in recreating the Standard Model observables. We then look at the supersymmetric (SUSY) spectrum, the dark matter sector, and further phenomenological results. Finally, we give a discussion of the effects on collider physics and experimental physics more generally.

5.4.1 Fermion masses and mixing

In this subsection we present the results of our scan for fermion masses and mixing parameters, which are put in as constraints as shown in Table 5.3. The results for the fermion masses are shown in Figure 5.4, while those for the mixing parameters are shown in Figures 5.6 and 5.7.

These results follow from the charged fermion Yukawa matrices at the GUT scale shown in Eqs. (5.2.18), together with the neutrino Dirac Yukawa matrix in Eq. (5.2.20) and the heavy right-handed neutrino mass matrix in Eq. (5.2.19). Note that the $(3,3)$ entries of the charged lepton and down type quark Yukawa matrices are equal at the GUT scale (yielding approximate bottom-tau unification $m_b = m_s$), while the $(2,2)$ entries of these matrices differ by the Georgi-Jarlskog (GJ) factor of 3 (yielding an approximate strange to muon mass ratio $m_s = m_\mu/3$ at the GUT scale).

The results for fermion masses in Figure 5.4 show that the above GJ relations do not lead to phenomenologically viable charged lepton and down type quark masses at low energy, in particular m_s, m_b and m_τ are not well fitted. This problem has also been noted by other authors, and possible solutions have been proposed based on various alternative choices of GUT scale Higgs leading to different phenomenologically successful mass ratios at the GUT scale [179, 180] but are beyond the scope of this study. Since the purpose of this study is to perform a comprehensive phenomenological analysis on an existing benchmark model, we shall not consider such alternative solutions here, but simply note that such solutions exist and could be readily applied.

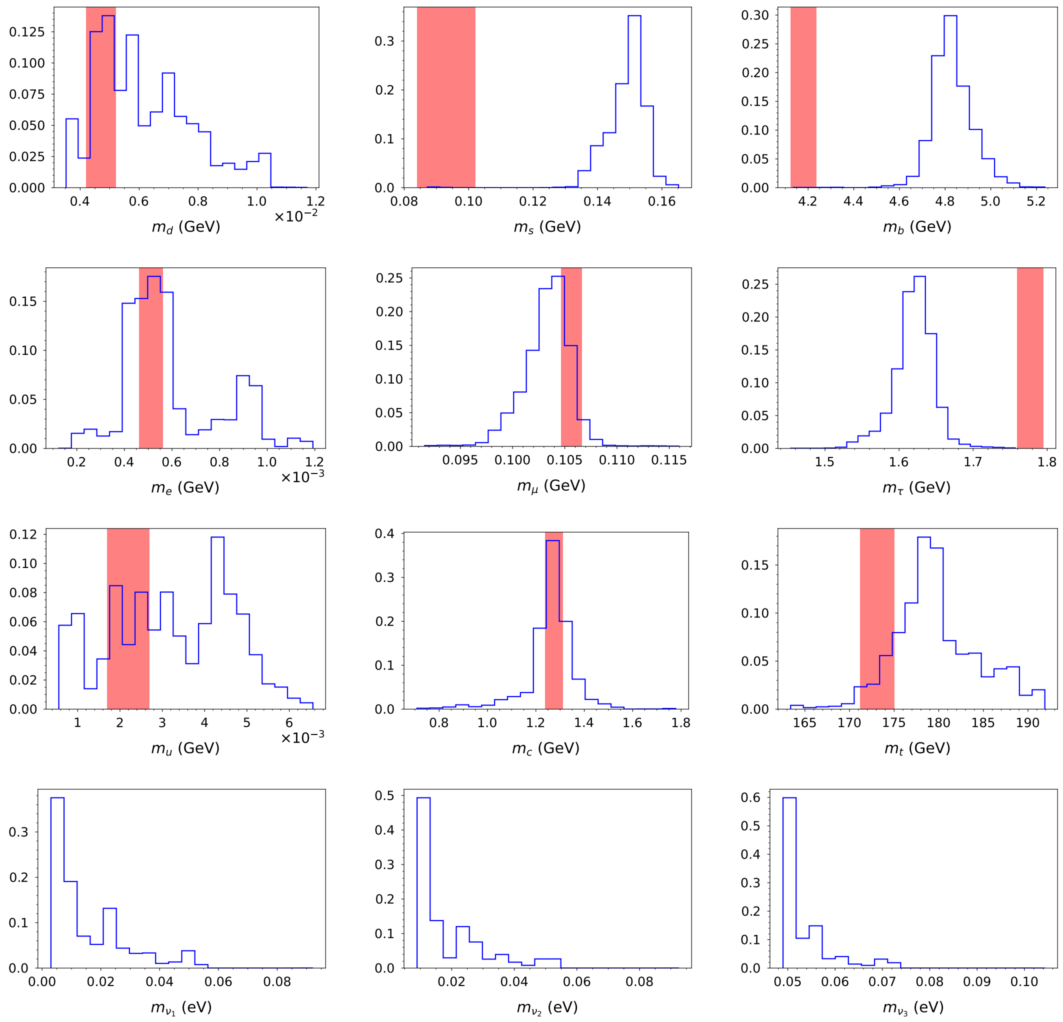

FIGURE 5.4: The fermion masses are displayed where the red region indicating the 1σ limits. The first generations are very well fitted. However, due to the link between the down type quarks and the leptons at the GUT scale, the second and third generation masses are slightly off. Furthermore, the top mass is also slightly poorly aligned due to the Higgs mass constraint. Note that few points exhibit neutrino masses above the visible part of the histograms.

Note that the absolute values of the neutrino masses in Figure 5.4 are genuine predictions of the model, since only the experimentally measured mass squared differences in Table 5.3 were put in as constraints. In particular, the lightest neutrino mass distribution is peaked around a few times 10^{-3} eV. This leads to an interesting prediction for neutrinoless double-beta becay. In Figure 5.5 we give the model prediction of the neutrinoless double-beta decay parameter m_{ee} against the mass of the lightest neutrino $m_{\nu 1}$. Future projections for CUORE rule out approximately 52% of the data set. Indeed, the model tends to favour relatively high values of m_{ee} as compared to the theoretically allowed region.

The results for the CKM and PMNS mixing parameters in Figures 5.6 and 5.7 show a good fit to the constraints. The PMNS mixing parameters $\sin\theta_{12}^{\text{PMNS}}$ and $\sin\theta_{13}^{\text{PMNS}}$ also

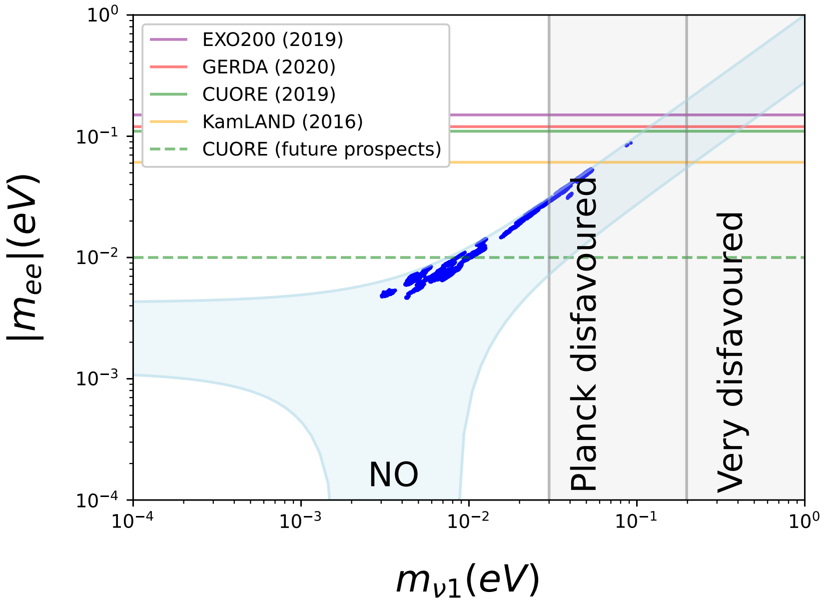

FIGURE 5.5: The dark blue points are the model prediction of the neutrinoless double beta decay parameter $|m_{ee}|$ vs the mass of the lightest neutrino $m_{\nu 1}$. The light blue shaded region shows the allowed range in this plane for a normal hierarchy as predicted by the model. The vertical grey shaded bands to the right show the current Planck disfavoured region [54], while the coloured horizontal lines show the limits on $|m_{ee}|$ from KamLAND [197], EXO-200 [198], CUORE [199], and GERDA [200]. We also indicate future prospects for CUORE [201].

fit very well. However the model prefers somewhat smaller values of $\sin\theta_{23}^{\rm PMNS}$, with the CP-oscillation phase $\delta^{\rm PMNS}$ being quite uniformly distributed.

The Majorana phases are also predicted and are highly correlated as shown in Figure 5.8. In principle, the fact that they are correlated is not surprising. The model only depends on two high scale phases, θ_2^d and θ_3^d, and the MCMC has two low scale constraints on the phases from δ^{CKM} and δ^{PMNS}. Therefore, the high scale phases, who determine the Majorana phases, must be correlated. However, the striking nature of the correlation is surprising. It seems that, roughly speaking, the Majorana phases must sum to a multiple of π. Of course, these phases are important with regards to CP-violating processes but this should suggest that their individual values should be multiples of π, not their sum. For the time being we leave this puzzle as a comment to be understood in greater detail.

5.4.2 SUSY spectrum

Figure 5.10 shows the distribution of the lightest charged sfermion masses. Typically, the lightest sleptonic state represents the lightest sfermion of the spectrum with the up and down squarks being larger and similar in mass to each other. Furthermore, as will

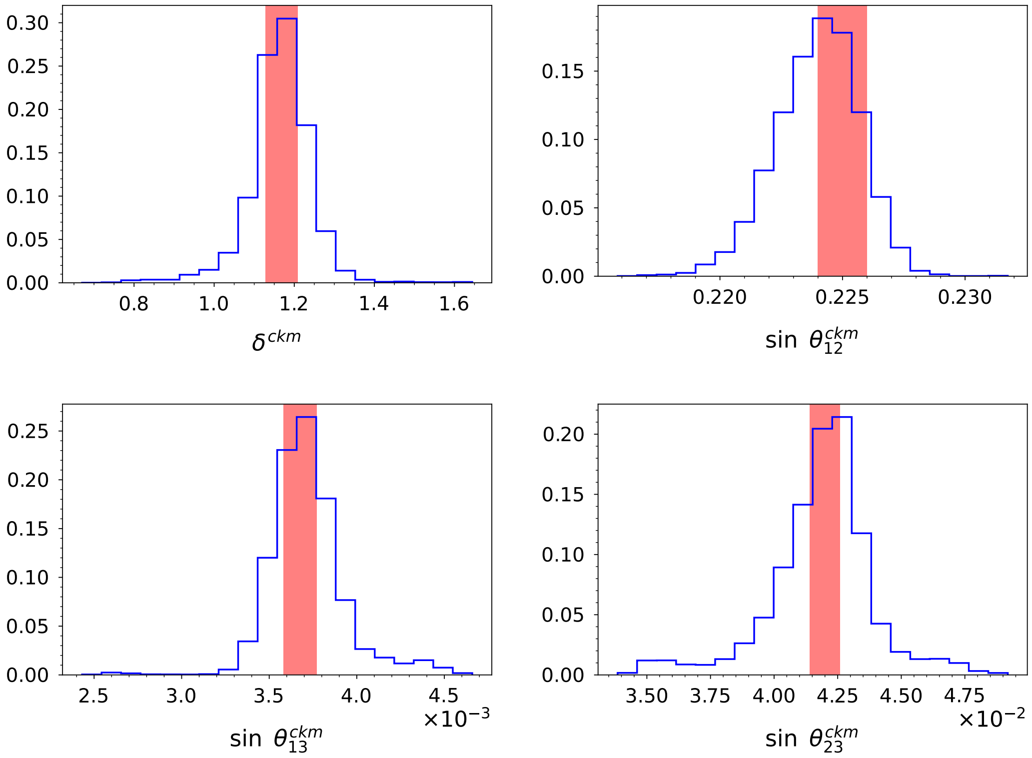

FIGURE 5.6: The CKM parameters are displayed where the red region indicating the 1σ limits. All parameters in the CKM are fitted very well with an approximately Gaussian distribution around the expected value.

be discussed later, large flavour mixing involving the first and second generation, is typical of these sfermionic states under this model. This is caused by the (1,1), (2,2) and (3,3) entries of the M_T and M_F soft matrices in Eq. (5.2.22). In M_T, as the (1,1) and (2,2) entries are given by b_{01}, their relative size in comparison with the (3,3) element, given by b_{02}, dictates the structure of the mixing matrix. In M_F, all diagonal entries are identical at the GUT scale. These structure peculiarities of the soft matrices stem from the flavour symmetry at the GUT scale: by construction the first two generations of (u_L, u_R, d_L, ℓ_R) are gathered in an S_4 doublet while the third generation forms a singlet. For (d_R, ℓ_L) the visible mass splitting difference is due to significantly larger third generation Yukawa coupling.

The neutralino, chargino, and gluino masses are displayed in Figure 5.11. Although the gluino mass is not particularly constrained, the two lightest neutralinos and the lightest chargino have a very constrained spectrum. As, a priori, the relic density is too high, the model requires a specific mechanism to reduce the dark matter relic density to phenomenological values. As much of the rest of the spectrum is large, the neutralinos and charginos supply an alternative mechanism via co-annihilation. In order to allow for such contributions, the lightest gauginos must be comparable in mass as will be seen in the dark matter dedicated section below.

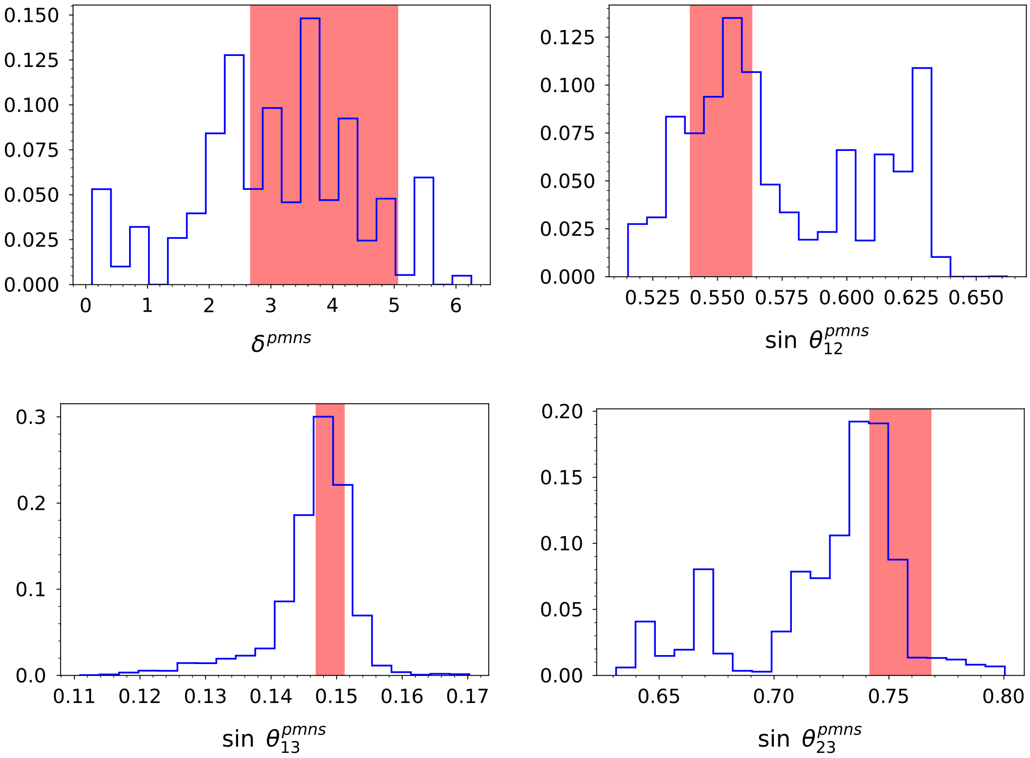

FIGURE 5.7: The PMNS parameters are displayed where the red region indicating the 1σ limits. Unlike the CKM parameters, the PMNS shows more variation due to the less stringent experimental constraints.

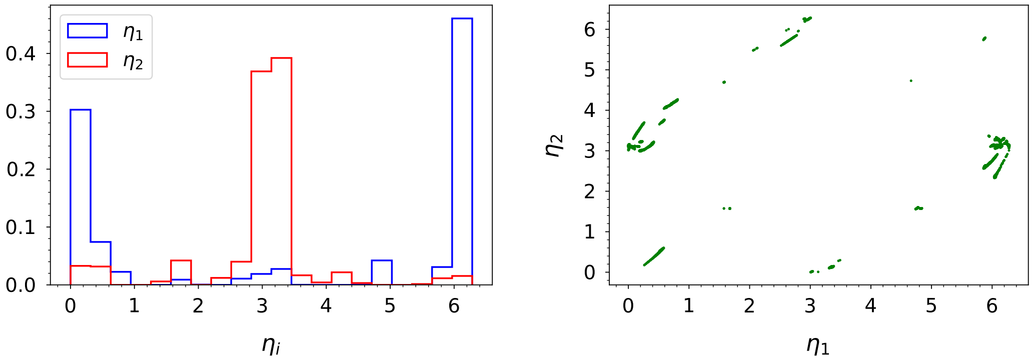

FIGURE 5.8: A representation of the Majorana phases is presented. The first panel shows the density of values for the two phases while the second shows their strong correlations.

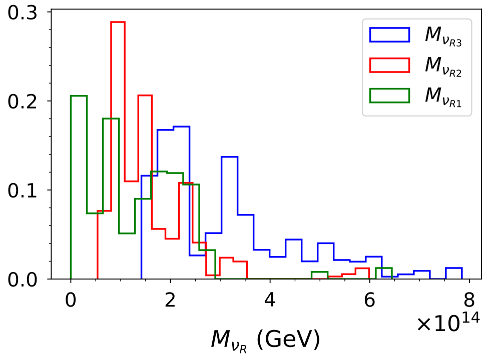

FIGURE 5.9: Mass distribution of right handed neutrinos. Overall, the masses are very large and approximately of the same order of magnitude (10^{14} GeV).

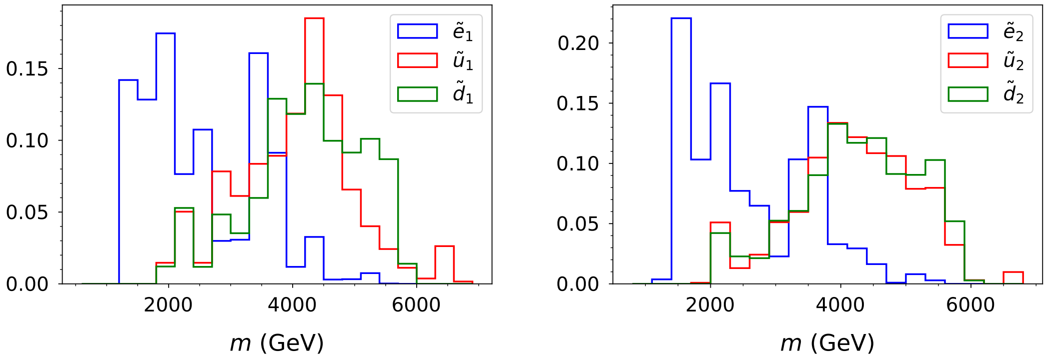

FIGURE 5.10: Distribution of masses for the lightest up-type, down-type sfermions and the lightest slepton. The slepton is the lightest of these particles.

The last panel of Figure 5.11 demonstrates the "decoupling limit" for two Higgs doublet models. In this limit, the three additional Higgs states have very large masses and are approximately degenerate.

5.4.3 Dark matter

We now come to the discussion of dark matter aspects of the model under consideration. As we have seen in Figure 5.3, the dark matter relic density given by the latest Planck results is well accommodated for in the parameter regions surviving the numerous imposed constraints. The corresponding parameter configurations feature essentially bino-like dark matter, which can be understood from Figure 5.12, where we depict the relevant bino and wino content of the lightest neutralino.

Looking at the gaugino masses (Figure 5.11), it can be seen that the second-lightest neutralino as well as the lighter chargino lie very close to the lightest neutralino. In other words, the bino and wino mass parameters are, at the SUSY scale, almost equal, the bino lying just below the wino mass. This feature is driven by co-annihilations

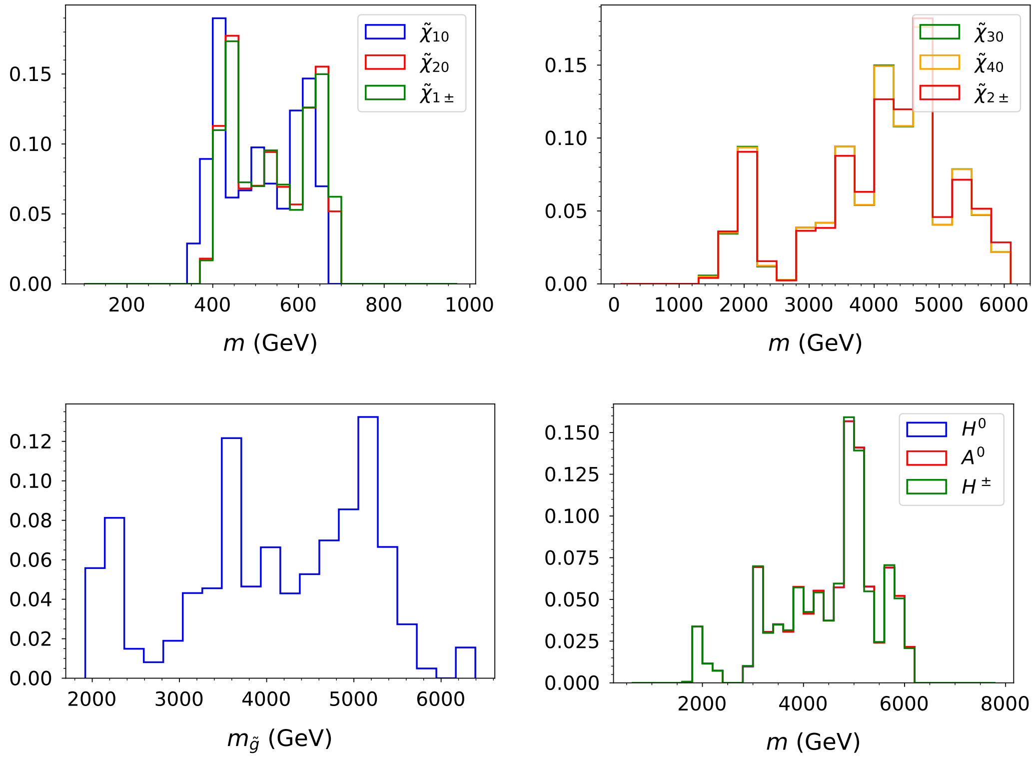

FIGURE 5.11: Distribution of the masses of the gauginos and higgses. The mass spectrum of the lightest chargino and two lightest neutralinos is compressed to provide co-annihilation mechanism for dark matter.

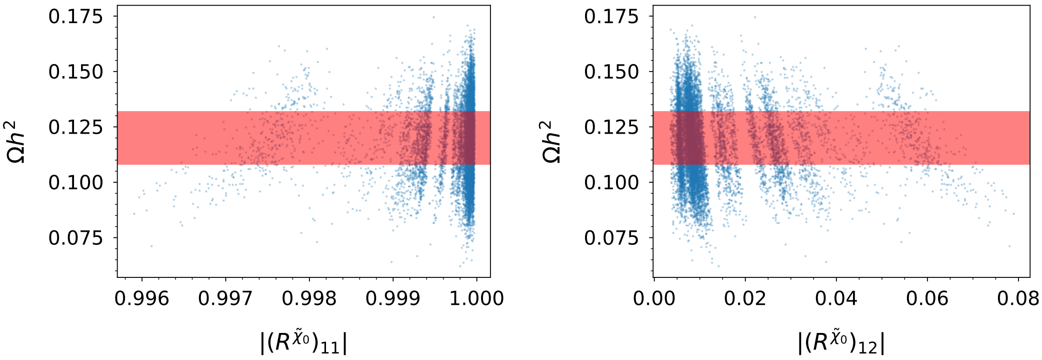

FIGURE 5.12: The bino ($|(R^{\tilde{\chi}^0})_{11}|$, left) and wino ($|(R^{\tilde{\chi}^0})_{12}|$, right) contents of the lightest neutrino shown against the corresponding dark matter relic density. The higgsino contents of the lightest neutralino are negligible and not shown here. The neutralino mixing matrix $R^{\tilde{\chi}^0}$ is defined according to the SLHA standard [187].

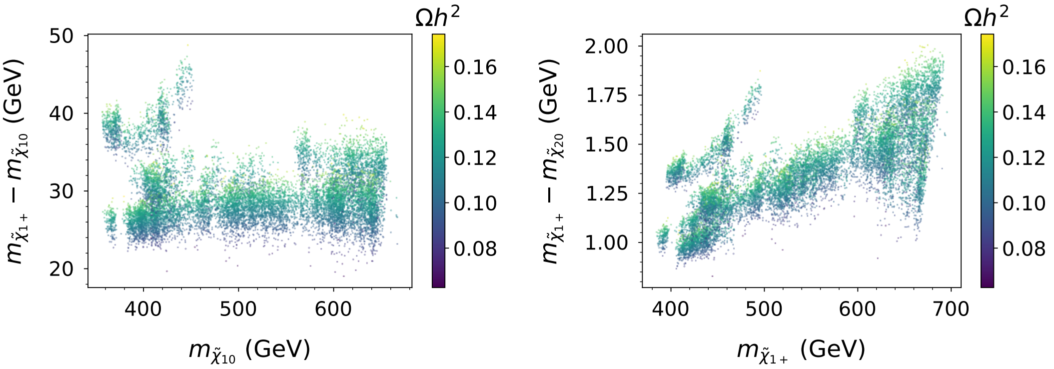

FIGURE 5.13: Mass differences between the lightest chargino (left) as well as the second-lightest neutralino (right) and the lightest neutralino displayed against the lightest neutralino mass. Correlations between the masses are displayed with the colour indicating the relic density. The relic density is controlled by co-annihilation channels whose strength are dictated by the mass gap between the relevant particles.

needed to achieve the required relic density. Note that this corresponds to a situation where the GUT-scale values of the bino and wino mass differ roughly by a factor of two.

It is interesting to note that, although the bino-like lightest neutralino $\tilde{\chi}_{10}$ is the dark matter candidate, the (co-)annihilation cross-section is dominated by the (co-)annihilaton of the wino-like states $\tilde{\chi}_{20}$ and $\tilde{\chi}_{1\pm}$. This is explained, on the one hand, by the very small mass difference between the wino-like states, and, on the other hand, by the enhanced annihilation cross-section for the latter as compared to the bino-like state. Typical final states of these (co-)annihilation channels are quark-antiquark pairs and gauge boson pairs (including Z^0, $W^\pm$, and γ). Neutrino final states are subdominant.

The presence of co-annihilation can also be understood through Figure 5.13 showing the correlation of the three lightest gaugino masses and the dark matter relic density. Let us finally note that scenarios with wino-like dark matter would give rise to insufficient relic density to align with the experimental evidence, as the wino (co-)annihilation cross-section is numerically more important as the one for the bino.

Coming to the direct dark matter detection, we can see from Figure 5.14 that this constraint is also well satisfied in the model under consideration, both for the spin-dependent and the spin-independent case. It is important to note that all points shown in Figure 5.14 lie also below the projected limits of the `XENONnT` experiment [202]. The fact that all points are found below this limit can be traced to the fact that we have applied a cut on the global likelihood value as explained in Section 5.3. This procedure discards the points which are too close to the current `XENON1T` limit, since they typically feature a somewhat lower likelihood value. This means that parameter

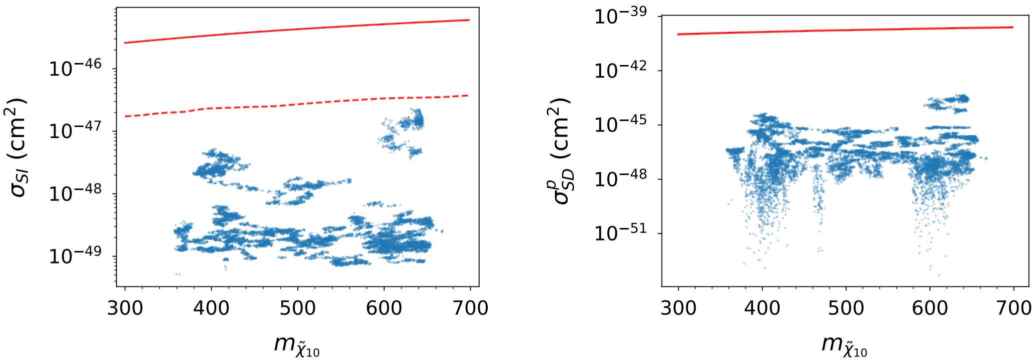

FIGURE 5.14: The direct detection limits for spin dependant and spin independent cross-sections are shown with the experimental limit plotted. The solid line indicates the `XENON1T` limits [195], while the dashed line in the first panel indicates the expected limit for the `XENONnT` [202] experiment. We have precluded a representation of the neutron direct detection calculation as all data points are far away from the exclusion limit, much like the proton calculation of the same.

configurations with reasonably high global likelihood values may not be challenged by direct detection experiments in a near future.

In summary, the relic density constraint implies a relatively small mass difference between the lightest neutralino and the next-to-lightest states, leading to final states with soft pions and leptons which are difficult to detect. The current bounds depend on the nature of the NLSP go up to masses of about 240 GeV [203–206]. This cuts slightly into the allowed parameter space.

5.4.4 Collider related aspects

As already mentioned in Section 5.4.2 the flavour structure of the lightest sfermions falls into two extreme case: For each sfermion type, we observe either a first and second generation fully mixed state or a strict third generation state. This feature is illustrated in Figure 5.15 where we show the distribution of the sum of the square of the mixing matrix entries.

While at first glance it seems that this particular prediction of the model would be quite interesting from a collider perspective, enabling potential flavour mixed search channels, the model also predicts rather high masses for sfermion states. The lightest squark masses are peaked around 4 TeV and stand well beyond any potential collider sensitivity reach (see for e.g. Ref. [139] where the limits are around 1.8 TeV squarks using simplifying assumptions that do not hold in our case). The lightest slepton on the other hand can be as light as 1 TeV. However, the production cross section drops significantly with respect to the QCD dominated squark ones. Furthermore, our model naturally predicts right-handed slepton states to be the lightest ones which

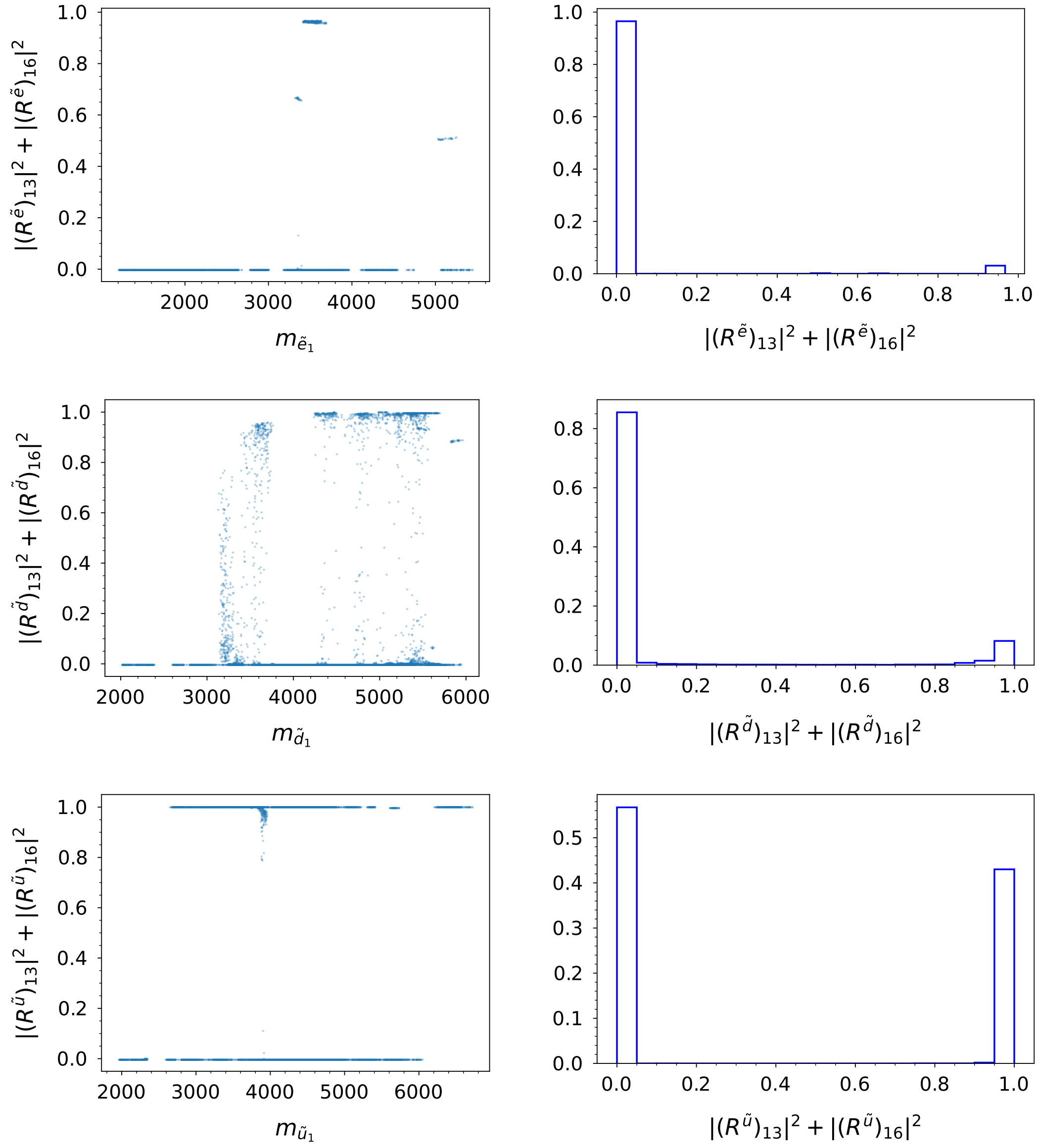

FIGURE 5.15: The mass of the lightest sparticle for up and down type squarks and sleptons is plotted against the third generation content for the given particle on the left panels. When the third generation content is close to 0, the sfermion features a second and first generation maximally mixed state. For low mass down squark and slepton states, an admixture of first and second generation is favoured. The right panels illustrate the actual proportion of points that belong to these two extreme flavour cases. The sfermion mixing matrices $R^{\tilde{f}}$ ($\tilde{f} = \tilde{u}, \tilde{d}, \tilde{e}$) are defined according to the SLHA 2 standard [188].

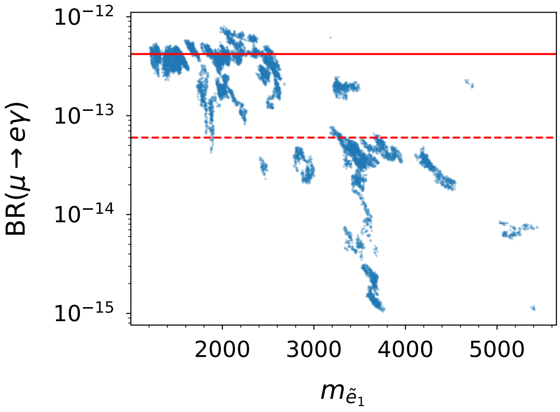

FIGURE 5.16: BR($\mu \to e\gamma$) as a function of $m_{\tilde{e}_1}$. Current experimental limit is represented by the red solid line while the dashed one corresponds to the future prospects of MEG II ($6 \cdot 10^{-14}$) [210].

further decreases the production cross section [207]. As an example, recent searches for flavour conserving channels with nearly helicity degenerated slepton states are excluding masses of the order 600 – 700 GeV [208] if $m_{\tilde{\chi}_{10}} < 150$ GeV (and limits are even weaker if this is not the case). In addition, current exclusion on τ flavoured sleptons masses are of order 390 GeV [209].

It turns out that our model predictions regarding the sfermionic sector are not very promising for potential collider searches. However this flavour mixing particularity leads to some interesting features from indirect searches perspectives. It is well known that slepton mixing can generate significant contributions to flavour violating decay constraints; in particular, if the mass of the slepton is rather light. In our case, BR($\mu \to e\gamma$) illustrates very well this feature as being one of the most stringent test for lepton flavour violation. Figure 5.16 shows the distribution of this branching ratio as a function of the mass of the lightest slepton. While the points are within the current experimental limits, it appears that future prospects in the current MEG II experiment [210] could rule out a vast majority of our light slepton points, implying the interesting conclusion that this particular constraint and other flavour violating constraints would have more discriminatory power than classic direct slepton searches and propose typical smoking guns for our framework.

Despite the sfermionic states being unreachable in near future collider searches, this is not necessarily the case for the other SUSY particles in our model. In particular, the model can predict rather light electroweakinos with sufficient mass gap for collider considerations. As a comparison, recent searches from ATLAS [211] put a lower bound on $m_{\tilde{\chi}_{10}}$ of 270 GeV when the mass gap with $m_{\tilde{\chi}_{1\pm}}$ is of order 50 GeV. While these very light masses are not present in our current framework, we can hope for more stringent limits from future LHC runs. Two example Feynman diagrams for

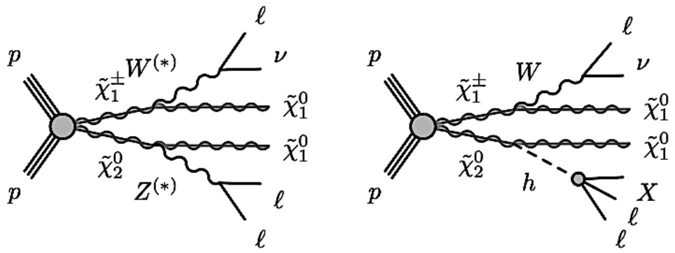

FIGURE 5.17: Feynman diagrams showing pair production of electroweakinos and subsequent decay into LSPs mediated by weak and Higgs bosons, with three leptons and a neutrino. The compressed mass gap of the light electroweakinos increases the significance of these channels. Such diagrams can be of interest for the model under discussion in future collider searches as the lower mass limits on the LSP increases. Figure from [211]

such searches are given in Figure 5.17. The compressed mass spectrum in the electroweakinos increases the relevance of such processes.

Similar conclusion can be derived regarding gluino searches. While the predicted masses lie in the 2 – 6 TeV range, ATLAS and CMS limits using simplified models [139, 212] reaches 1.8 TeV exclusion. Again, we can argue that future LHC runs might restrict our light spectrum parameter distributions.

To illustrate the collider phenomenology we present three benchmark points where relevant information is given in Table 5.5. The detailed information is added as supplementary material to the arXiv submission of the corresponding paper to this chapter. In particular, we list the masses of the electroweakinos for an illustrative point with low masses for the light gauginos and a relatively small mass gap. We also give the dominant decay channels and decay widths. All other particles are too heavy to be detected in the upcoming LHC run. We give a benchmark for a point which features, besides the light chargino and the neutralinos of BP1, a gluino with mass 2 TeV which should be in reach of the upcoming LHC run. Again, we give the masses, decay widths, and decay channels for the particles under examination. Regarding the third benchmark point, while having similar features as BP2 in view of collider physics, it further highlights the fully mixed nature of the lightest sleptons and the potential relevance for $\mu \to e\gamma$. Its branching of $4 \cdot 10^{-13}$ is close to the current experimental bound. However, even if this rare decay is discovered in an upcoming experiment, this example shows that it will be rather challenging to detect lepton flavour at a high energy collider as the sleptons are quite heavy.

	Particle	Mass	Decay Width	Decay Channels	Branching Ratio
BP1	$\tilde{\chi}_{10}$	402	0		
	$\tilde{\chi}_{20}$	442	1.76×10^{-11}	$\tilde{\chi}_{10}\,\bar{q}\,q$ $\tilde{\chi}_{10}\,\bar{b}\,b$ $\tilde{\chi}_{10}\,\nu_i\nu_i$	70% 13% 14%
	$\tilde{\chi}_{1+}$	444	1.5×10^{-8}	$\tilde{\chi}_{10}\,\bar{q}\,q$ $\tilde{\chi}_{10}\,\bar{l}\,\nu_i$	67% 33%
BP2	$\tilde{G}$	2000	1.87×10^{-1}	$\tilde{\chi}_{10}\,\bar{q}\,q$ $\tilde{\chi}_{1\pm}\,q^*\,q$ $\tilde{\chi}_{20}\,q^*\,q$	11% 46% 35%
BP3	$\tilde{e}_1$	1470	6.6	$\tilde{\chi}_{10}\,e$ $\tilde{\chi}_{10}\,\mu$	44% 56%
	$\tilde{e}_2$	1500	6.8	$\tilde{\chi}_{10}\,e$ $\tilde{\chi}_{10}\,\mu$	56% 44%
	$\tilde{\chi}_{10}$	413	0		
	$\tilde{\chi}_{20}$	439	3.72×10^{-11}	$\tilde{\chi}_{10}\,q^*\,q$ $\tilde{\chi}_{10}\,\nu\,\nu$	81% 15%
	$\tilde{\chi}_{1+}$	440	5.18×10^{-8}	$\tilde{\chi}_{10}\,q^*\,q$ $\tilde{\chi}_{10}\,\nu\,e^*$	67% 33%
	$\tilde{G}$	2110	0.228	$\tilde{\chi}_{10}\,q^*\,q$ $\tilde{\chi}_{1\pm}\,q^*\,q$ $\tilde{\chi}_{20}\,q^*\,q$	13% 50% 37%

TABLE 5.5: Selected benchmark points (BP) for phenomenology. The first BP exhibits rather light electroweakinos and might represent a challenge for future colliders. The second BP has a rather light gluino, which is already close to the current experimental limits from the LHC collaborations. Finally, the last BP is an example of maximally mixed lightest sleptons. All masses and widths are given in GeV.

5.5 Conclusion

In this chpater I have presented a detailed phenomenological analysis of a concrete Supersymmetric (SUSY) Grand Unified Theory (GUT) of flavour, based on $SU(5) \times S_4$. The model predicts charged fermion and neutrino mass and mixing, and where the mass matrices of both the Standard Model and the Supersymmetric particles are controlled by a common symmetry at the GUT scale, with only two input phases. The considered framework predicts small but non-vanishing non-minimal flavour violating effects, motivating a sophisticated data-driven parameter analysis to uncover the signatures and viability of the model.

The computer-intensive Markov-Chain-Monte-Carlo (MCMC) based analysis performed here, the first of its kind to include a large range of flavour as well as dark matter and SUSY observables, predicts distributions for a range of physical quantities which may be used to test the model. The predictions include maximally mixed sfermions, $\mu \to e\gamma$ close to its experimental limit and successful bino-like dark matter with nearby winos (making direct detection unlikely), implying good prospects for discovering winos and gluinos at forthcoming collider runs. The results also demonstrate that the Georgi-Jarlskog mechanism does not provide a good description of the splitting of down type quark masses and charged leptons. However neutrinoless double beta decay, which depends on a curious pattern of Majorana phases resulting from the two input phases, is predicted at observable rates.

The analysis here may be repeated for any given SUSY GUT of flavour, leading to corresponding predictions for fermion masses and mixing as well as SUSY masses and flavour violating physical observables at colliders and high precision experiments. The results here exemplify the synergy between the theory of quark and lepton (including neutrino) mass and mixing, dark matter and the SUSY particle spectrum and flavour violation, that is possible within such frameworks. It is only by systematically confronting the detailed predictions of concrete examples of SUSY GUTs of flavour with experiment that the underlying unified theory of quark and lepton flavour beyond the Standard Model may eventually be discovered.

Chapter 6

Conclusions

The Standard Model, although remarkably successful, has some critical weaknesses that preclude it as the final theory of nature. In order to solve these problems, while keeping its remarkable successes in hand, it is natural to try to extend the standard model. I have considered two such extensions both involving supersymmetry.

Despite the lack of direct experimental evidence, supersymmetry still represents a fascinating and promising model for theoretical physics beyond the Standard Model. Not only does it solve the hierarchy problem, but also supplies a framework for satisfying various flavour conundrums in modern physics, as well as its critical role in constructing GUT models. Although there is no direct evidence, a whole host of alternative experimental results constrain SUSY models making the role of phenomenologists critical in assessing the merits of SUSY models.

In this thesis I have displayed the analysis of two SUSY models. I first gave a brief review fo the SM as the bed rock for all theories moving forward. I then introduced SUSY and other BSM frameworks as critical pieces of infrastructure of the models I analysed. I then introduced two models, each focussing on different approaches to beyond the standard model phenomenology and displaying two different numerical techniques of analysis. Thereby, I have assessed their current theoretical validity in light of present experimental results and their potential to contribute to a more complete view of fundamental physics. I hope that this work can also serve to guide experimental colleagues in their searches and motivate further experimentation at colliders as well as the vast array of flavour physics, neutrino experiments, and dark matter searches.

In Chapter 4, I present the results of a no-scale Starobinsky inflation inspired SUGRA model. Such a model is well motivated by string theory as well as by its use of the Polonyi term to drive slow-roll inflation and thereby solving various cosmological problems. As the SUGRA parameter set is small and indeed the zero scalar mass requirement effectively removes another parameter, MonteCarlo analysis is used to assess the parameter space. We conducted two main scans, corresponding to zero and non-zero trilinear soft parameter and presented the results. First, leaving g-2 aside for a moment, we show how readily this frame work can accommodate the Higgs mass and the dark matter relic density. We also analyse the spectrum showing how the variance in the universal gaugino mass parameter (controlled by k) influences both the SUSY spectrum but also the mixing amongst the gauginos and therefore the relic density. By considering g-2 as well, we find the model is significantly more constrained. Indeed, $k < 0$ is required in order to satisfy the constraint to 2σ. Furthermore, the no-scale nature of the model naturally leads to light sleptons and light gauginos. Although the resultant parameter set can also satisfy collider constraints, this is non-trivial and requires some parameter tuning. Having said this, a large part of the parameter space satisfies g-2 very well when we allow for the right handed stau to supersede the lightest gaugino as the lightest sparticle. This could motivate R-parity violating models.

In Chapter 5, we present the results of a phenomenological scan of a SUSY GUT of flavour based on an $SU(5) \times S_4$ symmetry group. The model relaxes assumptions about the flavour structure of the SUSY breaking lagrangian instead controlling them and indeed the flavour structure of the SM, with the above symmetry. However, by allowing for NMFV parameters, the size of the parameter space is greatly increased as compared to the model in the previous chapter. Therefore, a more sophisticated MCMC approach was adopted in order to increase computer efficiency. In conjunction with the GUT symmetries imposed, we also include the seesaw mechanism such that the model also addresses the neutrino mass problem. By using a whole host of flavour constraints, we show that the Georgi-Jarlskog mechanism does not generate satisfactory SM masses. However, the model does successfully satisfy all other constraints. Furthermore, it predicts maximally mixed sfermions between the first and second generation. It also predicts $\mu \to e\gamma$ close to the experimental limit. Indeed, our analysis suggests that this result will be more powerful in constraining such models than near future collider runs. Having said this, the model predicts low mass gauginos and gluinos and observable rates of neutrino-less double beta decay.

In conclusion, I have presented the results of two interesting prospective SUSY models and in so doing, provided some understanding of the current state of BSM phenomenology. I have also demonstrated the use of different data techniques and their relative utility. I have considered many of latest experimental results and hope that many more exciting results are just around the corner.

Appendix A

SPheno

Our results have been obtained using the numerical code `SPheno` [114, 115], where we have implemented the model using `SARAH v4.14.0` [181–185] and then adapted the code for the model at hand. Here we describe the corresponding modifications.

In the standard version of `SPheno` the SM fermion masses, the CKM matrix, the mass of the Z-boson m_Z, the Fermi constant, the electromagnetic coupling α, and the strong coupling $\alpha_s(m_Z)$ serve as input. The latter can either be given in the Thomson limit or in the $\overline{\text{MS}}$-scheme at $Q = m_Z$. From these the three gauge couplings, the SM vacuum expectation value (VEV) v of the Higgs boson and the Yukawa couplings are calculated at the scale $Q = m_Z$. The couplings are then evolved up to the scale M_{SUSY} where the SM and the MSSM are matched including one-loop SUSY threshold corrections.

In the model at hand the Yukawa couplings are given at the GUT-scale and the fermion masses, the CKM-matrix and the PMNS-matrix are an output which required some changes to the code. The input which is done via the standard SUSY Les Houches format [187, 188] with the slight modification that the Yukawa couplings can be input at the GUT scale. The input is given at different scales as follows:

- at M_{GUT}: Y_ℓ, Y_ν, Y_d, Y_u, arg(μ) (in practice the sign of μ), as well as the soft SUSY breking terms in a non-universal form: scalar mass squares $m^2_{\tilde{f}}$ ($\tilde{f} = \ldots$), trilinear couplings $A_{\tilde{f}}$ ($\tilde{f} = \ldots$) and non-universal gaugino mass parameters M_1, M_2, M_3. All phases can be non-zero in principle.
- at M_{SUSY}: $\tan\beta$
- at $Q = m_Z$: G_F, m_Z, α_s, $\alpha_{em}(m_Z)$

The calculation is done in an iterative way:

1. The gauge couplings are evolved from the electroweak scale using the SUSY RGEs at the one-loop level to $M_{\mathrm{GUT}} = 2 \cdot 10^{16}$ GeV. We do not require unification at this scale. These couplings at this stage serve only as a starting point for our iteration.

2. All parameters are evolved from M_{GUT} to $M_{\mathrm{SUSY}} = \sqrt{(M_Q)_{33}(M_U)_{33}}$ using RGEs at the two-loop level. The right-handed neutrinos are decoupled at their respective mass scale during this evaluation and the contributions to the Weinberg operator are calculated at these scales as well. The running of this operator is taken into account as well.

3. The SUSY spectrum is calculated at the scale M_{SUSY} at the one-loop level and the heavy Higgs masses at two-loop level taking into account the contributions from third generation sfermions and fermions, see Ref. [196] for a summary. In addition the matching to the SM-parameters is performed as described in Ref. [213].

4. The SM-parameters are evolved from M_{SUSY} to m_Z using the two-loop SM RGEs. At m_Z, the masses of the SM fermions are calculated and the mass of the Higgs boson at the two-loop level. For these calculations we however take G_F, m_Z, $\alpha(m_Z)$ and $\alpha_s(m_Z)$ to calculate the gauge couplings and the VEV.

5. The gauge and Yukawa couplings as well as the quartic Higgs couplings are then evolved to M_{SUSY} using the two-loop RGEs. At this scale the SUSY threshold corrections to the gauge and Yukawa couplings are taken into account. The resulting couplings are evolved to $M_{\mathrm{GUT}} = 2 \cdot 10^{16}$ GeV. Then steps 2. to 4. are repeated until a relative precision of all masses at the level of 10^{-5} is reached.

6. Once the precision goal for the spectrum has been achieved, the flavour observables are calculated. Also here we have modified the procedure slightly: we have a quite heavy spectrum leading potentially large logs of the form $\ln(M_{\mathrm{SUSY}}/m_t)$. For this reason the calculation is done in two steps: (i) Calculate the SUSY contributions to the Wilson coefficients at $Q = M_{\mathrm{SUSY}}$. (ii) Calculate the SM contributions to the Wilson coefficients at $Q = m_t$. (iii) Add both contributions to calculate the relevant observables.

References

[1] Sheldon L. Glashow. Partial-symmetries of weak interactions. Nuclear Physics, 22(4):579–588, 1961. ISSN 0029-5582. . URL https://www.sciencedirect.com/science/article/pii/0029558261904692.

[2] Steven Weinberg. A model of leptons. Phys. Rev. Lett., 19:1264–1266, Nov 1967. . URL https://link.aps.org/doi/10.1103/PhysRevLett.19.1264.

[3] S. L. Glashow, J. Iliopoulos, and L. Maiani. Weak interactions with lepton-hadron symmetry. Phys. Rev. D, 2:1285–1292, Oct 1970. . URL https://link.aps.org/doi/10.1103/PhysRevD.2.1285.

[4] Steven Weinberg. Effects of a neutral intermediate boson in semileptonic processes. Phys. Rev. D, 5:1412–1417, Mar 1972. . URL https://link.aps.org/doi/10.1103/PhysRevD.5.1412.

[5] David J. Gross and Frank Wilczek. Asymptotically free gauge theories. i. Phys. Rev. D, 8:3633–3652, Nov 1973. . URL https://link.aps.org/doi/10.1103/PhysRevD.8.3633.

[6] David J. Gross and Frank Wilczek. Asymptotically free gauge theories. ii. Phys. Rev. D, 9:980–993, Feb 1974. . URL https://link.aps.org/doi/10.1103/PhysRevD.9.980.

[7] H David Politzer. Asymptotic freedom: An approach to strong interactions. Physics Reports, 14(4):129–180, 1974. ISSN 0370-1573. . URL https://www.sciencedirect.com/science/article/pii/0370157374900143.

[8] G. Arnison, A. Astbury, B. Aubert, C. Bacci, G. Bauer, A. Bézaguet, R. Böck, T.J.V. Bowcock, M. Calvetti, T. Carroll, P. Catz, P. Cennini, S. Centro, F. Ceradini, S. Cittolin, D. Cline, C. Cochet, J. Colas, M. Corden, D. Dallman, M. DeBeer, M. Della Negra, M. Demoulin, D. Denegri, A. Di Ciaccio, D. DiBitonto, L. Dobrzynski, J.D. Dowell, M. Edwards, K. Eggert, E. Eisenhandler, N. Ellis, P. Erhard, H. Faissner, G. Fontaine, R. Frey, R. Frühwirth, J. Garvey, S. Geer, C. Ghesquière, P. Ghez, K.L. Giboni, W.R. Gibson, Y. Giraud-Héraud, A. Givernaud, A. Gonidec, G. Grayer, P. Gutierrez, T. Hansl-Kozanecka, W.J.

Haynes, L.O. Hertzberger, C. Hodges, D. Hoffmann, H. Hoffmann, D.J. Holthuizen, R.J. Homer, A. Honma, W. Jank, G. Jorat, P.I.P. Kalmus, V. Karimäki, R. Keeler, I. Kenyon, A. Kernan, R. Kinnunen, H. Kowalski, W. Kozanecki, D. Kryn, F. Lacava, J.-P. Laugier, J.-P. Lees, H. Lehmann, K. Leuchs, A. Lévêque, E. Linglin, E. Locci, M. Loret, J.-J. Malosse, T. Markiewicz, G. Maurin, T. McMahon, J.-P. Mendiburu, M.-N. Minard, M. Moricca, H. Muirhead, F. Muller, A.K. Nandi, L. Naumann, A. Norton, A. Orkin-Lecourtois, L. Paoluzi, G. Petrucci, G.Piano Mortari, M. Pimiä, A. Placci, E. Radermacher, J. Ransdell, H. Reithler, J.-P. Revol, J. Rich, M. Rijssenbeek, C. Roberts, J. Rohlf, P. Rossi, C. Rubbia, B. Sadoulet, G. Sajot, G. Salvi, J. Salvini, J. Sass, A. Saudraix, A. Savoy-Navarro, D. Schinzel, W. Scott, T.P. Shah, M. Spiro, J. Strauss, K. Sumorok, F. Szoncso, D. Smith, C. Tao, G. Thompson, J. Timmer, E. Tscheslog, J. Tuominiemi, S. Van der Meer, J.-P. Vialle, J. Vrana, V. Vuillemin, H.D. Wahl, P. Watkins, J. Wilson, Y.G. Xie, M. Yvert, and E. Zurfluh. Experimental observation of isolated large transverse energy electrons with associated missing energy at s=540 gev. Physics Letters B, 122(1):103–116, 1983. ISSN 0370-2693. . URL `https://www.sciencedirect.com/science/article/pii/0370269383911772`.

[9] P. Bagnaia, M. Banner, R. Battiston, Ph. Bloch, F. Bonaudi, K. Borer, M. Borghini, J.-C. Chollet, A.G. Clark, C. Conta, P. Darriulat, L. Di Lella, J. Dines-Hansen, P.A. Dorsaz, L. Fayard, M. Fraternali, D. Froidevaux, G. Fumagalli, J.-M. Gaillard, O. Gildemeister, V.G. Goggi, H. Grote, B. Hahn, H. Hänni, J.R. Hansen, P. Hansen, T. Himel, V. Hungerbühler, P. Jenni, O. Kofoed-Hansen, E. Lançon, M. Livan, S. Loucatos, B. Madsen, P. Mani, B. Mansoulié, G.C. Mantovani, L. Mapelli, B. Merkel, M. Mermikides, R. Møllerud, B. Nilsson, C. Onions, G. Parrour, F. Pastore, H. Plothow-Besch, M. Polverel, J.-P. Repellin, A. Rimoldi, A. Rothenberg, A. Roussarie, G. Sauvage, J. Schacher, J.L. Siegrist, H.M. Steiner, G. Stimpfl, F. Stocker, J. Teiger, V. Vercesi, A.R. Weidberg, H. Zaccone, J.A. Zakrzewski, and W. Zeller. Evidence for $z_0 \rightarrow e^+e^-$ at the cern pp collider. Physics Letters B, 129(1):130–140, 1983. ISSN 0370-2693. . URL `https://www.sciencedirect.com/science/article/pii/037026938390744X`.

[10] Georges Aad et al. Observation of a new particle in the search for the Standard Model Higgs boson with the ATLAS detector at the LHC. Phys. Lett. B, 716: 1–29, 2012. .

[11] Serguei Chatrchyan et al. Observation of a New Boson at a Mass of 125 GeV with the CMS Experiment at the LHC. Phys. Lett. B, 716:30–61, 2012. .

[12] Katherine Garrett and Gintaras Duda. Dark Matter: A Primer. Adv. Astron., 2011:968283, 2011. .

[13] Andrew R. Liddle. An Introduction to cosmological inflation. In ICTP Summer School in High-Energy Physics and Cosmology, pages 260–295, 1 1999.

[14] T. Aoyama et al. The anomalous magnetic moment of the muon in the Standard Model. Phys. Rept., 887:1–166, 2020. .

[15] Tatsumi Aoyama, Masashi Hayakawa, Toichiro Kinoshita, and Makiko Nio. Complete Tenth-Order QED Contribution to the Muon g-2. Phys. Rev. Lett., 109: 111808, 2012. .

[16] Tatsumi Aoyama, Toichiro Kinoshita, and Makiko Nio. Theory of the Anomalous Magnetic Moment of the Electron. Atoms, 7(1):28, 2019. .

[17] Andrzej Czarnecki, William J. Marciano, and Arkady Vainshtein. Refinements in electroweak contributions to the muon anomalous magnetic moment. Phys. Rev. D, 67:073006, 2003. . [Erratum: Phys.Rev.D 73, 119901 (2006)].

[18] C. Gnendiger, D. Stöckinger, and H. Stöckinger-Kim. The electroweak contributions to $(g-2)_\mu$ after the Higgs boson mass measurement. Phys. Rev. D, 88:053005, 2013. .

[19] Michel Davier, Andreas Hoecker, Bogdan Malaescu, and Zhiqing Zhang. Reevaluation of the hadronic vacuum polarisation contributions to the Standard Model predictions of the muon $g-2$ and $\alpha(m_Z^2)$ using newest hadronic cross-section data. Eur. Phys. J. C, 77(12):827, 2017. .

[20] Alexander Keshavarzi, Daisuke Nomura, and Thomas Teubner. Muon $g-2$ and $\alpha(M_Z^2)$: a new data-based analysis. Phys. Rev. D, 97(11):114025, 2018. .

[21] Gilberto Colangelo, Martin Hoferichter, and Peter Stoffer. Two-pion contribution to hadronic vacuum polarization. JHEP, 02:006, 2019. .

[22] Martin Hoferichter, Bai-Long Hoid, and Bastian Kubis. Three-pion contribution to hadronic vacuum polarization. JHEP, 08:137, 2019. .

[23] M. Davier, A. Hoecker, B. Malaescu, and Z. Zhang. A new evaluation of the hadronic vacuum polarisation contributions to the muon anomalous magnetic moment and to $\boldsymbol{\alpha}(\mathbf{m_Z^2})$. Eur. Phys. J. C, 80(3):241, 2020. . [Erratum: Eur.Phys.J.C 80, 410 (2020)].

[24] Alexander Keshavarzi, Daisuke Nomura, and Thomas Teubner. $g-2$ of charged leptons, $\alpha(M_Z^2)$, and the hyperfine splitting of muonium. Phys. Rev. D, 101(1): 014029, 2020. .

[25] Alexander Kurz, Tao Liu, Peter Marquard, and Matthias Steinhauser. Hadronic contribution to the muon anomalous magnetic moment to next-to-next-to-leading order. Phys. Lett. B, 734:144–147, 2014. .

[26] Kirill Melnikov and Arkady Vainshtein. Hadronic light-by-light scattering contribution to the muon anomalous magnetic moment revisited. Phys. Rev. D, 70:113006, 2004. .

[27] Pere Masjuan and Pablo Sanchez-Puertas. Pseudoscalar-pole contribution to the $(g_\mu - 2)$: a rational approach. Phys. Rev. D, 95(5):054026, 2017. .

[28] Gilberto Colangelo, Martin Hoferichter, Massimiliano Procura, and Peter Stoffer. Dispersion relation for hadronic light-by-light scattering: two-pion contributions. JHEP, 04:161, 2017. .

[29] Martin Hoferichter, Bai-Long Hoid, Bastian Kubis, Stefan Leupold, and Sebastian P. Schneider. Dispersion relation for hadronic light-by-light scattering: pion pole. JHEP, 10:141, 2018. .

[30] Antoine Gérardin, Harvey B. Meyer, and Andreas Nyffeler. Lattice calculation of the pion transition form factor with $N_f = 2 + 1$ Wilson quarks. Phys. Rev. D, 100(3):034520, 2019. .

[31] Johan Bijnens, Nils Hermansson-Truedsson, and Antonio Rodríguez-Sánchez. Short-distance constraints for the HLbL contribution to the muon anomalous magnetic moment. Phys. Lett. B, 798:134994, 2019. .

[32] Gilberto Colangelo, Franziska Hagelstein, Martin Hoferichter, Laetitia Laub, and Peter Stoffer. Longitudinal short-distance constraints for the hadronic light-by-light contribution to $(g-2)_\mu$ with large-N_c Regge models. JHEP, 03: 101, 2020. .

[33] Thomas Blum, Norman Christ, Masashi Hayakawa, Taku Izubuchi, Luchang Jin, Chulwoo Jung, and Christoph Lehner. Hadronic Light-by-Light Scattering Contribution to the Muon Anomalous Magnetic Moment from Lattice QCD. Phys. Rev. Lett., 124(13):132002, 2020. .

[34] Gilberto Colangelo, Martin Hoferichter, Andreas Nyffeler, Massimo Passera, and Peter Stoffer. Remarks on higher-order hadronic corrections to the muon g−2. Phys. Lett. B, 735:90–91, 2014. .

[35] Y. Fukuda, T. Hayakawa, E. Ichihara, K. Inoue, K. Ishihara, H. Ishino, Y. Itow, T. Kajita, J. Kameda, S. Kasuga, K. Kobayashi, Y. Kobayashi, Y. Koshio, M. Miura, M. Nakahata, S. Nakayama, A. Okada, K. Okumura, N. Sakurai, M. Shiozawa, Y. Suzuki, Y. Takeuchi, Y. Totsuka, S. Yamada, M. Earl, A. Habig, E. Kearns, M. D. Messier, K. Scholberg, J. L. Stone, L. R. Sulak, C. W. Walter, M. Goldhaber, T. Barszczxak, D. Casper, W. Gajewski, P. G. Halverson, J. Hsu, W. R. Kropp, L. R. Price, F. Reines, M. Smy, H. W. Sobel, M. R. Vagins, K. S. Ganezer, W. E. Keig, R. W. Ellsworth, S. Tasaka, J. W. Flanagan, A. Kibayashi, J. G. Learned, S. Matsuno, V. J. Stenger, D. Takemori, T. Ishii, J. Kanzaki,

T. Kobayashi, S. Mine, K. Nakamura, K. Nishikawa, Y. Oyama, A. Sakai, M. Sakuda, O. Sasaki, S. Echigo, M. Kohama, A. T. Suzuki, T. J. Haines, E. Blaufuss, B. K. Kim, R. Sanford, R. Svoboda, M. L. Chen, Z. Conner, J. A. Goodman, G. W. Sullivan, J. Hill, C. K. Jung, K. Martens, C. Mauger, C. McGrew, E. Sharkey, B. Viren, C. Yanagisawa, W. Doki, K. Miyano, H. Okazawa, C. Saji, M. Takahata, Y. Nagashima, M. Takita, T. Yamaguchi, M. Yoshida, S. B. Kim, M. Etoh, K. Fujita, A. Hasegawa, T. Hasegawa, S. Hatakeyama, T. Iwamoto, M. Koga, T. Maruyama, H. Ogawa, J. Shirai, A. Suzuki, F. Tsushima, M. Koshiba, M. Nemoto, K. Nishijima, T. Futagami, Y. Hayato, Y. Kanaya, K. Kaneyuki, Y. Watanabe, D. Kielczewska, R. A. Doyle, J. S. George, A. L. Stachyra, L. L. Wai, R. J. Wilkes, and K. K. Young. Evidence for oscillation of atmospheric neutrinos. Phys. Rev. Lett., 81:1562–1567, Aug 1998. . URL `https://link.aps.org/doi/10.1103/PhysRevLett.81.1562`.

[36] Stephen P. Martin. A Supersymmetry primer. Adv. Ser. Direct. High Energy Phys., 18:1–98, 1998. .

[37] H. Fritzsch, M. Gell-Mann, and H. Leutwyler. Advantages of the color octet gluon picture. Physics Letters B, 47(4):365–368, 1973. ISSN 0370-2693. . URL `https://www.sciencedirect.com/science/article/pii/0370269373906254`.

[38] F. Englert and R. Brout. Broken symmetry and the mass of gauge vector mesons. Phys. Rev. Lett., 13:321–323, Aug 1964. . URL `https://link.aps.org/doi/10.1103/PhysRevLett.13.321`.

[39] Peter W. Higgs. Broken symmetries and the masses of gauge bosons. Phys. Rev. Lett., 13:508–509, Oct 1964. . URL `https://link.aps.org/doi/10.1103/PhysRevLett.13.508`.

[40] N. Cabibbo. Unitary Symmetry and Leptonic Decays. Phys. Rev. Lett., 10: 531–533, 1963. .

[41] M. Kobayashi and T. Maskawa. CP Violation in the Renormalizable Theory of Weak Interaction. Prog. Theor. Phys., 49:652–657, 1973. .

[42] Ziro Maki, Masami Nakagawa, and Shoichi Sakata. Remarks on the Unified Model of Elementary Particles. Progress of Theoretical Physics, 28(5):870–880, 11 1962. ISSN 0033-068X. . URL `https://doi.org/10.1143/PTP.28.870`.

[43] Gerhart Lüders. Proof of the tcp theorem. Annals of Physics, 2(1):1–15, 1957. ISSN 0003-4916. . URL `https://www.sciencedirect.com/science/article/pii/0003491657900325`.

[44] J. M. Cline, Baryogenesis [arXiv:hep-ph/0609145 [hep-ph]].

[45] S. Davidson, E. Nardi and Y. Nir, Phys. Rept. **466** (2008), 105-177 doi:10.1016/j.physrep.2008.06.002 [arXiv:0802.2962 [hep-ph]].

[46] S. O. Bilson-Thompson, F. Markopoulou and L. Smolin, Class. Quant. Grav. **24** (2007), 3975-3994 doi:10.1088/0264-9381/24/16/002 [arXiv:hep-th/0603022 [hep-th]].

[47] S. F. King. Unified Models of Neutrinos, Flavour and CP Violation. Prog. Part. Nucl. Phys., 94:217–256, 2017. .

[48] Ivan Esteban, M. C. Gonzalez-Garcia, Alvaro Hernandez-Cabezudo, Michele Maltoni, and Thomas Schwetz. Global analysis of three-flavour neutrino oscillations: synergies and tensions in the determination of θ_{23}, δ_{CP}, and the mass ordering. JHEP, 01:106, 2019. .

[49] P. A. R. Ade et al. Planck 2015 results. XIII. Cosmological parameters. Astron. Astrophys., 594:A13, 2016. .

[50] Vera C. Rubin and Jr. Ford, W. Kent. Rotation of the Andromeda Nebula from a Spectroscopic Survey of Emission Regions. ApJ, 159:379, February 1970. .

[51] V. C. Rubin, Jr. Ford, W. K., and N. Thonnard. Rotational properties of 21 SC galaxies with a large range of luminosities and radii, from NGC 4605 (R=4kpc) to UGC 2885 (R=122kpc). ApJ, 238:471–487, June 1980. .

[52] Maxim Markevitch. Chandra observation of the most interesting cluster in the universe. ESA Spec. Publ., 604:723, 2006.

[53] Douglas Clowe, Marusa Bradac, Anthony H. Gonzalez, Maxim Markevitch, Scott W. Randall, Christine Jones, and Dennis Zaritsky. A direct empirical proof of the existence of dark matter. Astrophys. J. Lett., 648:L109–L113, 2006. .

[54] N. Aghanim et al. Planck 2018 results. VI. Cosmological parameters. Astron. Astrophys., 641:A6, 2020. . [Erratum: Astron.Astrophys. 652, C4 (2021)].

[55] Kerstin E. Kunze. An introduction to cosmology. In 8th CERN–Latin-American School of High-Energy Physics, pages 177–212, 2016. .

[56] John Ellis, J.S. Hagelin, D.V. Nanopoulos, K. Olive, and M. Srednicki. Supersymmetric relics from the big bang. Nuclear Physics B, 238(2):453–476, 1984. ISSN 0550-3213. . URL https://www.sciencedirect.com/science/article/pii/0550321384904619.

[57] Gino Isidori and David M. Straub. Minimal Flavour Violation and Beyond. Eur. Phys. J. C, 72:2103, 2012. .

[58] Samuel J. Rowley, Jordan Bernigaud, Björn Herrmann, and Stephen F. King. Non-Minimal Flavour Violation in $A_4 \times SU(5)$ SUSY GUTs. In 54th Rencontres de Moriond on Electroweak Interactions and Unified Theories, pages 427–430, 2019.

[59] Jordan Bernigaud, Adam K. Forster, Björn Herrmann, Stephen F. King, Werner Porod, and Samuel J. Rowley. Data-driven analysis of a SUSY GUT of flavour. 11 2021.

[60] Adam K. Forster and Stephen F. King. Muon g-2, Dark Matter and the Higgs mass in No-Scale Supergravity. 9 2021.

[61] Peter Minkowski. $\mu \to e\gamma$ at a Rate of One Out of 1-Billion Muon Decays? Phys.Lett., B67:421, 1977. .

[62] Murray Gell-Mann, Pierre Ramond, and Richard Slansky. Complex Spinors and Unified Theories. Conf.Proc., C790927:315–321, 1979.

[63] Tsutomu Yanagida. Horizontal Symmetry and Masses of Neutrinos. Conf.Proc., C7902131:95–99, 1979.

[64] Rabindra N. Mohapatra and Goran Senjanovic. Neutrino Mass and Spontaneous Parity Violation. Phys.Rev.Lett., 44:912, 1980. .

[65] J. Schechter and J. W. F. Valle. Neutrino Masses in $SU(2) \times U(1)$ Theories. Phys. Rev., D22:2227, 1980. .

[66] S. F. King. Neutrino mass models. Rept. Prog. Phys., 67:107–158, 2004. .

[67] Rupert Coy and Michele Frigerio. Effective comparison of neutrino-mass models. 10 2021.

[68] Z. Maki, M. Nakagawa, and S. Sakata. Remarks on the unified model of elementary particles. Prog. Theor. Phys., 28:870–880, 1962. .

[69] B. Pontecorvo. Neutrino Experiments and the Problem of Conservation of Leptonic Charge. Sov. Phys. JETP, 26:984–988, 1968. [Zh. Eksp. Teor. Fiz.53,1717(1967)].

[70] Michelle J. Dolinski, Alan W. P. Poon, and Werner Rodejohann. Neutrinoless Double-Beta Decay: Status and Prospects. Ann. Rev. Nucl. Part. Sci., 69:219–251, 2019. .

[71] Howard Georgi and S. L. Glashow. Unity of all elementary-particle forces. Phys. Rev. Lett., 32:438–441, Feb 1974. . URL `https://link.aps.org/doi/10.1103/PhysRevLett.32.438`.

[72] Howard Georgi. The state of the art—gauge theories. AIP Conference Proceedings, 23(1):575–582, 1975. . URL `https://aip.scitation.org/doi/abs/10.1063/1.2947450`.

[73] Alan H. Guth. Inflationary universe: A possible solution to the horizon and flatness problems. PrD, 23(2):347–356, January 1981. .

[74] A. A. Starobinskiĭ. Spectrum of relict gravitational radiation and the early state of the universe. Soviet Journal of Experimental and Theoretical Physics Letters, 30:682, December 1979.

[75] G. W. Bennett et al. Final Report of the Muon E821 Anomalous Magnetic Moment Measurement at BNL. Phys. Rev. D, 73:072003, 2006. .

[76] B. Abi et al. Measurement of the Positive Muon Anomalous Magnetic Moment to 0.46 ppm. Phys. Rev. Lett., 126(14):141801, 2021. .

[77] Andrzej Czarnecki and William J. Marciano. The Muon anomalous magnetic moment: A Harbinger for 'new physics'. Phys. Rev. D, 64:013014, 2001. .

[78] Qaisar Shafi and Cem Salih Ün. Sparticle Spectroscopy at LHC-Run3 and LSP Dark Matter in light of Muon g-2. 7 2021.

[79] Shu-Min Zhao, Lu-Hao Su, Xing-Xing Dong, Tong-Tong Wang, and Tai-Fu Feng. Study muon g-2 at two-loop level in the $U(1)_X$SSM. 7 2021.

[80] Zhuang Li, Guo-Li Liu, Fei Wang, Jin Min Yang, and Yang Zhang. Gluino-SUGRA scenarios in light of FNAL muon g-2 anomaly. 6 2021.

[81] Fei Wang, Lei Wu, Yang Xiao, Jin Min Yang, and Yang Zhang. GUT-scale constrained SUSY in light of new muon g-2 measurement. Nucl. Phys. B, 970: 115486, 2021. .

[82] Yuchao Gu, Ning Liu, Liangliang Su, and Daohan Wang. Heavy bino and slepton for muon g − 2 anomaly. Nucl. Phys. B, 969:115481, 2021. .

[83] Chengcheng Han. Muon g-2 and CP violation in MSSM. 4 2021.

[84] Motoi Endo, Koichi Hamaguchi, Sho Iwamoto, and Teppei Kitahara. Muon $g-2$ vs LHC Run 2 in supersymmetric models. JHEP, 04:165, 2020. .

[85] Junjie Cao, Jingwei Lian, Yusi Pan, Di Zhang, and Pengxuan Zhu. Improved $(g-2)_\mu$ measurement and singlino dark matter in μ-term extended $\mathbb{Z}_3$-NMSSM. JHEP, 09:175, 2021. .

[86] A. B. Lahanas and Dimitri V. Nanopoulos. The Road to No Scale Supergravity. Phys. Rept., 145:1, 1987. .

[87] Alan H. Guth. The Inflationary Universe: A Possible Solution to the Horizon and Flatness Problems. Phys. Rev. D, 23:347–356, 1981. .

[88] Andrei D. Linde. A New Inflationary Universe Scenario: A Possible Solution of the Horizon, Flatness, Homogeneity, Isotropy and Primordial Monopole Problems. Phys. Lett. B, 108:389–393, 1982. .

[89] Viatcheslav F. Mukhanov and G. V. Chibisov. Quantum Fluctuations and a Nonsingular Universe. JETP Lett., 33:532–535, 1981.

[90] Andreas Albrecht and Paul J. Steinhardt. Cosmology for Grand Unified Theories with Radiatively Induced Symmetry Breaking. Phys. Rev. Lett., 48: 1220–1223, 1982. .

[91] Andrei D. Linde. Chaotic Inflation. Phys. Lett. B, 129:177–181, 1983. .

[92] Andrei D. Linde. Inflationary Cosmology. Lect. Notes Phys., 738:1–54, 2008. .

[93] Andrei D. Linde. Particle physics and inflationary cosmology, volume 5. 1990.

[94] David H. Lyth and Antonio Riotto. Particle physics models of inflation and the cosmological density perturbation. Phys. Rept., 314:1–146, 1999. .

[95] P. A. R. Ade et al. Planck 2015 results. XX. Constraints on inflation. Astron. Astrophys., 594:A20, 2016. .

[96] Jerome Martin, Christophe Ringeval, and Vincent Vennin. Encyclopædia Inflationaris. Phys. Dark Univ., 5-6:75–235, 2014. .

[97] Alexei A. Starobinsky. A New Type of Isotropic Cosmological Models Without Singularity. Phys. Lett. B, 91:99–102, 1980. .

[98] John R. Ellis, Dimitri V. Nanopoulos, Keith A. Olive, and K. Tamvakis. Fluctuations in a Supersymmetric Inflationary Universe. Phys. Lett. B, 120: 331–334, 1983. .

[99] John R. Ellis, Dimitri V. Nanopoulos, Keith A. Olive, and K. Tamvakis. Cosmological Inflation Cries Out for Supersymmetry. Phys. Lett. B, 118:335, 1982. .

[100] John R. Ellis, Dimitri V. Nanopoulos, Keith A. Olive, and K. Tamvakis. PRIMORDIAL SUPERSYMMETRIC INFLATION. Nucl. Phys. B, 221:524–548, 1983. .

[101] John R. Ellis, K. Enqvist, Dimitri V. Nanopoulos, Keith A. Olive, and M. Srednicki. SU(N,1) Inflation. Phys. Lett. B, 152:175, 1985. . [Erratum: Phys.Lett.B 156, 452 (1985)].

[102] Stefan Antusch, Mar Bastero-Gil, Koushik Dutta, Steve F. King, and Philipp M. Kostka. Chaotic Inflation in Supergravity with Heisenberg Symmetry. Phys. Lett. B, 679:428–432, 2009. .

[103] Stefan Antusch and Francesco Cefalà. SUGRA New Inflation with Heisenberg Symmetry. JCAP, 10:055, 2013. .

[104] Kazunori Nakayama, Fuminobu Takahashi, and Tsutomu T. Yanagida. Polynomial Chaotic Inflation in the Planck Era. Phys. Lett. B, 725:111–114, 2013. .

[105] Stephen C. Davis and Marieke Postma. SUGRA chaotic inflation and moduli stabilisation. JCAP, 03:015, 2008. .

[106] Renata Kallosh, Andrei Linde, Keith A. Olive, and Tomas Rube. Chaotic inflation and supersymmetry breaking. Phys. Rev. D, 84:083519, 2011. .

[107] D. H. Lyth. A Bound on Inflationary Energy Density From the Isotropy of the Microwave Background. Phys. Lett. B, 147:403, 1984. . [Erratum: Phys.Lett.B 150, 465 (1985)].

[108] John Ellis, Dimitri V. Nanopoulos, and Keith A. Olive. No-Scale Supergravity Realization of the Starobinsky Model of Inflation. Phys. Rev. Lett., 111:111301, 2013. . [Erratum: Phys.Rev.Lett. 111, 129902 (2013)].

[109] John Ellis, Dimitri V. Nanopoulos, and Keith A. Olive. Starobinsky-like Inflationary Models as Avatars of No-Scale Supergravity. JCAP, 10:009, 2013. .

[110] John Ellis, Dimitri V. Nanopoulos, and Keith A. Olive. A no-scale supergravity framework for sub-Planckian physics. Phys. Rev. D, 89(4):043502, 2014. .

[111] Miguel Crispim Romao and Stephen F. King. Starobinsky-like inflation in no-scale supergravity Wess-Zumino model with Polonyi term. JHEP, 07:033, 2017. .

[112] Stephen F. King and Elena Perdomo. Starobinsky-like inflation and soft-SUSY breaking. JHEP, 05:211, 2019. .

[113] Kwang Sik Jeong, Junichiro Kawamura, and Chan Beom Park. Mixed modulus and anomaly mediation in light of the muon $g-2$ anomaly. JHEP, 10:064, 2021. .

[114] Werner Porod. SPheno, a program for calculating supersymmetric spectra, SUSY particle decays and SUSY particle production at e+ e- colliders. Comput. Phys. Commun., 153:275–315, 2003. .

[115] W. Porod and F. Staub. SPheno 3.1: Extensions including flavour, CP-phases and models beyond the MSSM. Comput. Phys. Commun., 183:2458–2469, 2012. .

[116] S. Heinemeyer, W. Hollik, and G. Weiglein. FeynHiggs: A Program for the calculation of the masses of the neutral CP even Higgs bosons in the MSSM. Comput. Phys. Commun., 124:76–89, 2000. .

[117] G. Belanger, F. Boudjema, A. Pukhov, and A. Semenov. micrOMEGAs: Version 1.3. Comput. Phys. Commun., 174:577–604, 2006. .

[118] G. Belanger, F. Boudjema, A. Pukhov, and A. Semenov. MicrOMEGAs 2.0: A Program to calculate the relic density of dark matter in a generic model. Comput. Phys. Commun., 176:367–382, 2007. .

[119] G. Belanger, F. Boudjema, A. Pukhov, and A. Semenov. Dark matter direct detection rate in a generic model with micrOMEGAs 2.2. Comput. Phys. Commun., 180:747–767, 2009. .

[120] G. Belanger, F. Boudjema, A. Pukhov, and A. Semenov. micrOMEGAs: A Tool for dark matter studies. Nuovo Cim. C, 033N2:111–116, 2010. .

[121] G. Belanger, F. Boudjema, A. Pukhov, and A. Semenov. micrOMEGAs_3: A program for calculating dark matter observables. Comput. Phys. Commun., 185: 960–985, 2014. .

[122] Manuel Drees, Herbi Dreiner, Daniel Schmeier, Jamie Tattersall, and Jong Soo Kim. CheckMATE: Confronting your Favourite New Physics Model with LHC Data. Comput. Phys. Commun., 187:227–265, 2015. .

[123] Daniel Dercks, Nishita Desai, Jong Soo Kim, Krzysztof Rolbiecki, Jamie Tattersall, and Torsten Weber. CheckMATE 2: From the model to the limit. Comput. Phys. Commun., 221:383–418, 2017. .

[124] Jason L. Evans, Natsumi Nagata, and Keith A. Olive. A Minimal SU(5) SuperGUT in Pure Gravity Mediation. Eur. Phys. J. C, 79(6):490, 2019. .

[125] Kwang Sik Jeong, Junichiro Kawamura, and Chan Beom Park. Mixed modulus and anomaly mediation in light of the muon $g-2$ anomaly. JHEP, 10:064, 2021. .

[126] John R. Ellis, Keith A. Olive, Yudi Santoso, and Vassilis C. Spanos. Very constrained minimal supersymmetric standard models. Phys. Rev. D, 70:055005, 2004. .

[127] W. K. Hastings. Monte Carlo Sampling Methods Using Markov Chains and Their Applications. Biometrika, 57:97–109, 1970. .

[128] John Ellis, Jason L. Evans, Natsumi Nagata, Keith A. Olive, and L. Velasco-Sevilla. Low-Energy Probes of No-Scale SU(5) Super-GUTs. Eur. Phys. J. C, 81(2):120, 2021. .

[129] R. Frederix, S. Frixione, V. Hirschi, D. Pagani, H. S. Shao, and M. Zaro. The automation of next-to-leading order electroweak calculations. JHEP, 07:185, 2018. . [Erratum: JHEP 11, 085 (2021)].

[130] J. Alwall, R. Frederix, S. Frixione, V. Hirschi, F. Maltoni, O. Mattelaer, H. S. Shao, T. Stelzer, P. Torrielli, and M. Zaro. The automated computation of tree-level and

next-to-leading order differential cross sections, and their matching to parton shower simulations. JHEP, 07:079, 2014. .

[131] Torbjörn Sjöstrand, Stefan Ask, Jesper R. Christiansen, Richard Corke, Nishita Desai, Philip Ilten, Stephen Mrenna, Stefan Prestel, Christine O. Rasmussen, and Peter Z. Skands. An introduction to PYTHIA 8.2. Comput. Phys. Commun., 191: 159–177, 2015. .

[132] Torbjorn Sjostrand, Stephen Mrenna, and Peter Z. Skands. A Brief Introduction to PYTHIA 8.1. Comput. Phys. Commun., 178:852–867, 2008. .

[133] J. de Favereau, C. Delaere, P. Demin, A. Giammanco, V. Lemaître, A. Mertens, and M. Selvaggi. DELPHES 3, A modular framework for fast simulation of a generic collider experiment. JHEP, 02:057, 2014. .

[134] Matteo Cacciari and Gavin P. Salam. Dispelling the N^3 myth for the k_t jet-finder. Phys. Lett. B, 641:57–61, 2006. .

[135] Matteo Cacciari, Gavin P. Salam, and Gregory Soyez. FastJet User Manual. Eur. Phys. J. C, 72:1896, 2012. .

[136] Matteo Cacciari, Gavin P. Salam, and Gregory Soyez. The anti-k_t jet clustering algorithm. JHEP, 04:063, 2008. .

[137] Alexander L. Read. Presentation of search results: The CL(s) technique. J. Phys. G, 28:2693–2704, 2002. .

[138] Morad Aaboud et al. Search for dark matter and other new phenomena in events with an energetic jet and large missing transverse momentum using the ATLAS detector. JHEP, 01:126, 2018. .

[139] Georges Aad et al. Search for squarks and gluinos in final states with jets and missing transverse momentum using 139 fb^{-1} of $\sqrt{s}$ =13 TeV pp collision data with the ATLAS detector. JHEP, 02:143, 2021. .

[140] A. M. Sirunyan et al. Search for electroweak production of charginos and neutralinos in multilepton final states in proton-proton collisions at $\sqrt{s} = 13$ TeV. JHEP, 03:166, 2018. .

[141] G. Aad et al. Observation of a new particle in the search for the Standard Model Higgs boson with the ATLAS detector at the LHC. Phys. Lett., B716:1–29, 2012. .

[142] S. Chatrchyan et al. Observation of a new boson at a mass of 125 GeV with the CMS experiment at the LHC. Phys. Lett., B716:30–61, 2012. .

[143] M. Arana-Catania, S. Heinemeyer, and M. J. Herrero. Updated Constraints on General Squark Flavor Mixing. Phys. Rev. D, 90(7):075003, 2014. .

[144] Kamila Kowalska. Phenomenology of SUSY with General Flavour Violation. JHEP, 09:139, 2014. .

[145] Karen De Causmaecker, Benjamin Fuks, Bjoern Herrmann, Farvah Mahmoudi, Ben O'Leary, Werner Porod, Sezen Sekmen, and Nadja Strobbe. General squark flavour mixing: constraints, phenomenology and benchmarks. JHEP, 11:125, 2015. .

[146] A. Bartl, K. Hidaka, K. Hohenwarter-Sodek, T. Kernreiter, W. Majerotto, and W. Porod. Test of lepton flavor violation at LHC. Eur. Phys. J. C, 46:783–789, 2006. .

[147] Giuseppe Bozzi, Benjamin Fuks, Bjorn Herrmann, and Michael Klasen. Squark and gaugino hadroproduction and decays in non-minimal flavour violating supersymmetry. Nucl. Phys. B, 787:1–54, 2007. .

[148] A. Bartl, K. Hidaka, K. Hohenwarter-Sodek, T. Kernreiter, W. Majerotto, and Werner Porod. Impact of slepton generation mixing on the search for sneutrinos. Phys. Lett. B, 660:228–235, 2008. .

[149] F. del Aguila et al. Collider aspects of flavour physics at high Q. Eur. Phys. J. C, 57:183–308, 2008. .

[150] Tobias Hurth and Werner Porod. Flavour violating squark and gluino decays. JHEP, 08:087, 2009. .

[151] A. Bartl, K. Hidaka, K. Hohenwarter-Sodek, T. Kernreiter, W. Majerotto, and W. Porod. Impact of squark generation mixing on the search for gluinos at LHC. Phys. Lett. B, 679:260–266, 2009. .

[152] Matthias Bruhnke, Bjorn Herrmann, and Werner Porod. Signatures of bosonic squark decays in non-minimally flavour-violating supersymmetry. JHEP, 09:006, 2010. .

[153] A. Bartl, H. Eberl, B. Herrmann, K. Hidaka, W. Majerotto, and W. Porod. Impact of squark generation mixing on the search for squarks decaying into fermions at LHC. Phys. Lett. B, 698:380–388, 2011. . [Erratum: Phys.Lett.B 700, 390–390 (2011)].

[154] A. Bartl, H. Eberl, E. Ginina, B. Herrmann, K. Hidaka, W. Majerotto, and W. Porod. Flavour violating gluino three-body decays at LHC. Phys. Rev. D, 84:115026, 2011. .

[155] A. Bartl, H. Eberl, E. Ginina, B. Herrmann, K. Hidaka, W. Majerotto, and W. Porod. Flavor violating bosonic squark decays at LHC. Int. J. Mod. Phys. A, 29(07):1450035, 2014. .

[156] A. Bartl, H. Eberl, E. Ginina, K. Hidaka, and W. Majerotto. $h^0 \to c\bar{c}$ as a test case for quark flavor violation in the MSSM. Phys. Rev. D, 91(1):015007, 2015. .

[157] Monika Blanke, Benjamin Fuks, Iftah Galon, and Gilad Perez. Gluino Meets Flavored Naturalness. JHEP, 04:044, 2016. .

[158] G. Brooijmans et al. Les Houches 2017: Physics at TeV Colliders New Physics Working Group Report. In 10th Les Houches Workshop on Physics at TeV Colliders, 3 2018.

[159] Amit Chakraborty, Motoi Endo, Benjamin Fuks, Björn Herrmann, Mihoko M. Nojiri, Priscilla Pani, and Giacomo Polesello. Flavour-violating decays of mixed top-charm squarks at the LHC. Eur. Phys. J. C, 78(10):844, 2018. .

[160] Vernon Barger, Danny Marfatia, Azar Mustafayev, and Ali Soleimani. SUSY dark matter and lepton flavor violation. Phys. Rev. D, 80:076004, 2009. .

[161] D. Choudhury, R. Garani, and S. K. Vempati. Flavored Co-annihilations. JHEP, 06:014, 2012. .

[162] Bjorn Herrmann, Michael Klasen, and Quentin Le Boulc'h. Impact of squark flavour violation on neutralino dark matter. Phys. Rev. D, 84:095007, 2011. .

[163] Prateek Agrawal, Monika Blanke, and Katrin Gemmler. Flavored dark matter beyond Minimal Flavor Violation. JHEP, 10:072, 2014. .

[164] Ugo Amaldi, Wim de Boer, and Hermann Furstenau. Comparison of grand unified theories with electroweak and strong coupling constants measured at LEP. Phys. Lett. B, 260:447–455, 1991. .

[165] Alexander S. Belyaev, Steve F. King, and Patrick B. Schaefers. Muon g-2 and dark matter suggest nonuniversal gaugino masses: $SU(5) \times A_4$ case study at the LHC. Phys. Rev., **D97**(11):115002, 2018. .

[166] Maria Dimou, Stephen F. King, and Christoph Luhn. Phenomenological implications of an SU(5)×S_4 ×U(1) SUSY GUT of flavor. Phys. Rev., D93(7): 075026, 2016. .

[167] Maria Dimou, Stephen F. King, and Christoph Luhn. Approaching Minimal Flavour Violation from an $SU(5) \times S_4 \times U(1)$ SUSY GUT. JHEP, **02**:118, 2016. .

[168] Jordan Bernigaud, Björn Herrmann, Stephen F. King, and Samuel J. Rowley. Non-minimal flavour violation in A_4× SU(5) SUSY GUTs with smuon assisted dark matter. JHEP, 03:067, 2019. .

[169] N. Metropolis, A. W. Rosenbluth, M. N. Rosenbluth, A. H. Teller, and E. Teller. Equation of state calculations by fast computing machines. J. Chem. Phys., 21: 1087–1092, 1953. .

[170] W. K. Hastings. Monte Carlo Sampling Methods Using Markov Chains and Their Applications. Biometrika, 57:97–109, 1970. .

[171] A. A. Markov.
Extension of the limit theorems of probability theory to a sum of variables connected in a chain. reprinted in Appendix B of: R. Howard, *Dynamic Probabilistic Systems, volume 1: Markov Chains*, John Wiley and Sons, 1971.

[172] Claudia Hagedorn, Stephen F. King, and Christoph Luhn. A SUSY GUT of Flavour with S4 x SU(5) to NLO. JHEP, 06:048, 2010. .

[173] Claudia Hagedorn, Stephen F. King, and Christoph Luhn. SUSY $S_4 \times$ SU(5) revisited. Phys. Lett., B717:207–213, 2012. .

[174] D. J. H. Chung, L. L. Everett, G. L. Kane, S. F. King, Joseph D. Lykken, and Lian-Tao Wang. The Soft supersymmetry breaking Lagrangian: Theory and applications. Phys. Rept., 407:1–203, 2005. .

[175] Lincoln Wolfenstein. Parametrization of the Kobayashi-Maskawa Matrix. Phys. Rev. Lett., 51:1945, 1983. .

[176] Christoph Luhn. Trimaximal TM_1 neutrino mixing in S_4 with spontaneous CP violation. Nucl. Phys., B875:80–100, 2013. .

[177] Raoul Gatto, G. Sartori, and M. Tonin. Weak Selfmasses, Cabibbo Angle, and Broken $SU(2) \times SU(2)$. Phys. Lett., 28B:128–130, 1968. .

[178] Howard Georgi and C. Jarlskog. A New Lepton - Quark Mass Relation in a Unified Theory. Phys. Lett., 86B:297–300, 1979. .

[179] Stefan Antusch and Martin Spinrath. New GUT predictions for quark and lepton mass ratios confronted with phenomenology. Phys. Rev. D, 79:095004, 2009. .

[180] Stefan Antusch, Stephen F. King, and Martin Spinrath. GUT predictions for quark-lepton Yukawa coupling ratios with messenger masses from non-singlets. Phys. Rev. D, 89(5):055027, 2014. .

[181] F. Staub. SARAH. 2008.

[182] Florian Staub. SARAH 4 : A tool for (not only SUSY) model builders. Comput. Phys. Commun., 185:1773–1790, 2014. .

[183] Florian Staub. SARAH 3.2: Dirac Gauginos, UFO output, and more. Comput. Phys. Commun., 184:1792–1809, 2013. .

[184] Florian Staub. Automatic Calculation of supersymmetric Renormalization Group Equations and Self Energies. Comput. Phys. Commun., 182:808–833, 2011. .

[185] Florian Staub. From Superpotential to Model Files for FeynArts and CalcHep/CompHep. Comput. Phys. Commun., 181:1077–1086, 2010. .

[186] Werner Porod, Florian Staub, and Avelino Vicente. A Flavor Kit for BSM models. Eur. Phys. J. C, 74(8):2992, 2014. .

[187] Peter Z. Skands et al. SUSY Les Houches accord: Interfacing SUSY spectrum calculators, decay packages, and event generators. JHEP, 07:036, 2004. .

[188] B. C. Allanach et al. SUSY Les Houches Accord 2. Comput. Phys. Commun., 180:8–25, 2009. .

[189] P.A. Zyla et al. Review of Particle Physics. PTEP, 2020(8):083C01, 2020. .

[190] Unitarity triangle fit. `http://www.utfit.org/UTfit/WebHome`. Accessed: 2020-02-03.

[191] P. A. R. Ade et al. Planck 2015 results. XIII. Cosmological parameters. Astron. Astrophys., 594:A13, 2016. .

[192] G. Bélanger, F. Boudjema, A. Pukhov, and A. Semenov. MicrOMEGAs: A Program for calculating the relic density in the MSSM. Comput. Phys. Commun., 149:103–120, 2002. .

[193] D. Barducci, G. Belanger, J. Bernon, F. Boudjema, J. Da Silva, S. Kraml, U. Laa, and A. Pukhov. Collider limits on new physics within micrOMEGAs_4.3. Comput. Phys. Commun., 222:327–338, 2018. .

[194] E. Aprile et al. Dark Matter Search Results from a One Ton-Year Exposure of XENON1T. Phys. Rev. Lett., 121(11):111302, 2018. .

[195] E. Aprile et al. Constraining the spin-dependent WIMP-nucleon cross sections with XENON1T. Phys. Rev. Lett., 122(14):141301, 2019. .

[196] P. Slavich et al. Higgs-mass predictions in the MSSM and beyond. Eur. Phys. J. C, 81(5):450, 2021. .

[197] A. Gando et al. Search for Majorana Neutrinos near the Inverted Mass Hierarchy Region with KamLAND-Zen. Phys. Rev. Lett., 117(8):082503, 2016. . [Addendum: Phys.Rev.Lett. 117, 109903 (2016)].

[198] G. Anton et al. Search for Neutrinoless Double-β Decay with the Complete EXO-200 Dataset. Phys. Rev. Lett., 123(16):161802, 2019. .

[199] D. Q. Adams et al. Improved Limit on Neutrinoless Double-Beta Decay in ^{130}Te with CUORE. Phys. Rev. Lett., 124(12):122501, 2020. .

[200] M. Agostini et al. Final Results of GERDA on the Search for Neutrinoless Double-β Decay. Phys. Rev. Lett., 125(25):252502, 2020. .

[201] L. Canonica et al. Status and prospects for CUORE. J. Phys. Conf. Ser., 888(1): 012034, 2017. .

[202] E. Aprile et al. Projected WIMP sensitivity of the XENONnT dark matter experiment. JCAP, 11:031, 2020. .

[203] Morad Aaboud et al. Search for electroweak production of supersymmetric states in scenarios with compressed mass spectra at $\sqrt{s} = 13$ TeV with the ATLAS detector. Phys. Rev. D, 97(5):052010, 2018. .

[204] Albert M Sirunyan et al. Search for new physics in events with two soft oppositely charged leptons and missing transverse momentum in proton-proton collisions at $\sqrt{s} = 13$ TeV. Phys. Lett. B, 782:440–467, 2018. .

[205] Albert M Sirunyan et al. Search for supersymmetry with a compressed mass spectrum in the vector boson fusion topology with 1-lepton and 0-lepton final states in proton-proton collisions at $\sqrt{s} = 13$ TeV. JHEP, 08:150, 2019. .

[206] Georges Aad et al. Searches for electroweak production of supersymmetric particles with compressed mass spectra in $\sqrt{s} = 13$ TeV pp collisions with the ATLAS detector. Phys. Rev. D, 101(5):052005, 2020. .

[207] W. Beenakker, M. Klasen, M. Kramer, T. Plehn, M. Spira, and P. M. Zerwas. The Production of charginos / neutralinos and sleptons at hadron colliders. Phys. Rev. Lett., 83:3780–3783, 1999. . [Erratum: Phys.Rev.Lett. 100, 029901 (2008)].

[208] Georges Aad et al. Search for electroweak production of charginos and sleptons decaying into final states with two leptons and missing transverse momentum in $\sqrt{s} = 13$ TeV pp collisions using the ATLAS detector. Eur. Phys. J. C, 80(2): 123, 2020. .

[209] Georges Aad et al. Search for direct stau production in events with two hadronic τ-leptons in $\sqrt{s} = 13$ TeV pp collisions with the ATLAS detector. Phys. Rev. D, 101(3):032009, 2020. .

[210] A. M. Baldini et al. The design of the MEG II experiment. Eur. Phys. J. C, 78(5): 380, 2018. .

[211] Georges Aad et al. Search for chargino–neutralino pair production in final states with three leptons and missing transverse momentum in $\sqrt{s} = 13$ TeV pp collisions with the ATLAS detector. 6 2021.

[212] Albert M Sirunyan et al. Search for supersymmetry in proton-proton collisions at 13 TeV in final states with jets and missing transverse momentum. JHEP, 10: 244, 2019. .

[213] Florian Staub and Werner Porod. Improved predictions for intermediate and heavy Supersymmetry in the MSSM and beyond. Eur. Phys. J. C, 77(5):338, 2017.
.